Gilmer, A., Sparks, S., Rust, A., Tapster, S., Webb, A., & Barford, D. N. (2017). Geology of the Don Manuel igneous complex, central Chile: Implications for igneous processes in porphyry copper systems. *Geological Society of America Bulletin*, *129*(7-8), 920-946. https://doi.org/10.1130/B31524.1

Geology of the Don Manuel igneous complex, central Chile: implications for igneous processes in porphyry copper systems

Amy K. Gilmer[1], R. S. J. Sparks[1], Alison C. Rust[1], Simon Tapster[2], Adam D. Webb[3], and Dan N. Barfod[4]

[1]School of Earth Sciences, University of Bristol, Wills Memorial Building, Bristol, BS8 1RJ UK

[2]NERC Isotope Geoscience Laboratory, British Geological Survey, Keyworth, Nottingham, NG12 5GG, UK

[3]BHP Billiton, Cerro El Plomo 6000, Santiago, RM, Chile.

[4]NERC Argon Isotope Facility, SUERC, East Kilbride G75 0QF, UK

ABSTRACT

The Don Manuel igneous complex (DMIC) and associated porphyry copper mineralization in the Andean Cordillera of central Chile demonstrates similarities between intrusive complexes associated with porphyry copper deposits (PCDs) and arc volcanoes that generate porphyritic volcanics. The DMIC intrusions progressed from quartz monzonite through rhyolite and biotite tonalite, to intermediate porphyritic and basaltic andesite dikes which intrude the older units. Mineralization is associated with the biotite tonalite and intermediate porphyries, which also contain the greatest abundance of mafic enclaves. Zoning patterns within plagioclase phenocrysts suggest that the later intermediate porphyries comprise a hybridized suite formed by magma mixing. New zircon U-Pb ages and whole rock Ar-Ar ages indicate that the DMIC was emplaced between ca. 4 and 3.6 Ma. The timescale for the episodic intrusion of the DMIC units is similar to observed episodicity of eruption and degassing events in active arc volcanoes. Observations from

the DMIC are consistent with the close spatial and temporal association of mineralization with both episodic intrusion and interaction between silicic and mafic magmas during emplacement. The observations are also consistent with the hypothesis that mafic magma provides a source of sulfur for porphyry copper deposit formation.

INTRODUCTION

Porphyry copper deposits (PCDs) form in association with high-level hypabyssal dikes or stocks, which are commonly referred to as "sub-volcanic" (Gustafson and Hunt, 1975; Hedenquist and Lowenstern, 1994; Redmond et al., 2004; Sillitoe, 1973, 2010). These mineralized intrusions are thought to be connected to larger pluton-scale magma reservoirs at depth and many have suggested a genetic or physical connection with volcanoes (Sillitoe, 1973, 2010; Sinclair, 2007). Volcanoes in convergent plate margin settings and PCD-related intrusions are typically characterized by calc-alkaline, water-rich and oxidized magmas (Kelley and Cottrell, 2009; Richards, 2011) that form rocks with porphyritic textures (Cline and Bodnar, 1991; Sillitoe, 2010) and often exhibit evidence of magma mixing (Halter et al., 2005; Lickfold et al., 2007; Murphy et al., 1998). The petrological similarity of many arc volcanic rocks and hypabyssal porphyry intrusions is well established (Dilles, 1987; Halter et al., 2004; Longo et al., 2010; Maydagán et al., 2011; Sillitoe, 1973; Waite et al., 1997). The igneous connection is particularly well demonstrated in the Yerington district, Nevada, where mineralized dike swarms are rooted in a granite pluton and exposures extend into the overlying contemporaneous volcanics (Dilles, 1987).

Direct temporal and spatial volcanic-PCD connections are difficult to establish due to the spatial distance between the volcanic edifice on the surface and the formation of porphyry copper deposits typically at depths of 1 to 6 km (Seedorff et al., 2005). Volcanic edifices are not preserved where

46 erosion rates are high and associated rocks have been hydrothermally altered. Where evidence for
47 direct connections is lacking, other criteria must be used to compare the evolution of the igneous
48 systems associated with arc volcanoes and those associated with PCD formation.

49 Recent advances in understanding intermediate to silicic volcanic and plutonic systems show
50 periods of eruption and intense degassing occur on timescales of years to centuries, and are
51 interspersed with dormant periods lasting thousands to tens of thousands of years (Christopher et
52 al., 2015; Harford et al., 2002; Hildreth et al., 2003; Le Friant et al., 2008). Relevant to the
53 interpretation of intrusions associated with porphyry copper deposits, is the emerging evidence
54 from geochronology and thermal and diffusion modelling for the highly episodic assembly of
55 shallow crustal calc-alkaline plutons (Annen et al., 2015; Mercer et al., 2015; Tapster et al., 2016)
56 on timescales similar to those of eruptive and degassing periods observed at active volcanoes.
57 Important questions are: (1) whether PCD-related hypabyssal intrusive complexes are formed by
58 processes similar to the processes that form sub-volcanic conduit systems that supply arc
59 volcanoes; and (2) how do these processes relate to mineralization?

60 This paper is the first description of the geology, geochronology, and geochemistry of the Don
61 Manuel igneous complex (DMIC), associated with one of the youngest known porphyry copper
62 systems in the Andes. The complex is situated in the Miocene-Pliocene porphyry copper belt of
63 central Chile, between the giant El Teniente porphyry copper-molybdenum deposit and the active
64 Maipo volcano (Fig. 1). Although destructive hydrothermal alteration occurs locally in the DMIC,
65 there are many areas with weak to no alteration, enabling primary magmatic features associated
66 with a porphyry copper system to be investigated. We describe the units of the DMIC, including
67 their geological relationships, geochemical compositions, ages, and evidence for magma mixing
68 and mingling. We consider the similarities between the DMIC and arc magmas, in particular the

episodic character of arc volcanism and hypabyssal igneous complexes to highlight the potential role of mafic magma in PCD genesis and discuss the links between magmatic degassing, hypabyssal intrusion and mineralization.

GEOLOGIC SETTING

Regional Geology

The Don Manuel igneous complex is located in the Andean Cordillera of the O'Higgins Region of Chile, approximately 100 kilometers southeast of Santiago and 30 km southeast of the giant El Teniente porphyry copper-molybdenum deposit (Fig. 1). Tectonically, the DMIC sits within the South American plate in the Principal Cordillera. This area is part of the northern segment of the Southern Volcanic Zone (NSVZ). The NSVZ has been studied extensively to understand the dynamics of subduction-related magmatism (Dungan et al., 2001; Hildreth and Moorbath, 1988; Kay et al., 2005; Kay et al., 1991; Stern and Skewes, 1995). Moreover, the region has been the focus of intense research on porphyry copper deposits, as it is part of the central Chile Miocene-Pliocene metallogenic belt (Atkinson Jr et al., 1996; Cannell et al., 2005; Deckart et al., 2005; Hollings et al., 2005; Kay and Kurtz, 1995; Kurtz et al., 1997; Maksaev et al., 2004; Muñoz et al., 2012; Piquer et al., 2015; Reich et al., 2003; Serrano et al., 1996; Skewes and Stern, 1995; Stern et al., 2007; Stern and Skewes, 1995; Stern et al., 2011; Vry et al., 2010; Warnaars et al., 1985).

Just north of the DMIC and the NSVZ is the Chilean flat-slab segment (29°S-33°S) (Kay et al., 2005; Marot et al., 2014; Stern and Skewes, 1995) where the Nazca plate is subducting below the South American plate at an angle of ~10° (Farías et al., 2010; Yáñez et al., 2002). The marked change in subduction style compared with areas to the north and south has been attributed to subduction of the Juan Fernandez Ridge (JFR), which began at around 25 Ma and has progressively

moved southward (Yáñez et al., 2002; Yáñez et al., 2001). The flat slab region between 28° and 33°S lacks active arc volcanoes, whereas south of latitude 33°S, the slab subducts at ~30° (Fig.1) (Marot et al., 2014; Pardo et al., 2002; Yáñez et al., 2002), and active arc volcanism is represented by several Late Pliocene to Holocene volcanic centers. Near the 33°S change in slab dip, the flat slab may increase crustal compression and reduce asthenospheric mantle wedge temperatures in the NSVZ, resulting in lower magma production rates and longer ascent and residence times than areas of the SVZ further to the south underpinned by steeper subduction angles (Marot et al., 2014).

Magmatic activity in central Chile began in the Jurassic and was relatively stable until the Pliocene, at which point the arc progressively moved eastward to its current position (Camus, 2003; Kay et al., 2005; Stern, 2004; Stern and Skewes, 1995). Between the late Eocene and the late Oligocene, an extensional basin opened and was filled with lavas, volcaniclastic and lacustrine sediments of the Abanico Formation, equivalent to the Coya Machalí Formation further to the south (Charrier et al., 2002; Charrier et al., 1996; Godoy et al., 1999; Kay et al., 2005) and later by volcanic units of the Miocene Farellones Formation (Charrier et al., 2002; Kay et al., 2005; Vergara et al., 1988). In most areas of central Chile, the Farellones Formation unconformably overlies the Coya Machalí Formation. It ranges in age from 25 to 7.4 Ma (Vergara et al., 1988) and consists of up to 2,400 m of gently folded andesitic to rhyolitic lavas and volcaniclastic sequences (Charrier et al., 2002; Nyström et al., 2003). In the area of the DMIC (~34°20'S) it can be difficult to distinguish between the Farellones and Coya Machalí formations, as the volcanic sequences are very similar in composition and the contact between the two is transitional (Charrier et al., 2002). Both the Coya Machalí Formation and the lower member of the Farellones Formation have bimodal compositions and were emplaced during periods of extension, whereas the upper Farellones Formation formed during passive to mild contraction (Nyström et al., 2003). The Young Plutonic Complex, which

114 includes predominantly granodiorite intrusions, ranging in age from 6.6 to 5.5 Ma (Kay et al.,
115 2005; Kurtz et al., 1997), marks the eastward frontal migration of the arc.

116 The DMIC and associated porphyry copper prospect occur in country rock consisting of mostly
117 basaltic andesite lavas and volcaniclastic deposits interbedded with fluvial and lacustrine
118 sedimentary units of the Coya Machalí Formation (Fig. 2). The formation is up to 2,500 m thick
119 and late Eocene to early Miocene in age (Kay and Kurtz, 1995). Locally the sequence is strongly
120 folded and locally metamorphosed to lower greenschist facies (Godoy et al., 1999).

121 Structurally, the DMIC sits on the eastern edge of the late Eocene to late Oligocene Coya Machalí
122 extensional basin (also known as the Abanico basin) (Farías et al., 2010). Godoy et al. (1999)
123 suggested that the Coya Machalí basin was inverted in the late Oligocene to early Pliocene,
124 resulting in folds and out-of-sequence thrust faults and uplift. Basin inversion appears to have been
125 syn-depositional with both the Coya Machalí and Farellones formations, and shortening was
126 accommodated primarily by reactivation of the original extensional basin-bounding faults (Godoy
127 et al., 1999; Charrier et al., 2002; 2007). The DMIC lies just west of the El Fierro fault system,
128 one of the major reactivated basin-bounding faults (Candia et al., 2009; Godoy et al., 1999).

129 Regional deformation has been characterized by over 63 km of shortening in three main events
130 (Farías et al., 2008; Farías et al., 2010; Giambiagi and Ramos, 2002). Inversion of the Abanico
131 basin around 22 to 15 Ma was followed by development of a thin-skinned fold-and-thrust belt in
132 the eastern Principal Cordillera between 16 and 8.5 Ma and then by uplift of the Frontal Cordillera
133 and thrust faulting in the eastern Principal Cordillera between 8.5 and 4 Ma. Late Miocene thrust
134 faulting was contemporaneous with migration of magmatic activity to the west (Farías et al. 2010).

The closest active Holocene volcanic center to the DMIC is the stratovolcano Maipo, ~25 km to the northeast (Fig. 1). Maipo volcano sits within the much larger Diamante Caldera formed by eruption of rhyolitic ignimbrites ~450,000 years ago (Hynek et al., 2010). In the Cerro de la Laguna area just east of the Diamante Caldera, lavas, ignimbrites and lahar deposits record pre-caldera, volcanic activity dating to the Late Miocene (Sruoga et al., 2012; Sruoga et al., 2005).

Central Chile Miocene-Pliocene porphyry copper-molybdenum belt

The central Chile Miocene-Pliocene porphyry copper-molybdenum belt extends from approximately 32°S to 34°S along the western flank of the Principal Cordillera and consists of N-S (orogeny-parallel) aligned deposits of Miocene to Pliocene age; this belt hosts three of the world's largest porphyry copper deposits: El Teniente, Río Blanco-Los Bronces, and Los Pelambres-El Pachón (Fig. 1). The PCDs in this belt are hosted in multiple porphyritic intrusions and late magmatic-hydrothermal breccias (Atkinson Jr et al., 1996; Cannell et al., 2005; Deckart et al., 2005; Maksaev et al., 2007; Serrano et al., 1996; Warnaars et al., 1985). These porphyritic intrusions formed toward the end of a tectonic-magmatic cycle that began around 19 Ma and are considered to be the last gasp of magmatism prior to the eastward shift of the volcanic front to the present-day location (Kay et al., 2005; Skewes and Stern, 1995; Stern, 2004; Stern et al., 2007).

The association of this belt of world-class PCDs and associated intrusions that have adakite-like geochemical characteristics (Defant and Drummond, 1990; Kay, 1978; Loucks, 2014; Richards and Kerrich, 2007) has been explained by several different models. By definition, adakites have high Sr/Y and La/Yb in intermediate calc-alkaline igneous rocks (Defant and Drummond, 1990; Kay, 1978; Richards and Kerrich, 2007). They have been attributed to either partial melting of the down-going oceanic slab (Defant and Drummond, 1990, 1993; Kay, 1978; Oyarzun et al., 2001) or mid- to deep-crustal fractionation of amphibole and/or garnet, involving wet (>4% H_2O),

158 oxidized basalts/andesites (Castillo, 2012; Chiaradia, 2015; Richards, 2011; Richards and Kerrich,
159 2007; Zellmer et al., 2012). Changes in the residual mineralogy from plagioclase to amphibole ±
160 garnet to produce the adakite-like signature may be the consequence of increased crustal thickness
161 and resulting changes in the magma source region and may have supplied additional water for
162 PCD formation (Kay and Mpodozis; (2001).

163 **ANALYTICAL TECHNIQUES AND SAMPLING METHODS**

164 The study area is divided into two parts, the northern Paredones area and the southern Don Manuel
165 Principal area where 8 holes were drilled to explore for porphyry copper deposits (Fig. 3). Dikes
166 and small stock-like intrusions dominate outcrops in the Paredones area, but moraines, alluvium,
167 and glaciers cover much of the complex in the Don Manuel Principal area. This study is therefore
168 based on fieldwork in the Paredones area and logging of drill cores from the Don Manuel Principal
169 area.

170 Over 350 representative samples of the various intrusive and country rocks were collected from
171 the surface exposures in the Paredones area and the eight drill cores. Samples collected were
172 variably altered and were selected to characterize the original igneous textures and mineralogy as
173 well as the products of alteration associated with sulfide mineralization. A fresh to minimally
174 altered sub-set of these samples was selected for focused characterization of the primary mineral
175 assemblage, compositions, and sample textures. Samples were examined petrographically using
176 both transmitted and reflected light, as well as by scanning electron microscopy (SEM) at the
177 University of Bristol.

178 Whole rock major and trace elements were analyzed for 78 samples by inductively coupled plasma
179 optical emission spectrometry (ICP-OES) and inductively coupled plasma-mass spectrometry

(ICP-MS) at the Element Analysis Facility at Cardiff University (Table 1 and Supplementary material DR1 and Table DR1) following the procedures documented in McDonald and Viljoen (2006). For the purpose of identifying the primary igneous characteristics of the DMIC, only the least altered samples were used and visible veins were removed prior to analysis (see Table DR1 for alteration intensity). Total sulfur analyses of all 78 samples and Fe^{2+}/Fe^{3+} by iron titration analysis for a selected sub-set of 12 samples was performed at Acme Analytical Laboratories Ltd., Canada.

Quantitative plagioclase analyses were carried out using a Cameca SX100 electron microprobe at the University of Bristol. Analyses were performed using a 20 kV, 10 nA beam for major elements and a 100 nA beam for minor and trace elements (Table 2 and Table DR2). Counting times for most elements were 30s on peak and 15s on the background. Sodium mobility was not observed when Na was measured first. Minor and trace elements in plagioclase were analyzed using counting times of 40-120 s on peak for Sr, 40-200s for Ba, 90-150s for Fe, and 50-300s for Mg. A labradorite standard was run as an unknown at the beginning of each session. The results for these standards and all analyses are presented in Table DR2.

Zircon fractions from nine DMIC samples were analyzed at the NERC Isotope Geosciences Laboratory at the British Geological Survey by CA-ID-TIMS methods to determine ^{238}U-^{206}Pb dates (Table 3 and DR3). Zircons were separated from bulk rock samples using standard separation techniques. Grains chosen for CA-ID-TIMS were imaged under transmitted light and fractions with the fewest inclusions were selected. Additional zircons were mounted in epoxy, polished and imaged by cathodoluminescence (CL) techniques to assess the complexity of the zircon growth histories. As many of the DMIC zircons are small (~50-300 μm) and have low concentrations of radiogenic Pb, we favored dating whole zircons or fragments rather than those where volume had

been reduced by polishing for CL imaging. Zircons selected for analysis by CA-ID-TIMS were thermally annealed and chemically abraded following the methods of Mattison (2005). Analysis of DMIC samples is technically challenging, requiring a robust uncertainty model for the common Pb isotopic composition and extremely low common Pb laboratory blanks (average 0.6 pg) and due to the small sizes of zircons (<150 μm), their low U concentrations (typically <200 ppm for the intermediate porphyry dike zircons) and the young age of the DMIC. All dates are reported in millions of years (Ma); 2σ uncertainties are noted in the form of ± x/y/z, where x is the analytical uncertainty suitable only for inter-comparison of U-Pb within this study and other EARTHTIME tracer ID-TIMS dates, y is the uncertainty inclusive of tracer calibration, and z is the total uncertainty, including ^{238}U-^{206}Pb decay constant (Jaffey et al., 1971), required for comparison with dates yielded by additional isotopic systems, e.g., $^{40}Ar/^{39}Ar$. Full analytical methods, procedures and data handling are described in detail in supplementary material DR3.

Don Manuel Principal basaltic andesite groundmass separates were analyzed using $^{40}Ar/^{39}Ar$ method at the NERC Ar Isotope Facility (Table 4). Samples were crushed, sieved, and purified using a combination of magnetic separation and mild leaching in dilute HNO_3. Altered grains and/or phenocrysts were removed by hand picking under a binocular microscope. Additional analytical methods and procedures are described in detail in supplementary material DR4 and complete raw data reported according to Renne et al. (2009) are given in Table DR4.

DON MANUEL IGNEOUS COMPLEX

Don Manuel has been a prospect of recent interest for exploration as a consequence of its proximity to other major ore deposits such as El Teniente and the occurrence of similar indicators of hypogene PCD mineralization. We have focussed our study on this complex because locally there

is excellent preservation of primary igneous textures. Thus DMIC provides a remarkable opportunity to study the higher temperature igneous processes associated with mineralization that are commonly masked by the effects of strong alteration in many PCDs.

Six main intrusive/hypabyssal units have been recognized in the DMIC. Four of these units occur in the Don Manuel Principal area (Fig. 2 and Fig. 3) in the southern part of the study area. These include: quartz monzonite; biotite tonalite, a stock-like body which is volumetrically the most significant rock type; a suite of intermediate porphyry dikes; and basaltic andesite dikes which cross cut the other units. In all eight drill cores, these igneous units are hosted by the Coya Machalí Formation, which consists of volcanic and volcaniclastic deposits interbedded with fluvial and lacustrine sedimentary units. The biotite tonalite, intermediate porphyry dikes and Coya Machalí Formation crop out at the surface (Candia et al., 2009). In the Paredones area (Fig. 3), two additional igneous units were recognized: a rhyolite stock and basaltic andesite dikes. These units are also hosted by the Coya Machalí Formation (Fig. 3).

The DMIC in both the Don Manual Principal and Paredones areas is locally extensively altered. Within the drill cores, the alteration intensity varies and is locally discontinuous. Calc-silicate intervals in the Coya Machalí Formation have largely been altered to garnet-clinopyroxene-epidote skarn and a clinopyroxene-magnetite-actinolite-epidote skarn; other siliciclastic sedimentary facies, volcaniclastic facies, and volcanic hornfels exhibit secondary biotite adjacent to the biotite tonalite and intermediate porphyry dikes and more distally contain chlorite and epidote (Fig. 4A). Along the northwestern contact of the rhyolite in the Paredones area, the host rocks have been intensely hornfelsed and locally the rhyolite stock has been silicified.

Observed copper sulfides in the core from the Don Manuel Principal area are primarily hosted in the biotite tonalite, intermediate porphyry dikes, and sedimentary and volcaniclastic hornfels and skarn lithologies of the Coya Machalí Formation. The copper grades of the DMIC rocks are commercially confidential, but confirm the strong association of mineralization with the biotite tonalite and IPDs (Candia et al., 2009). Within the igneous units, copper sulfides occur in porphyry-style veins (Fig. 4B) and disseminated in the host rock. In the skarns, copper sulfides are massive, whereas they are disseminated and vein-hosted in the surrounding sedimentary and volcaniclastic hornfels. No copper sulfides were observed in the Paredones area.

Three main stages of mineralization and alteration can be recognized: an early stage characterized by silicification and pervasive magnetite and secondary biotite associated with K-silicate alteration; a primary mineralization stage, characterized by vein-hosted chalcopyrite associated with K-silicate alteration and distal propylitic alteration including abundant chlorite and actinolite; and a late mineralization stage of lower temperature produced localized chlorite-sericite and sericite and argillic alteration assemblages. The close temporal association of the peak mineralization with the major intrusions documented below has been confirmed by Re-Os dating of molybdenite in mineralized veins (Gilmer, 2016). A detailed account of the mineralization will be presented elsewhere.

Don Manuel Principal units

Quartz monzonite

The quartz monzonite (67-74 wt. % SiO_2) is fine- to medium-grained and locally porphyritic, and composed of plagioclase, microcline, quartz, and biotite (Fig. 4C). Accessory minerals include apatite, magnetite, and rutile. Where porphyritic, plagioclase phenocrysts range in size from 1 to 3.5 mm, and primary biotite phenocrysts are 0.5 to 1.3 mm (Fig. 5A and Fig. 6A). The quartz

monzonite occurs in short vertical intervals (less than 20 m) in two drill holes (DM2 and DM6) and is crosscut by intermediate porphyry and basaltic andesite porphyry dikes. Overall, this unit has a fine-grained equigranular groundmass, and locally, it is also strongly silicified and contains disseminated secondary biotite with minor secondary magnetite. In other narrow intervals, vein-related sodic-calcic alteration is characterized by growth of actinolite and magnetite and albitization mostly within vein selvages. Disseminated pyrite and pyrite veinlets are the only sulfides present in the quartz monzonite. Based on the absence of copper sulfides, and because this unit is cut by the intermediate porphyry dikes that have the most sulfide minerals and veins, it is interpreted to be pre-mineralization (Fig. 3B).

Biotite tonalite

The biotite tonalite (64-68 wt. % SiO_2) is the most common unit, observed in drill cores DM2, DM4, DM7, and DM8. Overall, this intrusion is medium- to coarse-grained, with typical plutonic texture, and has horizontal dimensions of at least 1.5 km. It constitutes over 80% of the 600 m of drill hole DM4. Drill holes DM7 and DM4 both terminate in biotite tonalite; with DM4 ending in brecciated biotite tonalite. Two textural varieties of biotite tonalite were identified in the drill core, one equigranular and one porphyritic (Fig. 4D and 4E). Drill holes DM4 and DM7 contain intervals of both varieties. Contacts between the two are rare, but where observed are sharp.

The biotite tonalite ranges from medium- to coarse-grained and is composed of subhedral to anhedral plagioclase, tabular biotite, microcline, quartz, and ± amphibole (Fig. 5B and 5C); small (0.5-1 mm) aggregates of quartz, plagioclase, biotite, and microcline are also present (Fig. 6B). Accessory minerals include apatite, anhydrite, titanite, magnetite, ilmenite, and zircon; however, the titanite is anhedral suggesting that this phase is secondary. The porphyritic biotite tonalite (Fig. 4E) contains plagioclase (1-4 mm), biotite (1-3 mm), and amphibole (1-4 mm long) phenocrysts.

The groundmass in the porphyritic phase has an intergranular texture comprising crystals ranging from 0.2-0.3 mm. Anhydrite inclusions are present in plagioclase in both variants. Mafic enclaves are common throughout the biotite tonalite (Fig. 4D) and show chilled margins where the hotter, more mafic magma cooled against the biotite tonalite. Crosscutting relationships indicate that the biotite tonalite is older than the intermediate porphyry dikes and basaltic andesite dikes (Fig. 3B).

The biotite tonalite contains pyrite, chalcopyrite and molybdenite in quartz veinlets with sericite halos, and disseminated in the interstitial space adjacent to quartz, biotite, and anhydrite. With the exception of the rare anhydrite inclusions in plagioclase, anhydrite occurrences are likely secondary. Later veins and cavities, primarily within the porphyritic phase, contain coarse-grained anhydrite, biotite, quartz and molybdenite, but no other sulfides. In the majority of core intercepts, the biotite tonalite is mineralized.

The biotite tonalite unit shows both propylitic and K-silicate alteration. Within the propylitically-altered zones, chlorite has replaced biotite, actinolite has replaced amphibole and plagioclase has been replaced by sericite, epidote and/or calcite. K-silicate alteration is characterized by pervasive secondary biotite replacing primary biotite and amphibole, and patchy areas (10-50 μm) of potassium feldspar replacing plagioclase. Relict amphiboles contain abundant titanite and rutile, which may be the result of late magmatic alteration of titanomagnetite or alteration of amphibole to biotite, the remaining titanium forming titanite and rutile.

Intermediate porphyry dikes

Numerous intermediate porphyry dikes intrude the biotite tonalite and Coya Machalí Formation. This suite of dikes shows a wide range of textures and modal compositions, ranging from dacite to andesite (59-68 wt. % SiO_2) (Fig. 4B and 4F). These porphyries vary from less than one to 60

meters in width, and occur in all drill cores (DM1-DM8). The distribution of textural types is spatially complex, and the suite displays sharp contacts as well as gradational contacts. Where the contacts are sharp, they dip steeply at ~10˚ to 25˚ to the subvertical drill core orientation. These sharp contacts may separate dikes of nearly identical composition or dikes of a distinctly different texture and composition within the intermediate suite. Contact-parallel flow foliations are common adjacent to these sharp contacts. Numerous features of magma mixing are observed in these dikes, including mafic enclaves and irregular contacts (Fig. 6F and Fig. 7). In some cases, undulating contacts suggest intrusion of one dike into partially solidified magma of another dike.

The intermediate porphyry dike phenocryst contents range from 30 to 60 modal %. The main phenocrysts are euhedral plagioclase (0.3-2 mm), ± subhedral to euhedral amphibole, ± biotite (0.2–2 mm), and ± quartz (0.2–1 mm) (Fig. 5C). The intermediate dikes can be divided into three types on the basis of the ferromagnesian phenocryst assemblage. Type 1 contains primary biotite phenocrysts, but no amphibole (Fig. 5D), Type 2 contains both primary biotite and amphibole phenocrysts (Fig. 5E), and Type 3 contains amphibole phenocrysts, but no biotite (Fig. 5F). Two of the Type 1 intermediate porphyry dikes also contain trace amounts of rounded and embayed quartz phenocrysts. The groundmass consists of plagioclase, amphibole, ± biotite, and quartz. Anhydrite inclusions in plagioclase were observed in all three types of intermediate porphyry dikes, although they are rare (n=5). Accessory minerals include apatite, titanite, magnetite, ilmenite, and zircon.

The intermediate porphyry dikes contain more copper than any other unit (based on commercially confidential assays, BHP Billiton personal communication, January 2014). Disseminated chalcopyrite, bornite, and pyrite occur within all three types of intermediate porphyry dikes; the dikes also contain veins and veinlets of quartz ± chalcopyrite-pyrite-bornite-specularite-

molybdenite; quartz ± chalcopyrite; quartz ±pyrite; quartz-chlorite± actinolite-pyrite; quartz-anhydrite ± chalcopyrite-pyrite-molybdenite; and quartz-molybdenite ± anhydrite.

The intermediate porphyry dikes show selective replacement of both amphibole and primary biotite by titanite, hydrothermal biotite, magnetite and sulfides. In some cases, the dikes exhibit chlorite, actinolite, and epidote replacement of biotite and amphibole, and minor sericite replacement of plagioclase phenocrysts. Overall, the alteration in the intermediate porphyry dikes has preferentially affected the groundmass and ferromagnesian phases. Many of the intermediate porphyry dikes also contain miarolitic cavities filled with quartz, apatite, anhydrite, epidote, and calcite, and some cavities also contain chalcopyrite and pyrite.

Basaltic andesite dikes

The Don Manuel Principal basaltic andesite dikes are the most mafic unit in the Don Manuel drill core (54-57 wt. % SiO_2). These dikes occur as short vertical intervals in all of the drill cores (DM1-DM8) and are typically less than 10 meters in thickness; they have near-vertical contacts with other units (Fig. 4G). The basaltic andesite dikes crosscut the intermediate porphyries. They are aphanitic to porphyritic with up to 20% phenocrysts (Fig. 5G). Where porphyritic, the main phenocrysts are euhedral to subhedral plagioclase (0.2–1.5 mm) and euhedral to subhedral, prismatic amphibole (0.2–1.3 mm) (Fig. 6E). Phenocrysts adjacent to dike contacts show contact-parallel alignment. The groundmass contains plagioclase, amphibole and biotite, with accessory apatite, titanite, magnetite and ilmenite (Fig. 5E). As seen in the intermediate porphyry dikes, several dikes also contain circular or irregular miarolitic cavities (1-5 mm diameter) infilled with quartz, anhydrite, apatite, biotite, and pyrite.

Pyrite is the only sulfide present in the basaltic andesite dikes; it occurs as pyrite veinlets, and pyrite + quartz veinlets, and disseminated. The basaltic andesite ranges from completely unaltered to weakly altered; in the altered dikes primary amphibole has been replaced by actinolite, and chlorite. Epidote and calcite may also locally occur in these dikes. They are interpreted to be late- to post-mineralization dikes.

Paredones units

Rhyolite porphyry

The rhyolite porphyry crops out in the northeastern corner of the Paredones field area, forming a ~1 km^2 subcircular, stock-like outcrop geometry (Fig. 3A). The rhyolite is predominately porphyritic; however, silicification has locally destroyed this texture, and is associated with abundant fractures. Prominent limonite (after pyrite) staining is observed. Where the primary texture is intact, the main phenocrysts comprise plagioclase (0.8-3.5 mm), biotite (0.3-2.5 mm), and rare quartz "eyes" (0.3-0.6 mm) (Fig. 6G and Fig. 8). Accessory minerals include apatite, titanite, and zircon. Secondary pyrite is locally disseminated. The rhyolite also contains rare mafic enclaves. Basaltic andesite porphyry dikes cut the rhyolite; the contacts are undulose and embayed (Fig. 8), typical of mafic intrusions into hot ductile silicic host rock (Blake et al., 1965). No copper minerals were observed in this unit.

Basaltic andesite dikes

Several vertical NW-SE striking dikes of basaltic andesite crop out in the Paredones area (Fig. 3). They are the most mafic unit in the study area (54-55 wt. % SiO_2). The dikes have a porphyritic texture with up to 60% phenocrysts, including plagioclase (0.1-1.5 mm), clinopyroxene (0.2 to 2 mm), biotite (0.3-1 mm) and minor amphibole (≤0.5 mm); the groundmass has the same mineralogy (Fig. 5h and 7). In places, the groundmass has a subophitic texture with plagioclase

laths enclosed by clinopyroxene. The presence of clinopyroxene phenocrysts distinguishes these basaltic andesite dikes from those encountered in the drill core. Samples collected adjacent to and cutting the rhyolite are strongly and pervasively altered; chlorite has completely replaced all ferromagnesian phases. Dikes that cut the volcaniclastic units of the Coya Machalí Formation are considerably less altered. No copper minerals were observed in this unit.

WHOLE ROCK COMPOSITIONS

Major and trace elements

The DMIC samples contain between 53 and 74 wt. % SiO_2 (Table 1; Table DR1; Fig. 9). The mafic enclaves have SiO_2 contents between those of the intermediate porphyry dikes and the basaltic andesite dikes. The DMIC samples follow a typical calc-alkaline trend and are metaluminous to peraluminous (Irvine and Baragar, 1971; Shand, 1951). Some mobile elements such as K, Na, Rb, and Cs show variation that is likely to be related to alteration. Although there is scatter in the compositions of the basaltic andesite dikes, mafic enclaves, and intermediate porphyry dikes, linear compositional trends are clear for most major oxides (Fig. 10). Within the DMIC, as SiO_2 increases, TiO_2, FeO*, Al_2O_3, P_2O_5, MgO, and CaO all decrease (Fig. 10). Overall Na_2O and K_2O increase with increasing SiO_2, although these components show more scatter, which is attributed to hydrothermal alteration. Alteration intensity for whole rock geochemical samples is noted in Table DR1 and alteration type is noted where justified.

Chondrite-normalized rare earth element (REE) patterns (Sun and McDonough, 1989) are similar across all samples and show patterns typical of subduction-related magmas (Pearce and Peate, 1995; Tatsumi, 1989). All DMIC samples show enrichment of Light REE (LREE) with respect to Heavy REE (HREE) (Fig. 11) and have similar ranges in REE abundances, however the

intermediate porphyries and mafic enclaves show the most variability. DMIC REE patterns show very little fractionation between the Middle REE (MREE) and HREE. Most samples in the DMIC do not show a negative Eu anomaly. Many of the DMIC units have high Sr/Y and La/Yb, the biotite tonalite and some intermediate porphyry dike samples in particular, and plot in the "adakite" fields of Defant and Drummond (1993) and Castillo et al. (1999) (Fig. 12). The less evolved samples of the DMIC have signatures more typical of arc rocks.

MAGMA MINGLING AND MIXING

Mafic enclaves and hybridization textures

Field, core and geochemical observations reveal conspicuous igneous contacts, structures and textures indicative of magma mingling, mixing and hybridization associated with the DMIC. Mafic enclaves can be found within the rhyolite, equigranular biotite tonalite, and in the intermediate porphyry dikes (Fig. 4D and 5A). These enclaves range in length from <1 cm to 15 cm, although intercepts within the drill core may not capture their full dimensions. Enclave morphologies range from subspherical to elongate and may have diffuse margins. They are most abundant in the biotite tonalite and intermediate porphyry dikes. Within the biotite tonalite enclaves can occur in clusters, which may represent intersections with enclave-rich syn-plutonic intrusions that are commonly attributed to dismemberment of a mafic dike intruded into a hot ductile pluton (Furman and Spera, 1985; Hallot et al., 1996) (Fig. 4D). Enclaves vary from aphanitic to porphyritic; phenocrysts consist of plagioclase, hornblende (often altered to secondary biotite), and biotite. The groundmass of the enclaves consists mainly of plagioclase and biotite with minor quartz.

Many of the enclaves display diktytaxitic textures, and some contain miarolitic cavities (Fig. 6D). Diktytaxitic textures likely result from exsolution of volatiles and consequent undercooling leading

to rapid crystallization (Bacon, 1986; Blake and Fink, 2000; Sparks and Marshall, 1986). Contacts between the enclaves and host can be crenulated and undulating or may show a more abrupt fine-grained chilled margin. In several instances, a phenocryst (plagioclase or hornblende) straddles the contact between the enclave and the host or appears to have become almost completely entrained by the enclave (Supplementary material Figure DR5.1). These are all classic features of mafic inclusions generated by mingling of mafic and more silicic magma (Bacon, 1986; Sparks and Marshall, 1986; Tepley et al., 2000; Vernon, 1984).

Within some intermediate porphyry dikes, there is evidence that interaction between the two magmas was more extensive, resulting in a more thoroughly mixed, hybridized texture (Fig. 7B). Amphibole crystals occur as glomerocrysts within the enclaves and as microenclaves within the adjacent host. These mafic clots (1 to 3 mm) may also include primary plagioclase, biotite, titanite, and magnetite. Amphibole crystals are euhedral to subhedral and range in size from 1 to 3 mm. These clots likely originated from disintegration of larger mafic enclaves (Humphreys et al., 2009).

The enclaves are commonly more altered (in the form of secondary biotite, epidote and chlorite) than their hosts because they contain additional ferromagnesian phases (Supplementary material Figure DR5.1). The mineralogical changes are consistent with the observed depletion in CaO and MgO and elevated K_2O and Na_2O values in some of the mafic enclaves (Fig. 10).

Plagioclase zoning and phenocryst assemblages

Plagioclase is the most common mineral in all of the DMIC units. Importantly, plagioclase zones preserve the original magmatic compositions and crystallization conditions because of sluggish, coupled substitution of the Si and Al pair (Grove et al., 1984). This attribute can be used to infer mixing between the magmas of different units and to determine whether this mixing involved a

447 mafic magma and/or was caused by convective self-mixing from hotter recharge magma of the
448 same composition (Couch et al., 2001; Humphreys et al., 2009; Streck, 2008).

449 Plagioclase phenocrysts from the Paredones rhyolite show the simplest zoning patterns, with minor
450 variations and little or no resorption (Fig. 13). All plagioclase phenocrysts in this unit show normal
451 zoning and have cores of An_{28-45} and rims of An_{6-28}. Plagioclase phenocrysts from the basaltic
452 andesite dikes show minor normal zoning and little or no resorption, and have cores of An_{75-85} and
453 rims of An_{50-70} (Fig. 13). In both of these units, the rim compositions are the same as the
454 surrounding groundmass plagioclase.

455 In contrast, plagioclase phenocrysts from the intermediate porphyry dikes show complex zoning
456 and resorption surfaces as well as diverse assemblages within a single dike. Five distinct types of
457 plagioclase phenocrysts were identified in the intermediate porphyry on the basis of optical and
458 SEM characteristics and electron microprobe analyses. Plagioclase phenocrysts selected for study
459 are unaltered (no albitization) and all zones are interpreted to be magmatic. These include: (1)
460 reversely zoned plagioclase phenocrysts that have broad cores of An_{23-38} and sieve-textured rims
461 with sharp transitions to An_{51-56} (Fig. 14); (2) oscillatory zoned phenocrysts that have high
462 amplitude, high frequency variations in An content, cores of An_{21-44} and rims that are normally
463 zoned, An_{51-32}; (3) patchy zoned phenocrysts containing An_{48-58} cores showing significant
464 resorption and rims that are An_{49-32} (Fig. 14); (4) largely unzoned, euhedral grains that have cores
465 of An_{51-58} and rims of An_{50-37}; and (5) patchy zoned phenocrysts commonly in glomerocrysts,
466 having cores of An_{87-66} and rims of An_{50-28} (Fig. 14). All five types of plagioclase phenocrysts can
467 be found within single thin sections of the intermediate porphyry dikes.

468 **GEOCHRONOLOGY**

A well-constrained chronology is a prerequisite for interpreting the durations of igneous processes and emplacement frequencies associated with the formation of PCDs, as well as for placing a deposit in the context of regional tectonics. We have employed both high-precision CA-ID-TIMS U-Pb and $^{40}Ar/^{39}Ar$ geochronological methods to provide time constraints for the DMIC.

U-Pb geochronology

Samples from the quartz monzonite (n=2), rhyolite (n=1), equigranular biotite tonalite (n=1), porphyritic biotite tonalite (n=1) and the intermediate porphyry dikes (n=4) were chosen for CA-ID-TIMS U-Pb dating. Dates and isotopic compositions of single zircon fractions are listed in Table 3 and weighted mean dates are presented in Figure 15 for grains of euhedral and elongate shapes, which showed no resorbed cores in CL images. Multifaceted grains were avoided where possible as these were shown to contain resorbed zones comparable to those discussed in Tapster et al. (2016), and therefore do not represent zircon growth upon emplacement. Both weighted mean dates and the youngest single fraction dates show a clear temporal progression that agrees with observed crosscutting relationships where observed. Best estimates for emplacement ages are interpreted from the weighted mean dates of the youngest clusters of zircon $^{238}U/^{206}Pb$ dates that form statistically acceptable mean squared weighted deviations (MSWDs) at the 95% confidence interval.

From the quartz monzonite, five zircons from DM6AG05 yielded a weighted mean date of 4.040 ± 0.015/0.016/0.016 Ma with an MSWD of 2.26 and six zircons from DM2AG33 yielded a weighted mean date of 3.975 ± 0.057/0.058/0.058 Ma with an MSWD of 1.2. Type 3 intermediate porphyry dike DM6AG21 yielded two clusters of dates, with a weighted mean of 4.058 ± 0.036/0.060/0.060 Ma (n=6; MSWD of 1.48) for the older cluster, and a weighted mean date (n=2) of 3.912 ± 0.057/0.066/0.066 Ma for the younger cluster that we take as our preferred emplacement

age. Rhyolite (DMN30) yielded a weighted mean date of 3.879 ± 0.017/0.018/0.018 Ma (MSWD=0.5, n=6). The equigranular biotite tonalite (DM2AG01) yielded a weighted mean date of 3.829 ± 0.009/0.010/0.011 Ma (MSWD=0.6, n=11) whereas the porphyritic biotite tonalite (DM4AG14) yielded a weighted mean date of 3.733 ± 0.012/0.012/0.013 Ma (MSWD=0.9, n=7). Six zircons from a Type 1 intermediate porphyry dike, sample DM8AG44, yielded a weighted mean date of 3.733 ± 0.048/0.050/0.050 Ma (MSWD of 1.5) which is closely comparable to that of DM4AG16. Six zircons from DM5AG32, a Type 2 intermediate porphyry dike, yielded a weighted mean date of 3.656 ± 0.028/0.029/0.029 Ma with an MSWD of 1.0 and DM3AG15, another Type 2 intermediate porphyry dike, yielded a near identical weighted mean date of 3.657 ± 0.031/0.032/0.032 Ma with an MSWD of 1. Zircon xenocrysts, with dates of ca. 8 Ma and ca. 5 Ma were noted in samples, DM2AG33, DMN30, DM8AG44 and DM3AG15 (Table 3).

$^{40}Ar/^{39}Ar$ geochronology

Two groundmass separates from the Don Manuel Principal basaltic andesite dikes were step heated using the $^{40}Ar/^{39}Ar$ method (see supplementary material DR4 for method details). The Paredones basaltic andesite dikes have not been dated. Samples analyzed are interpreted to be dikes that cross-cut either older volcaniclastic units or the equigranular biotite tonalite. Table 4 summarizes the geochronologic data and gives results for total fusion ages and inverse isochron ages in Ma. Plateau acceptance criteria are at least four consecutive age steps that are indistinguishable at the 2σ level and represent 50% or more of the total ^{39}Ar released during the experiment. The scatter between these steps should be low (MSWD approaching 1); for plateaus with excess scatter (MSWD>1), the uncertainty on the plateau age is multiplied by the square root of MSWD. Values for MSWD were below the cut-off criteria outlined in Wendt and Carl (1991) and no error expansion was applied. Furthermore, the trapped component derived from an inverse isochron analysis should be

indistinguishable from atmospheric composition. Samples DM4AG28 and DM7AG26 satisfied these criteria.

Sample DM7AG26 has a plateau age of 3.60 ± 0.06 Ma (Fig. 16A). This basaltic andesite dike cross cuts sedimentary hornfels. Sample DM4AG28, which was emplaced in the biotite tonalite, has a plateau age of 3.85 ± 0.19 Ma (Fig. 16B). This result is within uncertainty of the zircon U-Pb age for the equigranular biotite tonalite, and although it was interpreted as a small contemporaneous dike, it could also be a larger (relative to the drill core) mafic enclave.

DISCUSSION

Evolution of the Don Manuel Igneous complex

The DMIC represents a suite of hypabyssal and upper parts of plutonic intrusions, which like other porphyry copper-related intrusions, was emplaced within the upper crust (Cooke et al., 2014; Seedorff et al., 2008; Seedorff et al., 2005). Overall, the DMIC shows a temporal progression from dominantly silicic magmas with very minor mafic components (enclaves and intermediate dikes) to more mafic magmas represented by porphyritic intermediate and basaltic andesite dikes (Fig. 17). We attribute this trend to the tapping of progressively deeper parts of the transcrustal magmatic system (Cashman et al., 2017) together with mafic replenishment. Based on the new U-Pb dates, the silicic magmas in this system lasted for ~400 kyr (Fig. 17) beginning at ca. 4 Ma. The 3.85 ± 0.19 Ma and 3.60 ± 0.06 Ma Don Manuel Principal basaltic andesite dikes and the presence of mafic enclaves within the rhyolite, biotite tonalite, as well as evidence for magma mixing in the intermediate porphyry dikes, document the periodic emplacement of mafic magma into the upper crust throughout the lifetime of this magma system (Fig. 4 and Fig. 7).

Fractionation of the DMIC magmas occurred deeper than the level of final intrusion, under varying physical conditions. LREE enrichment, HREE depletion, a dip of MREE relative to HREE (Fig. 12) can be explained by fractionation of amphibole (Davidson et al., 2007). The high Sr/Y ratio and negligible Eu anomaly in the biotite tonalite and intermediate porphyry dikes ($Eu/Eu^* = 0.7$-1.2), and the small Eu anomaly in the rhyolite ($Eu/Eu^* = 0.68$-0.84), is attributed to suppression of plagioclase crystallization during magma evolution under high pH_2O and presumably deeper conditions (Moore and Carmichael, 1998; Müntener et al., 2001). Both the biotite tonalite and many of the intermediate porphyry dikes contain amphibole phenocrysts, which suggests relatively high water content (≥4 wt. % H_2O; (Naney, 1983; Richards, 2011; Richards et al., 2012). Within the intermediate porphyry dike suite, variations in Sr/Y and La/Yb suggest different amounts of amphibole fractionation prior to onset of plagioclase crystallization (Castillo, 2012; Castillo et al., 1999). A neglible Eu anomaly could also result from high oxidation conditions (e.g. Dilles et al., (2015). Primary anhydrite inclusions in plagioclase in the biotite tonalite and intermediate porphyry dikes are consistent with relatively oxidized magmas (NNO +1 to NNO +3) (Carroll and Rutherford, 1987; Luhr, 1990; Matjuschkin et al., 2016; Scaillet et al., 1998). We infer that the negative Eu anomaly reflects both high pH_2O and high oxidation conditions.

Episodic igneous processes and mineralization

Both PCDs and volcanoes are the top or near top expressions of upper crustal magma reservoirs (e.g. Dilles, 1987; Lipman, 2007; Scandone et al., 2007; Tapster et al., 2016). The DMIC developed over a timescale comparable to many arc volcanoes, contains a similar wide range of magma compositions, shows evidence of deeper fractionation of oxidized wet magmas, and displays features indicative of magma mixing and mingling. Although we cannot be sure that the DMIC connected directly to a volcano, it is reasonable to infer that volcanoes and porphyry-

559 associated hypabyssal intrusive complexes share some processes of magma ascent and degassing
560 from deeper in the crust. The specifics of these dynamic processes, however, determine whether
561 or not an ore deposit forms.

562 We first consider time scales as defined by the geochronology, geology of the intrusions, thermal
563 constraints and observations at active arc volcanoes. High-precision geochronological studies and
564 thermal modelling suggest that volcanic and shallow intrusive systems in arcs are highly pulsatory
565 (Annen et al., 2015; Michel et al., 2008; Sparks and Cashman, in press). Volcanic dome complexes
566 are, for example, characterized by short periods of extrusive activity fed by dikes separated by
567 much longer periods of repose. Dome complexes and stratovolcanoes typically have durations of
568 many hundreds of thousands of years (e.g. Clavero et al., 2004; Harford et al., 2002; Hoshizumi
569 et al., 1999), comparable to the ca. 400 kyrs duration of the DMIC. Many arc volcanoes are
570 characterized by highly episodic bursts of volcanic activity that last years to perhaps a few
571 centuries and are separated by dormant periods lasting thousands to tens of thousands of years (e.g.
572 Hildreth and Lanphere, 1994; Le Friant et al., 2008). In the Maipo volcanic center, ~25 km
573 northeast of DMIC, the large-volume eruption that produced the Diamante ignimbrite was
574 followed by a period of ca. 350 kyr. dormancy prior to post-caldera reactivation, during which
575 eruptive episodes occurred on the order of every 30 kyrs or less (Sruoga et al., 2005; Stern et al.,
576 1984).

577 Likewise, shallow intrusions in arcs involve multiple short bursts of intrusion separated by long
578 periods of inactivity (Barboni et al., 2015; Caricchi et al., 2012; Michel et al., 2008; Miller et al.,
579 2011). For example, emplacement of the Torres del Paine laccolith in Chile occurred in discrete,
580 short-lived pulses over 90 ± 30 kyrs, with large time gaps between pulses (Leuthold et al., 2012;
581 Michel et al., 2008). Thermal modelling (Annen et al., 2015) indicates that single pulses at Torres

582 del Paine lasted only hundreds of years at most. Other examples of episodic pluton emplacement
583 together with thermal modeling constraints are discussed in Barboni et al. (2015) and Annen et al.
584 (2015).

585 Cross-cutting relationships and age data indicate that the development of the DMIC was also
586 highly episodic. Based on our U-Pb ages and their 2σ uncertainties (Figs. 15 and 17) the time
587 intervals between emplacement of the major units are constrained to the order of 10's kyrs to ~100
588 kyrs: 95 ± 59 kyrs (2σ) (quartz monzonite and rhyolite), 51 ± 19 kyrs (2σ) (rhyolite and
589 equigranular biotite tonalite), and 96 ± 15 kyrs (2σ) (biotite tonalite and porphyritic biotite
590 tonalite).

591 With the exception of the biotite tonalite and the rhyolite, the numerous intrusions of DMIC are
592 dikes that have widths of meters to tens of meters at most. Conductive cooling times would range
593 from 1-10 years for meter scale dikes to 10^3 years for the 1500 m diameter rhyolite stock (Jaeger
594 et al., 1968). Emplacement times must be even shorter. These cooling times are orders of
595 magnitude shorter than the minimum age differences between the major intrusive units, thus
596 indicating that each unit would have solidified before the emplacement of the next intrusive unit.
597 The minimum time intervals between the quartz monzonite and the rhyolite stock and between the
598 rhyolite and the equigranular biotite tonalite intrusions are both constrained to ca. 30-35 kyrs (Fig.
599 17) and the different textural facies of the biotite tonalite (equigranular and porphyritic) have
600 distinctive ages, indicating a minimum time interval of ca. 80 kyrs. It is most probable, that this
601 represents the accumulation of multiple yet discrete magmatic pulses similar to the emplacement
602 of Torres del Paine, as cooling models would require an intrusion diameter of at least 2 km to
603 emplace the biotite tonalite over a duration of 80 kyrs or more (Annen, 2009). The observed sharp
604 contacts suggest, however, that two short-lived intrusive pulses of compositionally similar but

605 texturally contrasted magma is a more plausible explanation.

606 Conductive cooling times constrain the emplacement of individual hybrid porphyritic dikes of the
607 DMIC to be very short (<1 to 10^2 years), comparable to the typical time scales for emplacement
608 of feeder dikes associated with porphyritic lava dome eruptions (years to decades). In addition,
609 composite dikes observed in DMIC have undulose contacts (Supplementary material, Figure
610 DR6), recording the pulsed behavior of magma injection that must occur at timescales more rapid
611 than those defined by cooling (i.e. still ductile at the time of the next intrusion). The processes
612 causing pulsatory dike emplacement in the DMIC may be similar to those that lead to repetitive
613 cyclic lava dome extrusion over periods of weeks to years in many dike-fed lava dome eruptions
614 (Sparks, 1997). Composite dikes were, for example, encountered during the drilling of the Mt.
615 Unzen volcanic conduit that formed between 1991 and 1995 (Goto et al., 2008).

616 Pulsed porphyritic intrusions are a feature of PCDs elsewhere. The tens kyrs timescales
617 documented for the DMIC are similar to those documented by Tapster et al. (2016) in the Koloula
618 porphyry copper deposit in the Solomon Islands and by Buret et al. (2016) in the Bajo de la
619 Alumbrera porphyry copper deposit in Argentina. Additionally, detailed, high-resolution U-Pb
620 geochronology from other PCDs has shown that the entire duration of igneous activity associated
621 with mineralization episodes can be short, lasting only a few hundred thousand years or less and
622 that this activity is also episodic (Buret et al., 2016; Chelle-Michou et al., 2015; Tapster et al.,
623 2016; Von Quadt et al., 2011). As more high-precision data sets emerge from other studies of
624 geologically well-constrained PCDs such episodic igneous activity may become a well-recognized
625 feature of porphyry copper systems.

626 The spatial distribution and timing of mineralization are closely associated with hypabyssal
627 intrusions at DMIC, as is also the case at many other PCDs (e.g. Dilles (1987) and Spencer et al.
628 (2015)). Intrusions can create the pathways for mineralization fluids from deeper magma systems.
629 Observations of dike rocks and volcanic systems show that crustal permeability is created by dike
630 emplacement. Geophysical data show major fracturing around dikes due to high magma pressure
631 and wall-rock stress changes during dike emplacement (Roman and Cashman, 2006; Roman et al.,
632 2006). Dike-related earthquakes manifest themselves geologically as damage zones of fracture
633 systems along dike margins with marked increases in permeability (Farquharson et al., 2016).
634 Complex fracturing and brecciation at dike jogs create porosity and permeability for fluid flow
635 and alteration (e.g. Brown et al., 2007). In some eruptions, pathways for magmatic fluids to flow
636 to the surface from deep in the magmatic system closely follow dikes supplying the volcano (e.g.
637 Christopher et al., 2015). Based on observations of eruptions, geochronology, intrusive
638 relationships, and thermal models, time scales of igneous activity range from 1 to $<10^3$ years
639 (Sheldrake et al., 2016). In contrast, periods of non-intrusion or volcanic repose are typically $>10^3$
640 to 10^5 years. Our observations at Don Manuel fit this pattern well. For DMIC dikes with widths of
641 1 to 60 m, time scales of intrusion and solidification are in the range ~1 to $<10^2$ years while the
642 time span of repetitive intrusion associated with mineralization is of order 10^5 years (Figure 15).
643 Studies at other porphyry copper deposits (Cathles and Shannon, 2007; Mercer and Reed, 2013;
644 Reed et al., 2013) have inferred rapid expulsion of ore-forming fluids occurred on time scales
645 estimated at 20 to 900 years. Our observations, however, do not enable us to distinguish at DMIC
646 between rapid pulses of fluid release triggered by individual episodes of dike emplacement and
647 more continuous long-term release of fluids facilitated by the damaged regions created by multiple
648 intrusions.

Role of mafic and silicic magmas in mineralization

For DMIC, the early silicic intrusions, the quartz monzonite and rhyolite, were not mineralized. The onset of mineralization was associated with the mafic enclave-bearing biotite tonalite, reaching its peak with emplacement of the intermediate porphyry dikes, as indicated by high copper grades and abundance of Cu-Fe sulfides. These units associated with mineralization contain abundant hydrothermal biotite in addition to Cu-Fe sulfides indicating the presence of magmatic hydrothermal fluids. The hypabyssal intrusions themselves are far too small to provide the volumes of magmatic fluids necessary to form a porphyry copper deposit (e.g. Cline and Bodnar, 1991; Cloos, 2001; Sillitoe, 2010). These fluids must therefore derive from a much larger magmatic reservoir at depth (e.g. Yerington; Dilles and Einaudi, 1992; Dilles, 1987). We now discuss two models that have been developed to link the mineralizing fluids to the underlying magmatic system, placing observations at DMIC into context.

Many PCD models attribute mineralization to the release of a single magmatic fluid from a magma reservoir (Candela and Piccoli, 2005; Candela and Holland, 1984; Cline and Bodnar, 1991; Cloos, 2001; Cooke et al., 2014; Huber et al., 2012; Landtwing et al., 2005; Reed et al., 2013; Seedorff et al., 2005; Sillitoe, 2010; Weis et al., 2012). These models commonly postulate the steady release of fluids bearing Cu, Cl and S from a cooling and crystallizing silicic magma, along with interactions between the magmatic fluid and meteoric fluids. A single fluid model is not ruled out by our observations at DMIC, but the model does not explain the early period of barren silicic magmatism and the association of mineralization with mafic magma emplacement.

An alternative idea is that mafic magmas are the source of the S-rich, and in some models metal-rich, mineralizing magmatic fluids (Audetat and Pettke, 2006; Blundy et al., 2015; De Hoog et al., 2004; Halter et al., 2005; Hattori and Keith, 2001; Heinrich et al., 2005; Keith et al., 1997;

672 Maughan et al., 2002; Nadeau et al., 2010; Pollard et al., 2005; Sinclair, 2007; Zajacz and Halter,
673 2009). Blundy et al. (2015) developed this hypothesis further by invoking two different fluids: a
674 Cl-rich and Cu-rich brine derived from silicic magma and a S-rich fluid sourced from the influx of
675 mafic magma.

676 The early barren period of silicic magmatism at DMIC suggests early fluids lacked the right
677 geochemistry for mineralization, consistent with release of Cl-rich but S-poor hydrous fluids. We
678 cannot directly demonstrate that these fluids led to the accumulation of Cl and Cu-rich brines, as
679 required by the two fluid hypothesis of Blundy et al. (2015), but the period of early barren silicic
680 magmatism lasted ca. 200 kyr, providing time for discharge of hydrous fluids from the deeper
681 silicic system that sourced the hypabyssal intrusions. This 10^5 yr timescale of silicic magma
682 accumulation is directly comparable to the intrusive and antecrystic zircon record, well
683 documented at other PCDs (Buret et al., 2016; Tapster et al., 2016).

684 An open question concerns the processes that could enable S-rich fluids derived from mafic
685 magma to be involved in mineralization. Two possibilities have been discussed in the literature.
686 Sulfur derived from degassing mafic magma could have been stored temporarily as anhydrite and
687 then subsequently remobilized by breakdown of anhydrite in the shallow silicic magma reservoir
688 as has been suggested for Yanacocha (Chambefort et al., 2008; Chambefort et al., 2013). Here the
689 role of the mafic magma is to enrich the fluids within the silicic magma chamber in S leading to
690 mineralization by a single fluid. In the model of Blundy et al (2015) however,-metalliferous brine
691 accumulates as proto-ore prior to injection of pulsed S-rich fluids derived from mafic magma
692 injections. Our observations do not strongly favor one hypothesis over the other, but a prolonged
693 period of barren silicic magmatism prior to mineralization and evidence for mafic recharge (Fig.
694 17) is anticipated in the latter hypothesis but not by the former.

CONCLUSIONS

The DMIC units show magmatic complexity and chemical variation assembled in the upper crust in just over 400 kyr. The shallow-level intrusions within the DMIC represent short-lived injections of magma separated by periods of dormancy of 10s to 100s kyrs. The episodic emplacement and hybrid character of DMIC are features also found in arc volcanoes and other shallow intrusive complexes in arcs. These observations support the hypothesis that similar processes operate in the deeper portions of both arc volcanic and porphyry copper systems.

The DMIC evolved from barren silicic intrusions over about 100 kyrs to mineralized intrusions involving cogenetic mafic and silicic magmas. Based on petrographic and geochemical observations mingling and mixing between mafic and silicic magma occurred both in the deeper magma reservoir and during emplacement. These observations of the close association of mineralization with mafic magma intrusion are consistent with hypotheses of mafic magmas being a major source of sulfur.

ACKNOWLEDGMENTS

This work was conducted as part of the senior author's Ph.D. research at the University of Bristol, which was funded by BHP Billiton as part of the Bristol PCD Project. The U-Pb and ^{40}Ar-^{39}Ar geochronology work was funded by a NERC NIGL/AIF grant IP-1415-1113. BHP Billiton is also thanked for providing logistical support in the field and access to the core. We thank Stuart Kearns and Ben Buse (University of Bristol) and Iain McDonald (University of Cardiff) for help with the analytical data acquisition. Marit van Zalinge, Vladimir Matjuschkin, and Dan Condon are thanked for their insightful conversations and detailed critiques. The manuscript has benefited

717 greatly from the thorough and constructive reviews by Peter Hollings, Anthony Harris, Isabelle
718 Chambefort, Andreas Audétat, and Celeste Mercer and the careful editorial handling of Jocelyn
719 McPhie.

720

721 **REFERENCES CITED**

722

723 Annen, C., 2009, From plutons to magma chambers: thermal constraints on the accumulation of
724 eruptible silicic magma in the upper crust: Earth and Planetary Science Letters, v. 284,
725 no. 3, p. 409-416.
726 Annen, C., Blundy, J. D., Leuthold, J., and Sparks, R. S. J., 2015, Construction and evolution of
727 igneous bodies: Towards an integrated perspective of crustal magmatism: Lithos, v. 230,
728 p. 206-231.
729 Atkinson Jr, W., Souviron, A., Vehrs, T., and Faunes, A., 1996, Geology and mineral zoning of
730 the Los Pelambres porphyry copper deposit, Chile: Andean copper deposits: new
731 discoveries, mineralization, styles and metallogeny. Soc Econ Geol Spec Publ, v. 5, p.
732 131-156.
733 Audetat, A., and Pettke, T., 2006, Evolution of a porphyry-Cu mineralized magma system at
734 Santa Rita, New Mexico (USA): Journal of Petrology, v. 47, no. 10, p. 2021-2046.
735 Bacon, C. R., 1986, Magmatic inclusions in silicic and intermediate volcanic rocks: Journal of
736 Geophysical Research: Solid Earth (1978–2012), v. 91, no. B6, p. 6091-6112.
737 Barboni, M., Annen, C., and Schoene, B., 2015, Evaluating the construction and evolution of
738 upper crustal magma reservoirs with coupled U/Pb zircon geochronology and thermal
739 modeling: A case study from the Mt. Capanne pluton (Elba, Italy): Earth and Planetary
740 Science Letters, v. 432, p. 436-448.
741 Blake, D. H., Elwell, R. W. D., Gibson, I. L., Skelhorn, R. R., and Walker, G. P. L., 1965, Some
742 relationships resulting from the intimate association of acid and basic magmas: Quarterly
743 Journal of the Geological Society, v. 121, no. 1-4, p. 31-49.
744 Blake, S., and Fink, J., 2000, On the deformation and freezing of enclaves during magma
745 mixing: Journal of Volcanology and Geothermal Research, v. 95, no. 1, p. 1-8.
746 Blundy, J., Mavrogenes, J., Tattich, B., Sparks, S., and Gilmer, A., 2015, Generation of porphyry
747 copper deposits by gas–brine reaction in volcanic arcs: Nature, v. 8, p. 235–240.
748 Brown, R., Kavanagh, J., Sparks, R., Tait, M., and Field, M., 2007, Mechanically disrupted and
749 chemically weakened zones in segmented dike systems cause vent localization: Evidence
750 from kimberlite volcanic systems: Geology, v. 35, no. 9, p. 815-818.
751 Buret, Y., von Quadt, A., Heinrich, C., Selby, D., Wälle, M., and Peytcheva, I., 2016, From a
752 long-lived upper-crustal magma chamber to rapid porphyry copper emplacement:
753 Reading the geochemistry of zircon crystals at Bajo de la Alumbrera (NW Argentina):
754 Earth and Planetary Science Letters, v. 450, p. 120-131.
755 Camus, F., 2003, Geologia de los Systemas Porflricos en los Andes de Chile Santiago, Chile,
756 Servicio Nacional de Geologia y Mineria, 267 p.:

Candela, P., and Piccoli, P., 2005, Magmatic processes in the development of porphyry-type ore systems: Economic Geology 100th Anniversary Volume, p. 25-37.

Candela, P. A., and Holland, H. D., 1984, The partitioning of copper and molybdenum between silicate melts and aqueous fluids: Geochimica et Cosmochimica Acta, v. 48, no. 2, p. 373-380.

Candia, W., Oviedo, O., and Nuñez, E., 2009, Don Manuel Project Seasonal Report 2009: Unpublished report, Minera Aurex, p. 52 p.

Cannell, J., Cooke, D. R., Walshe, J. L., and Stein, H., 2005, Geology, mineralization, alteration, and structural evolution of the El Teniente porphyry Cu-Mo deposit: Economic Geology, v. 100, no. 5, p. 979-1003.

Caricchi, L., Annen, C., Rust, A., and Blundy, J., 2012, Insights into the mechanisms and timescales of pluton assembly from deformation patterns of mafic enclaves: Journal of Geophysical Research: Solid Earth (1978–2012), v. 117, no. B11.

Carroll, M. R., and Rutherford, M. J., 1987, The stability of igneous anhydrite: experimental results and implications for sulfur behavior in the 1982 El Chichon trachyandesite and other evolved magmas: Journal of Petrology, v. 28, no. 5, p. 781-801.

Castillo, P. R., 2012, Adakite petrogenesis: Lithos, v. 134, p. 304-316.

Castillo, P. R., Janney, P. E., and Solidum, R. U., 1999, Petrology and geochemistry of Camiguin Island, southern Philippines: insights to the source of adakites and other lavas in a complex arc setting: Contributions to Mineralogy and Petrology, v. 134, no. 1, p. 33-51.

Cathles, L., and Shannon, R., 2007, How potassium silicate alteration suggests the formation of porphyry ore deposits begins with the nearly explosive but barren expulsion of large volumes of magmatic water: Earth and Planetary Science Letters, v. 262, no. 1, p. 92-108.

Chambefort, I., Dilles, J. H., and Kent, A. J., 2008, Anhydrite-bearing andesite and dacite as a source for sulfur in magmatic-hydrothermal mineral deposits: Geology, v. 36, no. 9, p. 719-722.

Chambefort, I., Dilles, J. H., and Longo, A. A., 2013, Amphibole geochemistry of the Yanacocha Volcanics, Peru: Evidence for diverse sources of magmatic volatiles related to gold ores: Journal of Petrology, v. 54, p. 1017-1046.

Charrier, R., Baeza, O., Elgueta, S., Flynn, J. J., Gans, P., Kay, S. M., Munoz, N., Wyss, A. R., and Zurita, E., 2002, Evidence for Cenozoic extensional basin development and tectonic inversion south of the flat-slab segment, southern central Andes, Chile (33°-36°S): Journal of South American Earth Sciences, v. 15, no. 117-139.

Charrier, R., Wyss, A., Flynn, J. J., Swisher III, C. C., Norell, M. A., Zapatta, F., McKenna, M. C., and Novacek, M. J., 1996, New evidence for late Mesozoic-early Cenozoic evolution of the Chilean Andes in the upper Tinguiririca valley (35 S), central Chile: Journal of South American Earth Sciences, v. 9, no. 5, p. 393-422.

Chelle-Michou, C., Chiaradia, M., Selby, D., Ovtcharova, M., and Spikings, R. A., 2015, High-Resolution Geochronology of the Coroccohuayco Porphyry-Skarn Deposit, Peru: A Rapid Product of the Incaic Orogeny: Economic Geology, v. 110, no. 2, p. 423-443.

Chiaradia, M., 2015, Crustal thickness control on Sr/Y signatures of recent arc magmas: an Earth scale perspective: Scientific Reports, v. 5.

Christopher, T., Blundy, J., Cashman, K., Cole, P., Edmonds, M., Smith, P., Sparks, R., and Stinton, A., 2015, Crustal-scale degassing due to magma system destabilization and

magma-gas decoupling at Soufrière Hills Volcano, Montserrat: Geochemistry, Geophysics, Geosystems, v. 16, p. 2797-2811.
Cline, J. S., and Bodnar, R. J., 1991, Can economic porphyry copper mineralization be generated by a typical calc-alkaline melt?: Journal of Geophysical Research: Solid Earth (1978–2012), v. 96, no. B5, p. 8113-8126.
Cloos, M., 2001, Bubbling magma chambers, cupolas, and porphyry copper deposits: International geology review, v. 43, no. 4, p. 285-311.
Cooke, D., Hollings, P., Wilkinson, J., and Tosdal, R., 2014, Geochemistry of porphyry deposits: Treatise on Geochemistry, p. 357-381.
Couch, S., Sparks, R., and Carroll, M., 2001, Mineral disequilibrium in lavas explained by convective self-mixing in open magma chambers: Nature, v. 411, no. 6841, p. 1037-1039.
De Hoog, J., Hattori, K., and Hoblitt, R., 2004, Oxidized sulfur-rich mafic magma at Mount Pinatubo, Philippines: Contributions to Mineralogy and Petrology, v. 146, no. 6, p. 750-761.
Deckart, K., Clark, A. H., Celso, A. A., Ricardo, V. R., Bertens, A. N., Mortensen, J. K., and Fanning, M., 2005, Magmatic and hydrothermal chronology of the giant Rio Blanco porphyry copper deposit, central Chile: implications of an integrated U-Pb and 40Ar/39Ar database: Economic Geology, v. 100, no. 5, p. 905-934.
Defant, M. J., and Drummond, M. S., 1990, Derivation of some modern arc magmas by melting of young subducted lithosphere: Nature, v. 347, no. 6294, p. 662-665.
-, 1993, Mount St. Helens: potential example of the partial melting of the subducted lithosphere in a volcanic arc: Geology, v. 21, no. 6, p. 547-550.
Dilles, J. H., 1987, Petrology of the Yerington Batholith, Nevada; evidence for evolution of porphyry copper ore fluids: Economic Geology, v. 82, no. 7, p. 1750-1789.
Dilles, J. H., and Einaudi, M. T., 1992, Wall-rock alteration and hydrothermal flow paths about the Ann-Mason porphyry copper deposit, Nevada; a 6-km vertical reconstruction: Economic Geology, v. 87, no. 8, p. 1963-2001.
Dilles, J. H., Kent, A. J., Wooden, J. L., Tosdal, R. M., Koleszar, A., Lee, R. G., and Farmer, L. P., 2015, Zircon compositional evidence for sulfur-degassing from ore-forming arc magmas: Economic Geology, v. 110, no. 1, p. 241-251.
Dungan, M. A., Wulff, A., and Thompson, R., 2001, Eruptive stratigraphy of the Tatara–San Pedro complex, 36 S, Southern Volcanic Zone, Chilean Andes: reconstruction method and implications for magma evolution at long-lived arc volcanic centers: Journal of Petrology, v. 42, no. 3, p. 555-626.
Farías, M., Charrier, R., Carretier, S., Martinod, J., Fock, A., Campbell, D., Cáceres, J., and Comte, D., 2008, Late Miocene high and rapid surface uplift and its erosional response in the Andes of central Chile (33–35 S): Tectonics, v. 27, no. 1.
Farías, M., Comte, D., Charrier, R., Martinod, J., David, C., Tassara, A., Tapia, F., and Fock, A., 2010, Crustal-scale structural architecture in central Chile based on seismicity and surface geology: Implications for Andean mountain building: Tectonics, v. 29, no. 3.
Furman, T., and Spera, F. J., 1985, Co-mingling of acid and basic magma with implications for the origin of mafic I-type xenoliths: field and petrochemical relations of an unusual dike complex at Eagle Lake, Sequoia National Park, California, USA: Journal of Volcanology and Geothermal Research, v. 24, no. 1, p. 151-178.

847 Giambiagi, L., and Ramos, V., 2002, Structural evolution of the Andes in a transitional zone
848 between flat and normal subduction (33 30′–33 45′ S), Argentina and Chile: Journal of
849 South American Earth Sciences, v. 15, no. 1, p. 101-116.
850 Godoy, E., Yáñez, G., and Vera, E., 1999, Inversion of an Oligocene volcano-tectonic basin and
851 uplifting of its superimposed Miocene magmatic arc in the Chilean Central Andes: first
852 seismic and gravity evidences: Tectonophysics, v. 306, no. 2, p. 217-236.
853 Goto, Y., Nakada, S., Kurokawa, M., Shimano, T., Sugimoto, T., Sakuma, S., Hoshizumi, H.,
854 Yoshimoto, M., and Uto, K., 2008, Character and origin of lithofacies in the conduit of
855 Unzen volcano, Japan: Journal of Volcanology and Geothermal Research, v. 175, no. 1,
856 p. 45-59.
857 Grove, T. L., Baker, M. B., and Kinzler, R. J., 1984, Coupled CaAl-NaSi diffusion in plagioclase
858 feldspar: experiments and applications to cooling rate speedometry: Geochimica et
859 Cosmochimica Acta, v. 48, no. 10, p. 2113-2121.
860 Gustafson, L. B., and Hunt, J. P., 1975, The porphyry copper deposit at El Salvador, Chile:
861 Economic Geology, v. 70, no. 5, p. 857-912.
862 Hallot, E., Davy, P., de Bremond d'Ars, J., Auvray, B., Martin, H., and Van Damme, H., 1996,
863 Non-Newtonian effects during injection in partially crystallised magmas: Journal of
864 volcanology and geothermal research, v. 71, no. 1, p. 31-44.
865 Halter, W. E., Bain, N., Becker, K., Heinrich, C. A., Landtwing, M., VonQuadt, A., Clark, A. H.,
866 Sasso, A. M., Bissig, T., and Tosdal, R. M., 2004, From andesitic volcanism to the
867 formation of a porphyry Cu-Au mineralizing magma chamber: the Farallón Negro
868 Volcanic Complex, northwestern Argentina: Journal of Volcanology and Geothermal
869 Research, v. 136, no. 1, p. 1-30.
870 Halter, W. E., Heinrich, C. A., and Pettke, T., 2005, Magma evolution and the formation of
871 porphyry Cu–Au ore fluids: evidence from silicate and sulfide melt inclusions:
872 Mineralium Deposita, v. 39, no. 8, p. 845-863.
873 Harford, C., Pringle, M., Sparks, R., and Young, S., 2002, The volcanic evolution of Montserrat
874 using 40Ar/39Ar geochronology: Geological Society, London, Memoirs, v. 21, no. 1, p.
875 93-113.
876 Hattori, K. H., and Keith, J. D., 2001, Contribution of mafic melt to porphyry copper
877 mineralization: evidence from Mount Pinatubo, Philippines, and Bingham Canyon, Utah,
878 USA: Mineralium Deposita, v. 36, no. 8, p. 799-806.
879 Hedenquist, J. W., and Lowenstern, J. B., 1994, The role of magmas in the formation of
880 hydrothermal ore deposits: Nature, v. 370, no. 6490, p. 519-527.
881 Heinrich, C., Halter, W., Landtwing, M., and Pettke, T., 2005, The formation of economic
882 porphyry copper (-gold) deposits: constraints from microanalysis of fluid and melt
883 inclusions: Special Publication Geological Society of London, v. 248, p. 247.
884 Hildreth, W., Fierstein, J., and Lanphere, M., 2003, Eruptive history and geochronology of the
885 Mount Baker volcanic field, Washington: Geological Society of America Bulletin, v.
886 115, no. 6, p. 729-764.
887 Hildreth, W., and Lanphere, M. A., 1994, Potassium-argon geochronology of a basalt-andesite-
888 dacite arc system: The Mount Adams volcanic field, Cascade Range of southern
889 Washington: Geological Society of America Bulletin, v. 106, no. 11, p. 1413-1429.
890 Hildreth, W., and Moorbath, S., 1988, Crustal contributions to arc magmatism in the Andes of
891 central Chile: Contributions to Mineralogy and Petrology, v. 98, no. 4, p. 455-489.

892 Hollings, P., Cooke, D., and Clark, A., 2005, Regional geochemistry of Tertiary igneous rocks in
893 central Chile: Implications for the geodynamic environment of giant porphyry copper and
894 epithermal gold mineralization: Economic Geology, v. 100, no. 5, p. 887-904.
895 Huber, C., Bachmann, O., Vigneresse, J. L., Dufek, J., and Parmigiani, A., 2012, A physical
896 model for metal extraction and transport in shallow magmatic systems: Geochemistry,
897 Geophysics, Geosystems, v. 13, no. 8.
898 Humphreys, M. C., Christopher, T., and Hards, V., 2009, Microlite transfer by disaggregation of
899 mafic inclusions following magma mixing at Soufrière Hills volcano, Montserrat:
900 Contributions to Mineralogy and Petrology, v. 157, no. 5, p. 609-624.
901 Hynek, S. A., Marchetti, D. W., Fernandez, D. P., and Cerling, T. E., 2010, Composition, pre-
902 eruptive zonation, and geochronologic significance of the~ 450ka Diamante Tuff, Andean
903 Cordillera (34° S), Argentina: Quaternary Geochronology, v. 5, no. 5, p. 591-601.
904 Irvine, T., and Baragar, W., 1971, A guide to the chemical classification of the common volcanic
905 rocks: Canadian journal of earth sciences, v. 8, no. 5, p. 523-548.
906 Jaeger, J., Hess, H., and Poldevaart, A., 1968, The Poldervaart treatise on rocks of basaltic
907 composition.
908 Jaffey, A., Flynn, K., Glendenin, L., Bentley, W. t., and Essling, A., 1971, Precision
909 measurement of half-lives and specific activities of U 235 and U 238: Physical Review C,
910 v. 4, no. 5, p. 1889.
911 Kay, R., 1978, Aleutian magnesian andesites: melts from subducted Pacific Ocean crust: Journal
912 of Volcanology and Geothermal Research, v. 4, no. 1, p. 117-132.
913 Kay, S., and Kurtz, A., 1995, Magmatic and tectonic characterization of the El Teniente region:
914 CODELCO (unpublished report).
915 Kay, S. M., Godoy, E., and Kurtz, A., 2005, Episodic arc migration, crustal thickening,
916 subduction erosion, and magmatism in the south-central Andes: Geological Society of
917 America Bulletin, v. 117, no. 1-2, p. 67-88.
918 Kay, S. M., and Mpodozis, C., 2001, Central Andean ore deposits linked to evolving shallow
919 subduction systems and thickening crust: GSA TODAY, v. 11, no. 3, p. 4-9.
920 Kay, S. M., Mpodozis, C., Ramos, V. A., and Munizaga, F., 1991, Magma source variations for
921 mid–late Tertiary magmatic rocks associated with a shallowing subduction zone and a
922 thickening crust in the central Andes (28 to 33 S): Geological Society of America Special
923 Papers, v. 265, p. 113-138.
924 Keith, J., Whitney, J., Hattori, K., Ballantyne, G., Christiansen, E., Barr, D., Cannan, T., and
925 Hook, C., 1997, The role of magmatic sulfides and mafic alkaline magmas in the
926 Bingham and Tintic mining districts, Utah: Journal of Petrology, v. 38, no. 12, p. 1679-
927 1690.
928 Kelley, K. A., and Cottrell, E., 2009, Water and the oxidation state of subduction zone magmas:
929 Science, v. 325, no. 5940, p. 605-607.
930 Kurtz, A. C., Kay, S. M., Charrier, R., and Farrar, E., 1997, Geochronology of Miocene plutons
931 and exhumation history of the El Teniente region, Central Chile (34-35° 8): Andean
932 Geology, v. 24, no. 1, p. 75-90.
933 Landtwing, M. R., Pettke, T., Halter, W. E., Heinrich, C. A., Redmond, P. B., Einaudi, M. T.,
934 and Kunze, K., 2005, Copper deposition during quartz dissolution by cooling magmatic–
935 hydrothermal fluids: the Bingham porphyry: Earth and Planetary Science Letters, v. 235,
936 no. 1, p. 229-243.

Le Friant, A., Lock, E., Hart, M., Boudon, G., Sparks, R., Leng, M., Smart, C. W., Komorowski, J.-C., Deplus, C., and Fisher, J., 2008, Late Pleistocene tephrochronology of marine sediments adjacent to Montserrat, Lesser Antilles volcanic arc: Journal of the Geological Society, v. 165, no. 1, p. 279-289.

Le Maitre, R. W., Streckeisen, A., Zanettin, B., Le Bas, M., Bonin, B., and Bateman, P., 2002, Igneous rocks: a classification and glossary of terms: recommendations of the International Union of Geological Sciences Subcommission on the Systematics of Igneous Rocks, Cambridge University Press.

Leuthold, J., Müntener, O., Baumgartner, L. P., Putlitz, B., Ovtcharova, M., and Schaltegger, U., 2012, Time resolved construction of a bimodal laccolith (Torres del Paine, Patagonia): Earth and Planetary Science Letters, v. 325, p. 85-92.

Lickfold, V., Cooke, D., Crawford, A., and Fanning, C., 2007, Shoshonitic magmatism and the formation of the Northparkes porphyry Cu–Au deposits, New South Wales: Australian Journal of Earth Sciences, v. 54, no. 2-3, p. 417-444.

Lipman, P. W., 2007, Incremental assembly and prolonged consolidation of Cordilleran magma chambers: Evidence from the Southern Rocky Mountain volcanic field: Geosphere, v. 3, no. 1, p. 42-70.

Longo, A. A., Dilles, J. H., Grunder, A. L., and Duncan, R., 2010, Evolution of calc-alkaline volcanism and associated hydrothermal gold deposits at Yanacocha, Peru: Economic Geology, v. 105, no. 7, p. 1191-1241.

Luhr, J. F., 1990, Experimental phase relations of water-and sulfur-saturated arc magmas and the 1982 eruptions of El Chichón volcano: Journal of Petrology, v. 31, no. 5, p. 1071-1114.

Maksaev, V., Munizaga, F., McWilliams, M., Fanning, M., Mathur, R., Ruiz, J., and Zentilli, M., 2004, New chronology for El Teniente, Chilean Andes, from U/Pb, 40Ar/39Ar, Re/Os and fission-track dating: implications for the evolution of a supergiant porphyry Cu-Mo deposit: Andean Metallogeny: New Discoveries, Concepts Update. Society of Economic Geologists, Special Publication, v. 11, p. 15-54.

Maksaev, V., Townley, B., Palacios, C., and Camus, F., 2007, Metallic ore deposits: The geology of Chile. The Geological Society, London, p. 179-199.

Marot, M., Monfret, T., Gerbault, M., Nolet, G., Ranalli, G., and Pardo, M., 2014, Flat versus normal subduction zones: a comparison based on 3-D regional traveltime tomography and petrological modelling of central Chile and western Argentina (29°–35° S): Geophysical Journal International, v. 199, no. 3, p. 1633-1654.

Matjuschkin, V., Blundy, J. D., and Brooker, R. A., 2016, The effect of pressure on sulphur speciation in mid-to deep-crustal arc magmas and implications for the formation of porphyry copper deposits: Contributions to Mineralogy and Petrology, v. 171, no. 7, p. 1-25.

Mattinson, J. M., 2005, Zircon U–Pb chemical abrasion ("CA-TIMS") method: combined annealing and multi-step partial dissolution analysis for improved precision and accuracy of zircon ages: Chemical Geology, v. 220, no. 1, p. 47-66.

Maughan, D. T., Keith, J. D., Christiansen, E. H., Pulsipher, T., Hattori, K., and Evans, N. J., 2002, Contributions from mafic alkaline magmas to the Bingham porphyry Cu–Au–Mo deposit, Utah, USA: Mineralium Deposita, v. 37, no. 1, p. 14-37.

Maydagán, L., Franchini, M., Chiaradia, M., Pons, J., Impiccini, A., Toohey, J., and Rey, R., 2011, Petrology of the Miocene igneous rocks in the Altar region, main Cordillera of San

Juan, Argentina. A geodynamic model within the context of the Andean flat-slab segment and metallogenesis: Journal of South American Earth Sciences, v. 32, no. 1, p. 30-48.
McDonald, I., and Viljoen, K., 2006, Platinum-group element geochemistry of mantle eclogites: a reconnaissance study of xenoliths from the Orapa kimberlite, Botswana: Applied Earth Science: Transactions of the Institutions of Mining and Metallurgy: Section B, v. 115, no. 3, p. 81-93.
Mercer, C. N., and Reed, M. H., 2013, Porphyry Cu-Mo Stockwork Formation by Dynamic, Transient Hydrothermal Pulses: Mineralogic Insights from the Deposit at Butte, Montana: Economic Geology, v. 108, no. 6, p. 1347-1377.
Mercer, C. N., Reed, M. H., and Mercer, C. M., 2015, Time scales of porphyry Cu deposit formation: insights from titanium diffusion in quartz: Economic Geology, v. 110, no. 3, p. 587-602.
Michel, J., Baumgartner, L., Putlitz, B., Schaltegger, U., and Ovtcharova, M., 2008, Incremental growth of the Patagonian Torres del Paine laccolith over 90 ky: Geology, v. 36, no. 6, p. 459-462.
Miller, C. F., Furbish, D. J., Walker, B. A., Claiborne, L. L., Koteas, G. C., Bleick, H. A., and Miller, J. S., 2011, Growth of plutons by incremental emplacement of sheets in crystal-rich host: evidence from Miocene intrusions of the Colorado River region, Nevada, USA: Tectonophysics, v. 500, no. 1, p. 65-77.
Moore, G., and Carmichael, I., 1998, The hydrous phase equilibria (to 3 kbar) of an andesite and basaltic andesite from western Mexico: constraints on water content and conditions of phenocryst growth: Contributions to Mineralogy and Petrology, v. 130, no. 3-4, p. 304-319.
Murphy, M., Sparks, R., Barclay, J., Carroll, M., Lejeune, A. M., Brewer, T., Macdonald, R., Black, S., and Young, S., 1998, The role of magma mixing in triggering the current eruption at the Soufriere Hills volcano, Montserrat, West Indies: Geophysical Research Letters, v. 25, no. 18, p. 3433-3436.
Muñoz, M., Charrier, R., Fanning, C., Maksaev, V., and Deckart, K., 2012, Zircon trace element and O–Hf isotope analyses of mineralized intrusions from El Teniente ore deposit, Chilean Andes: Constraints on the source and magmatic evolution of porphyry Cu–Mo related magmas: Journal of Petrology, p. egs010.
Müntener, O., Kelemen, P. B., and Grove, T. L., 2001, The role of H2O during crystallization of primitive arc magmas under uppermost mantle conditions and genesis of igneous pyroxenites: an experimental study: Contributions to Mineralogy and Petrology, v. 141, no. 6, p. 643-658.
Nadeau, O., Williams-Jones, A. E., and Stix, J., 2010, Sulphide magma as a source of metals in arc-related magmatic hydrothermal ore fluids: Nature Geoscience, v. 3, no. 7, p. 501-505.
Naney, M., 1983, Phase equilibria of rock-forming ferromagnesian silicates in granitic systems: American journal of science, v. 283, no. 10, p. 993-1033.
Nyström, J. O., Vergara, M., Morata, D., and Levi, B., 2003, Tertiary volcanism during extension in the Andean foothills of central Chile (33 15′–33 45′ S): Geological Society of America Bulletin, v. 115, no. 12, p. 1523-1537.
Oyarzun, R., Márquez, A., Lillo, J., López, I., and Rivera, S., 2001, Giant versus small porphyry copper deposits of Cenozoic age in northern Chile: adakitic versus normal calc-alkaline magmatism: Mineralium Deposita, v. 36, no. 8, p. 794-798.

Pardo, M., Comte, D., and Monfret, T., 2002, Seismotectonic and stress distribution in the central Chile subduction zone: Journal of South American Earth Sciences, v. 15, no. 1, p. 11-22.
Pearce, J. A., and Peate, D. W., 1995, Tectonic implications of the composition of volcanic arc magmas: Annual Review of Earth and Planetary Sciences, v. 23, p. 251-286.
Piquer, J., Skarmeta, J., and Cooke, D. R., 2015, Structural Evolution of the Rio Blanco-Los Bronces District, Andes of Central Chile: Controls on Stratigraphy, Magmatism, and Mineralization: Economic Geology, v. 110, no. 8, p. 1995-2023.
Pollard, P. J., Taylor, R. G., and Peters, L., 2005, Ages of intrusion, alteration, and mineralization at the Grasberg Cu-Au deposit, Papua, Indonesia: Economic Geology, v. 100, no. 5, p. 1005-1020.
Redmond, P., Einaudi, M., Inan, E., Landtwing, M., and Heinrich, C., 2004, Copper deposition by fluid cooling in intrusion-centered systems: new insights from the Bingham porphyry ore deposit, Utah: Geology, v. 32, no. 3, p. 217-220.
Reed, M., Rusk, B., and Palandri, J., 2013, The Butte magmatic-hydrothermal system: One fluid yields all alteration and veins: Economic Geology, v. 108, no. 6, p. 1379-1396.
Reich, M., Parada, M. A., Palacios, C., Dietrich, A., Schultz, F., and Lehmann, B., 2003, Adakite-like signature of Late Miocene intrusions at the Los Pelambres giant porphyry copper deposit in the Andes of central Chile: metallogenic implications: Mineralium Deposita, v. 38, no. 7, p. 876-885.
Renne, P. R., Deino, A. L., Hames, W. E., Heizler, M. T., Hemming, S. R., Hodges, K. V., Koppers, A. A., Mark, D. F., Morgan, L. E., and Phillips, D., 2009, Data reporting norms for 40 Ar/39 Ar geochronology: Quaternary Geochronology, v. 4, no. 5, p. 346-352.
Richards, J. P., 2011, High Sr/Y arc magmas and porphyry Cu±Mo±Au deposits: just add water: Economic Geology, v. 106, no. 7, p. 1075-1081.
Richards, J. P., and Kerrich, R., 2007, Special paper: adakite-like rocks: their diverse origins and questionable role in metallogenesis: Economic Geology, v. 102, no. 4, p. 537-576.
Richards, J. P., Spell, T., Rameh, E., Razique, A., and Fletcher, T., 2012, High Sr/Y magmas reflect arc maturity, high magmatic water content, and porphyry Cu±Mo±Au potential: examples from the Tethyan arcs of Central and Eastern Iran and Western Pakistan: Economic Geology, v. 107, no. 2, p. 295-332.
Scaillet, B., Clémente, B., Evans, B. W., and Pichavant, M., 1998, Redox control of sulfur degassing in silicic magmas: Journal of Geophysical Research Solid Earth, v. 103, no. B10, p. 23,937-923,949.
Scandone, R., Cashman, K. V., and Malone, S. D., 2007, Magma supply, magma ascent and the style of volcanic eruptions: Earth and Planetary Science Letters, v. 253, no. 3, p. 513-529.
Seedorff, E., Dilles, J., Proffett, J., Einaudi, M., Zurcher, L., Stavast, W., Johnson, D., and Barton, M., 2005, Porphyry deposits: characteristics and origin of hypogene features: Economic Geology 100th Anniversary Volume, v. 29, p. 251-298.
Serrano, L., Vargas, R., Stambuk, V., Aguilar, C., Galeb, M., Holmgren, C., Contreras, A., Godoy, S., Vela, I., and Skewes, M., 1996, The late miocene to early pliocene Río Blanco-Los Bronces copper deposit, central Chilean Andes: Andean copper deposits: new discoveries, mineralization, styles and metallogeny. Soc Econ Geol Spec Publ, v. 5, p. 119-129.
Shand, S., 1951, Eruptive rocks; their genesis, classification, and their relation to ore deposits. John Wiley & Sons, New York, NY.

1073 Sillitoe, R. H., 1973, The tops and bottoms of porphyry copper deposits: Economic Geology, v.
1074 68, no. 6, p. 799-815.
1075 -, 2010, Porphyry copper systems: Economic Geology, v. 105, no. 1, p. 3-41.
1076 Sinclair, W., 2007, Porphyry deposits: Mineral deposits of Canada: A synthesis of major deposit-
1077 types, district metallogeny, the evolution of geological provinces, and exploration
1078 methods: Geological Association of Canada, Mineral Deposits Division, Special
1079 Publication, v. 5, p. 223-243.
1080 Skewes, M. A., and Stern, C. R., 1995, Genesis of the giant late Miocene to Pliocene copper
1081 deposits of central Chile in the context of Andean magmatic and tectonic evolution:
1082 International Geology Review, v. 37, no. 10, p. 893-909.
1083 Sparks, R., and Marshall, L., 1986, Thermal and mechanical constraints on mixing between
1084 mafic and silicic magmas: Journal of Volcanology and Geothermal Research, v. 29, no. 1,
1085 p. 99-124.
1086 Sparks, R. S. J., 1997, Causes and consequences of pressurisation in lava dome eruptions: Earth
1087 and Planetary Science Letters, v. 150, no. 3, p. 177-189.
1088 Sruoga, P., Etcheverría, M. P., Feineman, M., Rosas, M., Burkert, C., and Ibañes, O., 2012,
1089 Complejo caldera Diamante-Volcan Maipo (34° 10´ S): Evolucion Volcanologica y
1090 geoquimica e implicancias en su peligrosidad: Revista de la Asociación Geológica
1091 Argentina, v. 69, no. 4, p. 508-530.
1092 Sruoga, P., Llambías, E. J., Fauqué, L., Schonwandt, D., and Repol, D. G., 2005, Volcanological
1093 and geochemical evolution of the Diamante Caldera–Maipo volcano complex in the
1094 southern Andes of Argentina (34 10′ S): Journal of South American Earth Sciences, v.
1095 19, no. 4, p. 399-414.
1096 Stern, C. R., 2004, Active Andean volcanism: its geologic and tectonic setting: Revista geológica
1097 de Chile, v. 31, no. 2, p. 161-206.
1098 Stern, C. R., Amini, H., Charrier, R., Godoy, E., Herve, F., and Varela, J., 1984, Petrochemistry
1099 and age of rhyolitic pyroclastic flows which occur along the drainage valleys of the Rio
1100 Maipo and Rio Cachapoal (Chile) and the Rio Yaucha and Rio Papagayos (Argentina). :
1101 Revista Geologica de Chile, v. 23, p. 39-52.
1102 Stern, C. R., Funk, J. A., Skewes, M. A., and Arévalo, A., 2007, Magmatic anhydrite in plutonic
1103 rocks at the El Teniente Cu-Mo deposit, Chile, and the role of sulfur-and copper-rich
1104 magmas in its formation: Economic geology, v. 102, no. 7, p. 1335-1344.
1105 Stern, C. R., and Skewes, M. A., 1995, Miocene to present magmatic evolution at the northern
1106 end of the Andean Southern Volcanic Zone, Central Chile: Andean Geology, v. 22, no. 2,
1107 p. 261-272.
1108 Stern, C. R., Skewes, M. A., and Arévalo, A., 2011, Magmatic evolution of the giant El Teniente
1109 Cu–Mo deposit, central Chile: Journal of Petrology, v. 52, no. 7-8, p. 1591-1617.
1110 Streck, M. J., 2008, Mineral textures and zoning as evidence for open system processes: Reviews
1111 in Mineralogy and Geochemistry, v. 69, no. 1, p. 595-622.
1112 Sun, S.-S., and McDonough, W. F., 1989, Chemical and isotopic systematics of oceanic basalts:
1113 implications for mantle composition and processes: Geological Society, London, Special
1114 Publications, v. 42, no. 1, p. 313-345.
1115 Tapster, S., Condon, D., Naden, J., Noble, S., Petterson, M., Roberts, N., Saunders, A., and
1116 Smith, D., 2016, Rapid thermal rejuvenation of high-crystallinity magma linked to
1117 porphyry copper deposit formation; evidence from the Koloula Porphyry Prospect,
1118 Solomon Islands: Earth and Planetary Science Letters.

Tatsumi, Y., 1989, Migration of fluid phases and genesis of basalt magmas in subduction zones: Journal of Geophysical Research: Solid Earth (1978–2012), v. 94, no. B4, p. 4697-4707.
Tepley, F., Davidson, J., Tilling, R., and Arth, J., 2000, Magma mixing, recharge and eruption histories recorded in plagioclase phenocrysts from El Chichon Volcano, Mexico: Journal of Petrology, v. 41, no. 9, p. 1397-1411.
Vergara, M., Charrier, R., Munizaga, F., Rivano, S., Sepúlveda, P., Thiele, R., and Drake, R., 1988, Miocene volcanism in the central Chilean Andes (31 30′ S–34 35′ S): Journal of South American Earth Sciences, v. 1, no. 2, p. 199-209.
Vernon, R., 1984, Microgranitoid enclaves in granites—globules of hybrid magma quenched in a plutonic environment: Nature, v. 309, no. 5967, p. 438-439.
Von Quadt, A., Erni, M., Martinek, K., Moll, M., Peytcheva, I., and Heinrich, C. A., 2011, Zircon crystallization and the lifetimes of ore-forming magmatic-hydrothermal systems: Geology, v. 39, no. 8, p. 731-734.
Vry, V., Wilkinson, J., Seguel, J., and Millán, J., 2010, Multistage intrusion, brecciation, and veining at El Teniente, Chile: Evolution of a nested porphyry system: Economic Geology, v. 105, no. 1, p. 119-153.
Waite, K. A., Keith, J. D., Christiansen, E. H., Whitney, J. A., Hattori, K., Tingey, D. G., and Hook, C. J., 1997, Petrogenesis of the volcanic and intrusive rocks associated with the Bingham Canyon porphyry Cu–Au–Mo deposit, Utah: Soc Econ Geol Guidebook Ser, v. 29, p. 91-128.
Warnaars, F. W., Holmgren, C., and Barassi, S., 1985, Porphyry copper and tourmaline breccias at Los Bronces-Río Blanco, Chile: Economic Geology, v. 80, no. 6, p. 1544-1565.
Weis, P., Driesner, T., and Heinrich, C., 2012, Porphyry-copper ore shells form at stable pressure-temperature fronts within dynamic fluid plumes: Science, v. 338, no. 6114, p. 1613-1616.
Annen, C., 2009, From plutons to magma chambers: thermal constraints on the accumulation of eruptible silicic magma in the upper crust: Earth and Planetary Science Letters, v. 284, no. 3, p. 409-416.
Annen, C., Blundy, J. D., Leuthold, J., and Sparks, R. S. J., 2015, Construction and evolution of igneous bodies: Towards an integrated perspective of crustal magmatism: Lithos, v. 230, p. 206-231.
Atkinson Jr, W., Souviron, A., Vehrs, T., and Faunes, A., 1996, Geology and mineral zoning of the Los Pelambres porphyry copper deposit, Chile: Andean copper deposits: new discoveries, mineralization, styles and metallogeny. Soc Econ Geol Spec Publ, v. 5, p. 131-156.
Audetat, A., and Pettke, T., 2006, Evolution of a porphyry-Cu mineralized magma system at Santa Rita, New Mexico (USA): Journal of Petrology, v. 47, no. 10, p. 2021-2046.
Bacon, C. R., 1986, Magmatic inclusions in silicic and intermediate volcanic rocks: Journal of Geophysical Research: Solid Earth (1978–2012), v. 91, no. B6, p. 6091-6112.
Barboni, M., Annen, C., and Schoene, B., 2015, Evaluating the construction and evolution of upper crustal magma reservoirs with coupled U/Pb zircon geochronology and thermal modeling: A case study from the Mt. Capanne pluton (Elba, Italy): Earth and Planetary Science Letters, v. 432, p. 436-448.
Blake, D. H., Elwell, R. W. D., GIBSON, I. L., Skelhorn, R. R., and Walker, G. P. L., 1965, Some relationships resulting from the intimate association of acid and basic magmas: Quarterly Journal of the Geological Society, v. 121, no. 1-4, p. 31-49.

Blake, S., and Fink, J., 2000, On the deformation and freezing of enclaves during magma mixing: Journal of Volcanology and Geothermal Research, v. 95, no. 1, p. 1-8.

Blundy, J., Mavrogenes, J., Tattich, B., Sparks, S., and Gilmer, A., 2015, Generation of porphyry copper deposits by gas–brine reaction in volcanic arcs: Nature, v. 8, p. 235–240.

Brown, R., Kavanagh, J., Sparks, R., Tait, M., and Field, M., 2007, Mechanically disrupted and chemically weakened zones in segmented dike systems cause vent localization: Evidence from kimberlite volcanic systems: Geology, v. 35, no. 9, p. 815-818.

Buret, Y., von Quadt, A., Heinrich, C., Selby, D., Wälle, M., and Peytcheva, I., 2016, From a long-lived upper-crustal magma chamber to rapid porphyry copper emplacement: Reading the geochemistry of zircon crystals at Bajo de la Alumbrera (NW Argentina): Earth and Planetary Science Letters, v. 450, p. 120-131.

Camus, F., 2003, Geologia de los Systemas Porflricos en los Andes de Chile Santiago, Chile, Servicio Nacional de Geologia y Mineria, 267 p.:

Candela, P., and Piccoli, P., 2005, Magmatic processes in the development of porphyry-type ore systems: Economic Geology 100th Anniversary Volume, p. 25-37.

Candela, P. A., and Holland, H. D., 1984, The partitioning of copper and molybdenum between silicate melts and aqueous fluids: Geochimica et Cosmochimica Acta, v. 48, no. 2, p. 373-380.

Candia, W., Oviedo, O., and Nuñez, E., 2009, Don Manuel Project Seasonal Report 2009: Unpublished report, Minera Aurex, p. 52 p.

Cannell, J., Cooke, D. R., Walshe, J. L., and Stein, H., 2005, Geology, mineralization, alteration, and structural evolution of the El Teniente porphyry Cu-Mo deposit: Economic Geology, v. 100, no. 5, p. 979-1003.

Caricchi, L., Annen, C., Rust, A., and Blundy, J., 2012, Insights into the mechanisms and timescales of pluton assembly from deformation patterns of mafic enclaves: Journal of Geophysical Research: Solid Earth (1978–2012), v. 117, no. B11.

Carroll, M. R., and Rutherford, M. J., 1987, The stability of igneous anhydrite: experimental results and implications for sulfur behavior in the 1982 El Chichon trachyandesite and other evolved magmas: Journal of Petrology, v. 28, no. 5, p. 781-801.

Cashman, K. V., Sparks, R. S. J., and Blundy, J. D., 2017, Vertically extensive and unstable crystal mushes: a unifying view of igneous processes associated with volcanoes: Science, v. in press.

Castillo, P. R., 2012, Adakite petrogenesis: Lithos, v. 134, p. 304-316.

Castillo, P. R., Janney, P. E., and Solidum, R. U., 1999, Petrology and geochemistry of Camiguin Island, southern Philippines: insights to the source of adakites and other lavas in a complex arc setting: Contributions to Mineralogy and Petrology, v. 134, no. 1, p. 33-51.

Cathles, L., and Shannon, R., 2007, How potassium silicate alteration suggests the formation of porphyry ore deposits begins with the nearly explosive but barren expulsion of large volumes of magmatic water: Earth and Planetary Science Letters, v. 262, no. 1, p. 92-108.

Chambefort, I., Dilles, J. H., and Kent, A. J., 2008, Anhydrite-bearing andesite and dacite as a source for sulfur in magmatic-hydrothermal mineral deposits: Geology, v. 36, no. 9, p. 719-722.

Chambefort, I., Dilles, J. H., and Longo, A. A., 2013, Amphibole geochemistry of the Yanacocha Volcanics, Peru: Evidence for diverse sources of magmatic volatiles related to gold ores: Journal of Petrology, v. 54, p. 1017-1046.

Charrier, R., Baeza, O., Elgueta, S., Flynn, J. J., Gans, P., Kay, S. M., Munoz, N., Wyss, A. R., and Zurita, E., 2002, Evidence for Cenozoic extensional basin development and tectonic inversion south of the flat-slab segment, southern central Andes, Chile (33°-36°S): Journal of South American Earth Sciences, v. 15, no. 117-139.

Charrier, R., Wyss, A., Flynn, J. J., Swisher III, C. C., Norell, M. A., Zapatta, F., McKenna, M. C., and Novacek, M. J., 1996, New evidence for late Mesozoic-early Cenozoic evolution of the Chilean Andes in the upper Tinguiririca valley (35 S), central Chile: Journal of South American Earth Sciences, v. 9, no. 5, p. 393-422.

Chelle-Michou, C., Chiaradia, M., Selby, D., Ovtcharova, M., and Spikings, R. A., 2015, High-Resolution Geochronology of the Coroccohuayco Porphyry-Skarn Deposit, Peru: A Rapid Product of the Incaic Orogeny: Economic Geology, v. 110, no. 2, p. 423-443.

Chiaradia, M., 2015, Crustal thickness control on Sr/Y signatures of recent arc magmas: an Earth scale perspective: Scientific Reports, v. 5.

Christopher, T., Blundy, J., Cashman, K., Cole, P., Edmonds, M., Smith, P., Sparks, R., and Stinton, A., 2015, Crustal-scale degassing due to magma system destabilization and magma-gas decoupling at Soufrière Hills Volcano, Montserrat: Geochemistry, Geophysics, Geosystems, v. 16, p. 2797-2811.

Clavero, J., Sparks, R., Pringle, M., Polanco, E., and Gardeweg, M., 2004, Evolution and volcanic hazards of Taapaca volcanic complex, Central Andes of northern Chile: Journal of the Geological Society, v. 161, no. 4, p. 603-618.

Cline, J. S., and Bodnar, R. J., 1991, Can economic porphyry copper mineralization be generated by a typical calc-alkaline melt?: Journal of Geophysical Research: Solid Earth (1978–2012), v. 96, no. B5, p. 8113-8126.

Cloos, M., 2001, Bubbling magma chambers, cupolas, and porphyry copper deposits: International geology review, v. 43, no. 4, p. 285-311.

Cooke, D., Hollings, P., Wilkinson, J., and Tosdal, R., 2014, Geochemistry of porphyry deposits: Treatise on Geochemistry, p. 357-381.

Couch, S., Sparks, R., and Carroll, M., 2001, Mineral disequilibrium in lavas explained by convective self-mixing in open magma chambers: Nature, v. 411, no. 6841, p. 1037-1039.

Davidson, J., Turner, S., Handley, H., Macpherson, C., and Dosseto, A., 2007, Amphibole "sponge" in arc crust?: Geology, v. 35, no. 9, p. 787-790.

De Hoog, J., Hattori, K., and Hoblitt, R., 2004, Oxidized sulfur-rich mafic magma at Mount Pinatubo, Philippines: Contributions to Mineralogy and Petrology, v. 146, no. 6, p. 750-761.

Deckart, K., Clark, A. H., Celso, A. A., Ricardo, V. R., Bertens, A. N., Mortensen, J. K., and Fanning, M., 2005, Magmatic and hydrothermal chronology of the giant Rio Blanco porphyry copper deposit, central Chile: implications of an integrated U-Pb and 40Ar/39Ar database: Economic Geology, v. 100, no. 5, p. 905-934.

Defant, M. J., and Drummond, M. S., 1990, Derivation of some modern arc magmas by melting of young subducted lithosphere: Nature, v. 347, no. 6294, p. 662-665.

-, 1993, Mount St. Helens: potential example of the partial melting of the subducted lithosphere in a volcanic arc: Geology, v. 21, no. 6, p. 547-550.

Dilles, J. H., 1987, Petrology of the Yerington Batholith, Nevada; evidence for evolution of porphyry copper ore fluids: Economic Geology, v. 82, no. 7, p. 1750-1789.

1256 Dilles, J. H., and Einaudi, M. T., 1992, Wall-rock alteration and hydrothermal flow paths about
1257 the Ann-Mason porphyry copper deposit, Nevada; a 6-km vertical reconstruction:
1258 Economic Geology, v. 87, no. 8, p. 1963-2001.
1259 Dilles, J. H., Kent, A. J., Wooden, J. L., Tosdal, R. M., Koleszar, A., Lee, R. G., and Farmer, L.
1260 P., 2015, Zircon compositional evidence for sulfur-degassing from ore-forming arc
1261 magmas: Economic Geology, v. 110, no. 1, p. 241-251.
1262 Dungan, M. A., Wulff, A., and Thompson, R., 2001, Eruptive stratigraphy of the Tatara–San
1263 Pedro complex, 36 S, Southern Volcanic Zone, Chilean Andes: reconstruction method
1264 and implications for magma evolution at long-lived arc volcanic centers: Journal of
1265 Petrology, v. 42, no. 3, p. 555-626.
1266 Farquharson, J. I., Heap, M. J., and Baud, P., 2016, Strain-induced permeability increase in
1267 volcanic rock: Geophysical Research Letters, v. 43, no. 22.
1268 Farías, M., Charrier, R., Carretier, S., Martinod, J., Fock, A., Campbell, D., Cáceres, J., and
1269 Comte, D., 2008, Late Miocene high and rapid surface uplift and its erosional response in
1270 the Andes of central Chile (33–35 S): Tectonics, v. 27, no. 1.
1271 Farías, M., Comte, D., Charrier, R., Martinod, J., David, C., Tassara, A., Tapia, F., and Fock, A.,
1272 2010, Crustal-scale structural architecture in central Chile based on seismicity and
1273 surface geology: Implications for Andean mountain building: Tectonics, v. 29, no. 3.
1274 Furman, T., and Spera, F. J., 1985, Co-mingling of acid and basic magma with implications for
1275 the origin of mafic I-type xenoliths: field and petrochemical relations of an unusual dike
1276 complex at Eagle Lake, Sequoia National Park, California, USA: Journal of Volcanology
1277 and Geothermal Research, v. 24, no. 1, p. 151-178.
1278 Giambiagi, L., and Ramos, V., 2002, Structural evolution of the Andes in a transitional zone
1279 between flat and normal subduction (33 30′–33 45′ S), Argentina and Chile: Journal of
1280 South American Earth Sciences, v. 15, no. 1, p. 101-116.
1281 Gilmer, A. K., 2016, Petrogenesis of the Don Manuel Igneous Complex and porphyry copper
1282 system, central Chile PhD Thesis University of Bristol.
1283 Godoy, E., Yáñez, G., and Vera, E., 1999, Inversion of an Oligocene volcano-tectonic basin and
1284 uplifting of its superimposed Miocene magmatic arc in the Chilean Central Andes: first
1285 seismic and gravity evidences: Tectonophysics, v. 306, no. 2, p. 217-236.
1286 Goto, Y., Nakada, S., Kurokawa, M., Shimano, T., Sugimoto, T., Sakuma, S., Hoshizumi, H.,
1287 Yoshimoto, M., and Uto, K., 2008, Character and origin of lithofacies in the conduit of
1288 Unzen volcano, Japan: Journal of Volcanology and Geothermal Research, v. 175, no. 1,
1289 p. 45-59.
1290 Grove, T. L., Baker, M. B., and Kinzler, R. J., 1984, Coupled CaAl-NaSi diffusion in plagioclase
1291 feldspar: experiments and applications to cooling rate speedometry: Geochimica et
1292 Cosmochimica Acta, v. 48, no. 10, p. 2113-2121.
1293 Gustafson, L. B., and Hunt, J. P., 1975, The porphyry copper deposit at El Salvador, Chile:
1294 Economic Geology, v. 70, no. 5, p. 857-912.
1295 Hallot, E., Davy, P., de Bremond d'Ars, J., Auvray, B., Martin, H., and Van Damme, H., 1996,
1296 Non-Newtonian effects during injection in partially crystallised magmas: Journal of
1297 volcanology and geothermal research, v. 71, no. 1, p. 31-44.
1298 Halter, W. E., Bain, N., Becker, K., Heinrich, C. A., Landtwing, M., VonQuadt, A., Clark, A. H.,
1299 Sasso, A. M., Bissig, T., and Tosdal, R. M., 2004, From andesitic volcanism to the
1300 formation of a porphyry Cu-Au mineralizing magma chamber: the Farallón Negro

Volcanic Complex, northwestern Argentina: Journal of Volcanology and Geothermal Research, v. 136, no. 1, p. 1-30.
Halter, W. E., Heinrich, C. A., and Pettke, T., 2005, Magma evolution and the formation of porphyry Cu–Au ore fluids: evidence from silicate and sulfide melt inclusions: Mineralium Deposita, v. 39, no. 8, p. 845-863.
Harford, C., Pringle, M., Sparks, R., and Young, S., 2002, The volcanic evolution of Montserrat using 40Ar/39Ar geochronology: Geological Society, London, Memoirs, v. 21, no. 1, p. 93-113.
Hattori, K. H., and Keith, J. D., 2001, Contribution of mafic melt to porphyry copper mineralization: evidence from Mount Pinatubo, Philippines, and Bingham Canyon, Utah, USA: Mineralium Deposita, v. 36, no. 8, p. 799-806.
Hedenquist, J. W., and Lowenstern, J. B., 1994, The role of magmas in the formation of hydrothermal ore deposits: Nature, v. 370, no. 6490, p. 519-527.
Heinrich, C., Halter, W., Landtwing, M., and Pettke, T., 2005, The formation of economic porphyry copper (-gold) deposits: constraints from microanalysis of fluid and melt inclusions: SPECIAL PUBLICATION-GEOLOGICAL SOCIETY OF LONDON, v. 248, p. 247.
Hildreth, W., Fierstein, J., and Lanphere, M., 2003, Eruptive history and geochronology of the Mount Baker volcanic field, Washington: Geological Society of America Bulletin, v. 115, no. 6, p. 729-764.
Hildreth, W., and Lanphere, M. A., 1994, Potassium-argon geochronology of a basalt-andesite-dacite arc system: The Mount Adams volcanic field, Cascade Range of southern Washington: Geological Society of America Bulletin, v. 106, no. 11, p. 1413-1429.
Hildreth, W., and Moorbath, S., 1988, Crustal contributions to arc magmatism in the Andes of central Chile: Contributions to Mineralogy and Petrology, v. 98, no. 4, p. 455-489.
Hollings, P., Cooke, D., and Clark, A., 2005, Regional geochemistry of Tertiary igneous rocks in central Chile: Implications for the geodynamic environment of giant porphyry copper and epithermal gold mineralization: Economic Geology, v. 100, no. 5, p. 887-904.
Hoshizumi, H., Uto, K., and Watanabe, K., 1999, Geology and eruptive history of Unzen volcano, Shimabara peninsula, Kyushu, SW Japan: Journal of Volcanology and Geothermal Research, v. 89, no. 1, p. 81-94.
Huber, C., Bachmann, O., Vigneresse, J. L., Dufek, J., and Parmigiani, A., 2012, A physical model for metal extraction and transport in shallow magmatic systems: Geochemistry, Geophysics, Geosystems, v. 13, no. 8.
Humphreys, M. C., Christopher, T., and Hards, V., 2009, Microlite transfer by disaggregation of mafic inclusions following magma mixing at Soufrière Hills volcano, Montserrat: Contributions to Mineralogy and Petrology, v. 157, no. 5, p. 609-624.
Hynek, S. A., Marchetti, D. W., Fernandez, D. P., and Cerling, T. E., 2010, Composition, pre-eruptive zonation, and geochronologic significance of the~ 450ka Diamante Tuff, Andean Cordillera (34° S), Argentina: Quaternary Geochronology, v. 5, no. 5, p. 591-601.
Irvine, T., and Baragar, W., 1971, A guide to the chemical classification of the common volcanic rocks: Canadian journal of earth sciences, v. 8, no. 5, p. 523-548.
Jaeger, J., Hess, H., and Poldevaart, A., 1968, The Poldervaart treatise on rocks of basaltic composition.

1345 Jaffey, A., Flynn, K., Glendenin, L., Bentley, W. t., and Essling, A., 1971, Precision
1346 measurement of half-lives and specific activities of U 235 and U 238: Physical Review C,
1347 v. 4, no. 5, p. 1889.
1348 Kay, R., 1978, Aleutian magnesian andesites: melts from subducted Pacific Ocean crust: Journal
1349 of Volcanology and Geothermal Research, v. 4, no. 1, p. 117-132.
1350 Kay, S., and Kurtz, A., 1995, Magmatic and tectonic characterization of the El Teniente region:
1351 CODELCO (unpublished report).
1352 Kay, S. M., Godoy, E., and Kurtz, A., 2005, Episodic arc migration, crustal thickening,
1353 subduction erosion, and magmatism in the south-central Andes: Geological Society of
1354 America Bulletin, v. 117, no. 1-2, p. 67-88.
1355 Kay, S. M., and Mpodozis, C., 2001, Central Andean ore deposits linked to evolving shallow
1356 subduction systems and thickening crust: GSA TODAY, v. 11, no. 3, p. 4-9.
1357 Kay, S. M., Mpodozis, C., Ramos, V. A., and Munizaga, F., 1991, Magma source variations for
1358 mid–late Tertiary magmatic rocks associated with a shallowing subduction zone and a
1359 thickening crust in the central Andes (28 to 33 S): Geological Society of America Special
1360 Papers, v. 265, p. 113-138.
1361 Keith, J., Whitney, J., Hattori, K., Ballantyne, G., Christiansen, E., Barr, D., Cannan, T., and
1362 Hook, C., 1997, The role of magmatic sulfides and mafic alkaline magmas in the
1363 Bingham and Tintic mining districts, Utah: Journal of Petrology, v. 38, no. 12, p. 1679-
1364 1690.
1365 Kelley, K. A., and Cottrell, E., 2009, Water and the oxidation state of subduction zone magmas:
1366 Science, v. 325, no. 5940, p. 605-607.
1367 Kurtz, A. C., Kay, S. M., Charrier, R., and Farrar, E., 1997, Geochronology of Miocene plutons
1368 and exhumation history of the El Teniente region, Central Chile (34-35° 8): Andean
1369 Geology, v. 24, no. 1, p. 75-90.
1370 Landtwing, M. R., Pettke, T., Halter, W. E., Heinrich, C. A., Redmond, P. B., Einaudi, M. T.,
1371 and Kunze, K., 2005, Copper deposition during quartz dissolution by cooling magmatic–
1372 hydrothermal fluids: the Bingham porphyry: Earth and Planetary Science Letters, v. 235,
1373 no. 1, p. 229-243.
1374 Le Friant, A., Lock, E., Hart, M., Boudon, G., Sparks, R., Leng, M., Smart, C. W., Komorowski,
1375 J.-C., Deplus, C., and Fisher, J., 2008, Late Pleistocene tephrochronology of marine
1376 sediments adjacent to Montserrat, Lesser Antilles volcanic arc: Journal of the Geological
1377 Society, v. 165, no. 1, p. 279-289.
1378 Le Maitre, R. W., Streckeisen, A., Zanettin, B., Le Bas, M., Bonin, B., and Bateman, P., 2002,
1379 Igneous rocks: a classification and glossary of terms: recommendations of the
1380 International Union of Geological Sciences Subcommission on the Systematics of
1381 Igneous Rocks, Cambridge University Press.
1382 Leuthold, J., Müntener, O., Baumgartner, L. P., Putlitz, B., Ovtcharova, M., and Schaltegger, U.,
1383 2012, Time resolved construction of a bimodal laccolith (Torres del Paine, Patagonia):
1384 Earth and Planetary Science Letters, v. 325, p. 85-92.
1385 Lickfold, V., Cooke, D., Crawford, A., and Fanning, C., 2007, Shoshonitic magmatism and the
1386 formation of the Northparkes porphyry Cu–Au deposits, New South Wales: Australian
1387 Journal of Earth Sciences, v. 54, no. 2-3, p. 417-444.
1388 Lipman, P. W., 2007, Incremental assembly and prolonged consolidation of Cordilleran magma
1389 chambers: Evidence from the Southern Rocky Mountain volcanic field: Geosphere, v. 3,
1390 no. 1, p. 42-70.

1391 Longo, A. A., Dilles, J. H., Grunder, A. L., and Duncan, R., 2010, Evolution of calc-alkaline
1392 volcanism and associated hydrothermal gold deposits at Yanacocha, Peru: Economic
1393 Geology, v. 105, no. 7, p. 1191-1241.
1394 Loucks, R., 2014, Distinctive composition of copper-ore-forming arcmagmas: Australian Journal
1395 of Earth Sciences, v. 61, no. 1, p. 5-16.
1396 Luhr, J. F., 1990, Experimental phase relations of water-and sulfur-saturated arc magmas and the
1397 1982 eruptions of El Chichón volcano: Journal of Petrology, v. 31, no. 5, p. 1071-1114.
1398 Maksaev, V., Munizaga, F., McWilliams, M., Fanning, M., Mathur, R., Ruiz, J., and Zentilli, M.,
1399 2004, New chronology for El Teniente, Chilean Andes, from U/Pb, 40Ar/39Ar, Re/Os
1400 and fission-track dating: implications for the evolution of a supergiant porphyry Cu-Mo
1401 deposit: Andean Metallogeny: New Discoveries, Concepts Update. Society of Economic
1402 Geologists, Special Publication, v. 11, p. 15-54.
1403 Maksaev, V., Townley, B., Palacios, C., and Camus, F., 2007, Metallic ore deposits: The
1404 geology of Chile. The Geological Society, London, p. 179-199.
1405 Marot, M., Monfret, T., Gerbault, M., Nolet, G., Ranalli, G., and Pardo, M., 2014, Flat versus
1406 normal subduction zones: a comparison based on 3-D regional traveltime tomography
1407 and petrological modelling of central Chile and western Argentina (29°–35° S):
1408 Geophysical Journal International, v. 199, no. 3, p. 1633-1654.
1409 Matjuschkin, V., Blundy, J. D., and Brooker, R. A., 2016, The effect of pressure on sulphur
1410 speciation in mid-to deep-crustal arc magmas and implications for the formation of
1411 porphyry copper deposits: Contributions to Mineralogy and Petrology, v. 171, no. 7, p. 1-
1412 25.
1413 Mattinson, J. M., 2005, Zircon U–Pb chemical abrasion ("CA-TIMS") method: combined
1414 annealing and multi-step partial dissolution analysis for improved precision and accuracy
1415 of zircon ages: Chemical Geology, v. 220, no. 1, p. 47-66.
1416 Maughan, D. T., Keith, J. D., Christiansen, E. H., Pulsipher, T., Hattori, K., and Evans, N. J.,
1417 2002, Contributions from mafic alkaline magmas to the Bingham porphyry Cu–Au–Mo
1418 deposit, Utah, USA: Mineralium Deposita, v. 37, no. 1, p. 14-37.
1419 Maydagán, L., Franchini, M., Chiaradia, M., Pons, J., Impiccini, A., Toohey, J., and Rey, R.,
1420 2011, Petrology of the Miocene igneous rocks in the Altar region, main Cordillera of San
1421 Juan, Argentina. A geodynamic model within the context of the Andean flat-slab segment
1422 and metallogenesis: Journal of South American Earth Sciences, v. 32, no. 1, p. 30-48.
1423 McDonald, I., and Viljoen, K., 2006, Platinum-group element geochemistry of mantle eclogites:
1424 a reconnaissance study of xenoliths from the Orapa kimberlite, Botswana: Applied Earth
1425 Science: Transactions of the Institutions of Mining and Metallurgy: Section B, v. 115, no.
1426 3, p. 81-93.
1427 Mercer, C. N., and Reed, M. H., 2013, Porphyry Cu-Mo Stockwork Formation by Dynamic,
1428 Transient Hydrothermal Pulses: Mineralogic Insights from the Deposit at Butte,
1429 Montana: Economic Geology, v. 108, no. 6, p. 1347-1377.
1430 Mercer, C. N., Reed, M. H., and Mercer, C. M., 2015, Time scales of porphyry Cu deposit
1431 formation: insights from titanium diffusion in quartz: Economic Geology, v. 110, no. 3,
1432 p. 587-602.
1433 Michel, J., Baumgartner, L., Putlitz, B., Schaltegger, U., and Ovtcharova, M., 2008, Incremental
1434 growth of the Patagonian Torres del Paine laccolith over 90 ky: Geology, v. 36, no. 6, p.
1435 459-462.

1436 Miller, C. F., Furbish, D. J., Walker, B. A., Claiborne, L. L., Koteas, G. C., Bleick, H. A., and
1437 Miller, J. S., 2011, Growth of plutons by incremental emplacement of sheets in crystal-
1438 rich host: evidence from Miocene intrusions of the Colorado River region, Nevada, USA:
1439 Tectonophysics, v. 500, no. 1, p. 65-77.
1440 Moore, G., and Carmichael, I., 1998, The hydrous phase equilibria (to 3 kbar) of an andesite and
1441 basaltic andesite from western Mexico: constraints on water content and conditions of
1442 phenocryst growth: Contributions to Mineralogy and Petrology, v. 130, no. 3-4, p. 304-
1443 319.
1444 Murphy, M., Sparks, R., Barclay, J., Carroll, M., Lejeune, A. M., Brewer, T., Macdonald, R.,
1445 Black, S., and Young, S., 1998, The role of magma mixing in triggering the current
1446 eruption at the Soufriere Hills volcano, Montserrat, West Indies: Geophysical Research
1447 Letters, v. 25, no. 18, p. 3433-3436.
1448 Muñoz, M., Charrier, R., Fanning, C., Maksaev, V., and Deckart, K., 2012, Zircon trace element
1449 and O–Hf isotope analyses of mineralized intrusions from El Teniente ore deposit,
1450 Chilean Andes: Constraints on the source and magmatic evolution of porphyry Cu–Mo
1451 related magmas: Journal of Petrology, p. egs010.
1452 Müntener, O., Kelemen, P. B., and Grove, T. L., 2001, The role of H2O during crystallization of
1453 primitive arc magmas under uppermost mantle conditions and genesis of igneous
1454 pyroxenites: an experimental study: Contributions to Mineralogy and Petrology, v. 141,
1455 no. 6, p. 643-658.
1456 Nadeau, O., Williams-Jones, A. E., and Stix, J., 2010, Sulphide magma as a source of metals in
1457 arc-related magmatic hydrothermal ore fluids: Nature Geoscience, v. 3, no. 7, p. 501-505.
1458 Naney, M., 1983, Phase equilibria of rock-forming ferromagnesian silicates in granitic systems:
1459 American journal of science, v. 283, no. 10, p. 993-1033.
1460 Nyström, J. O., Vergara, M., Morata, D., and Levi, B., 2003, Tertiary volcanism during
1461 extension in the Andean foothills of central Chile (33 15′–33 45′ S): Geological Society
1462 of America Bulletin, v. 115, no. 12, p. 1523-1537.
1463 Oyarzun, R., Márquez, A., Lillo, J., López, I., and Rivera, S., 2001, Giant versus small porphyry
1464 copper deposits of Cenozoic age in northern Chile: adakitic versus normal calc-alkaline
1465 magmatism: Mineralium Deposita, v. 36, no. 8, p. 794-798.
1466 Pardo, M., Comte, D., and Monfret, T., 2002, Seismotectonic and stress distribution in the
1467 central Chile subduction zone: Journal of South American Earth Sciences, v. 15, no. 1, p.
1468 11-22.
1469 Pearce, J. A., and Peate, D. W., 1995, Tectonic implications of the composition of volcanic arc
1470 magmas: Annual Review of Earth and Planetary Sciences, v. 23, p. 251-286.
1471 Piquer, J., Skarmeta, J., and Cooke, D. R., 2015, Structural Evolution of the Rio Blanco-Los
1472 Bronces District, Andes of Central Chile: Controls on Stratigraphy, Magmatism, and
1473 Mineralization: Economic Geology, v. 110, no. 8, p. 1995-2023.
1474 Pollard, P. J., Taylor, R. G., and Peters, L., 2005, Ages of intrusion, alteration, and
1475 mineralization at the Grasberg Cu-Au deposit, Papua, Indonesia: Economic Geology, v.
1476 100, no. 5, p. 1005-1020.
1477 Redmond, P., Einaudi, M., Inan, E., Landtwing, M., and Heinrich, C., 2004, Copper deposition
1478 by fluid cooling in intrusion-centered systems: new insights from the Bingham porphyry
1479 ore deposit, Utah: Geology, v. 32, no. 3, p. 217-220.
1480 Reed, M., Rusk, B., and Palandri, J., 2013, The Butte magmatic-hydrothermal system: One fluid
1481 yields all alteration and veins: Economic Geology, v. 108, no. 6, p. 1379-1396.

Reich, M., Parada, M. A., Palacios, C., Dietrich, A., Schultz, F., and Lehmann, B., 2003, Adakite-like signature of Late Miocene intrusions at the Los Pelambres giant porphyry copper deposit in the Andes of central Chile: metallogenic implications: Mineralium Deposita, v. 38, no. 7, p. 876-885.

Renne, P. R., Deino, A. L., Hames, W. E., Heizler, M. T., Hemming, S. R., Hodges, K. V., Koppers, A. A., Mark, D. F., Morgan, L. E., and Phillips, D., 2009, Data reporting norms for 40 Ar/39 Ar geochronology: Quaternary Geochronology, v. 4, no. 5, p. 346-352.

Richards, J. P., 2011, High Sr/Y arc magmas and porphyry Cu±Mo±Au deposits: just add water: Economic Geology, v. 106, no. 7, p. 1075-1081.

Richards, J. P., and Kerrich, R., 2007, Special paper: adakite-like rocks: their diverse origins and questionable role in metallogenesis: Economic Geology, v. 102, no. 4, p. 537-576.

Richards, J. P., Spell, T., Rameh, E., Razique, A., and Fletcher, T., 2012, High Sr/Y magmas reflect arc maturity, high magmatic water content, and porphyry Cu±Mo±Au potential: examples from the Tethyan arcs of Central and Eastern Iran and Western Pakistan: Economic Geology, v. 107, no. 2, p. 295-332.

Scaillet, B., Clémente, B., Evans, B. W., and Pichavant, M., 1998, Redox control of sulfur degassing in silicic magmas: Journal of Geophysical Research Solid Earth, v. 103, no. B10, p. 23,937-923,949.

Scandone, R., Cashman, K. V., and Malone, S. D., 2007, Magma supply, magma ascent and the style of volcanic eruptions: Earth and Planetary Science Letters, v. 253, no. 3, p. 513-529.

Seedorff, E., Barton, M. D., Stavast, W. J., and Maher, D. J., 2008, Root zones of porphyry systems: Extending the porphyry model to depth: Economic Geology, v. 103, no. 5, p. 939-956.

Seedorff, E., Dilles, J., Proffett, J., Einaudi, M., Zurcher, L., Stavast, W., Johnson, D., and Barton, M., 2005, Porphyry deposits: characteristics and origin of hypogene features: Economic Geology 100th Anniversary Volume, v. 29, p. 251-298.

Serrano, L., Vargas, R., Stambuk, V., Aguilar, C., Galeb, M., Holmgren, C., Contreras, A., Godoy, S., Vela, I., and Skewes, M., 1996, The late miocene to early pliocene Río Blanco-Los Bronces copper deposit, central Chilean Andes: Andean copper deposits: new discoveries, mineralization, styles and metallogeny. Soc Econ Geol Spec Publ, v. 5, p. 119-129.

Shand, S., 1951, Eruptive Rocks. New York: J, Wiley. STAMPFLI, G., MOSAR, J., FAURE, P., PILLEVUIT, A. &.

Sheldrake, T. E., Sparks, R., Cashman, K., Wadge, G., and Aspinall, W., 2016, Similarities and differences in the historical records of lava dome-building volcanoes: Implications for understanding magmatic processes and eruption forecasting: Earth-Science Reviews, v. 160, p. 240-263.

Sillitoe, R. H., 1973, The tops and bottoms of porphyry copper deposits: Economic Geology, v. 68, no. 6, p. 799-815.

-, 2010, Porphyry copper systems: Economic Geology, v. 105, no. 1, p. 3-41.

Sinclair, W., 2007, Porphyry deposits: Mineral deposits of Canada: A synthesis of major deposit-types, district metallogeny, the evolution of geological provinces, and exploration methods: Geological Association of Canada, Mineral Deposits Division, Special Publication, v. 5, p. 223-243.

Skewes, M. A., and Stern, C. R., 1995, Genesis of the giant late Miocene to Pliocene copper deposits of central Chile in the context of Andean magmatic and tectonic evolution: International Geology Review, v. 37, no. 10, p. 893-909.

Sparks, R., and Marshall, L., 1986, Thermal and mechanical constraints on mixing between mafic and silicic magmas: Journal of Volcanology and Geothermal Research, v. 29, no. 1, p. 99-124.

Sparks, R. S. J., 1997, Causes and consequences of pressurisation in lava dome eruptions: Earth and Planetary Science Letters, v. 150, no. 3, p. 177-189.

Sparks, R. S. J., and Cashman, K., in press, The implications of magma system models for forecasting volcanic activity: Elements.

Spencer, E. T., Wilkinson, J. J., Creaser, R. A., and Seguel, J., 2015, The distribution and timing of molybdenite mineralization at the El Teniente cu-mo porphyry deposit, Chile: Economic Geology, v. 110, no. 2, p. 387-421.

Sruoga, P., Etcheverría, M. P., Feineman, M., Rosas, M., Burkert, C., and Ibañes, O., 2012, Complejo Caldera Diamante-Volcán Maipo (34°10´S): Evolución volcanológica y geoquímica e implicancias su IMPLICANCIAS EN SU PELIGROSIDAD: Revista de la Asociación Geológica Argentina, v. 69, no. 4, p. 508-530.

Sruoga, P., Llambías, E. J., Fauqué, L., Schonwandt, D., and Repol, D. G., 2005, Volcanological and geochemical evolution of the Diamante Caldera–Maipo volcano complex in the southern Andes of Argentina (34 10′ S): Journal of South American Earth Sciences, v. 19, no. 4, p. 399-414.

Stern, C. R., 2004, Active Andean volcanism: its geologic and tectonic setting: Revista geológica de Chile, v. 31, no. 2, p. 161-206.

Stern, C. R., Amini, H., Charrier, R., Godoy, E., Herve, F., and Varela, J., 1984, Petrochemistry and age of rhyolitic pyroclastic flows which occur along the drainage valleys of the Rio Maipo and Rio Cachapoal (Chile) and the Rio Yaucha and Rio Papagayos (Argentina). : Revista Geologica de Chile, v. 23, p. 39-52.

Stern, C. R., Funk, J. A., Skewes, M. A., and Arévalo, A., 2007, Magmatic anhydrite in plutonic rocks at the El Teniente Cu-Mo deposit, Chile, and the role of sulfur-and copper-rich magmas in its formation: Economic geology, v. 102, no. 7, p. 1335-1344.

Stern, C. R., and Skewes, M. A., 1995, Miocene to present magmatic evolution at the northern end of the Andean Southern Volcanic Zone, Central Chile: Andean Geology, v. 22, no. 2, p. 261-272.

Stern, C. R., Skewes, M. A., and Arévalo, A., 2011, Magmatic evolution of the giant El Teniente Cu–Mo deposit, central Chile: Journal of Petrology, v. 52, no. 7-8, p. 1591-1617.

Streck, M. J., 2008, Mineral textures and zoning as evidence for open system processes: Reviews in Mineralogy and Geochemistry, v. 69, no. 1, p. 595-622.

Sun, S.-S., and McDonough, W. F., 1989, Chemical and isotopic systematics of oceanic basalts: implications for mantle composition and processes: Geological Society, London, Special Publications, v. 42, no. 1, p. 313-345.

Tapster, S., Condon, D., Naden, J., Noble, S., Petterson, M., Roberts, N., Saunders, A., and Smith, D., 2016, Rapid thermal rejuvenation of high-crystallinity magma linked to porphyry copper deposit formation; evidence from the Koloula Porphyry Prospect, Solomon Islands: Earth and Planetary Science Letters.

Tatsumi, Y., 1989, Migration of fluid phases and genesis of basalt magmas in subduction zones: Journal of Geophysical Research: Solid Earth (1978–2012), v. 94, no. B4, p. 4697-4707.

Tepley, F., Davidson, J., Tilling, R., and Arth, J., 2000, Magma mixing, recharge and eruption histories recorded in plagioclase phenocrysts from El Chichon Volcano, Mexico: Journal of Petrology, v. 41, no. 9, p. 1397-1411.
Vergara, M., Charrier, R., Munizaga, F., Rivano, S., Sepúlveda, P., Thiele, R., and Drake, R., 1988, Miocene volcanism in the central Chilean Andes (31 30′ S–34 35′ S): Journal of South American Earth Sciences, v. 1, no. 2, p. 199-209.
Vernon, R., 1984, Microgranitoid enclaves in granites—globules of hybrid magma quenched in a plutonic environment: Nature, v. 309, no. 5967, p. 438-439.
Von Quadt, A., Erni, M., Martinek, K., Moll, M., Peytcheva, I., and Heinrich, C. A., 2011, Zircon crystallization and the lifetimes of ore-forming magmatic-hydrothermal systems: Geology, v. 39, no. 8, p. 731-734.
Vry, V., Wilkinson, J., Seguel, J., and Millán, J., 2010, Multistage intrusion, brecciation, and veining at El Teniente, Chile: Evolution of a nested porphyry system: Economic Geology, v. 105, no. 1, p. 119-153.
Waite, K. A., Keith, J. D., Christiansen, E. H., Whitney, J. A., Hattori, K., Tingey, D. G., and Hook, C. J., 1997, Petrogenesis of the volcanic and intrusive rocks associated with the Bingham Canyon porphyry Cu–Au–Mo deposit, Utah: Soc Econ Geol Guidebook Ser, v. 29, p. 91-128.
Warnaars, F. W., Holmgren, C., and Barassi, S., 1985, Porphyry copper and tourmaline breccias at Los Bronces-Río Blanco, Chile: Economic Geology, v. 80, no. 6, p. 1544-1565.
Weis, P., Driesner, T., and Heinrich, C., 2012, Porphyry-copper ore shells form at stable pressure-temperature fronts within dynamic fluid plumes: Science, v. 338, no. 6114, p. 1613-1616.
Yáñez, G., Cembrano, J., Pardo, M., Ranero, C., and Selles, D., 2002, The Challenger–Juan Fernández–Maipo major tectonic transition of the Nazca–Andean subduction system at 33–34 S: geodynamic evidence and implications: Journal of South American Earth Sciences, v. 15, no. 1, p. 23-38.
Yáñez, G. A., Ranero, C. R., Huene, R., and Díaz, J., 2001, Magnetic anomaly interpretation across the southern central Andes (32–34 S): The role of the Juan Fernández Ridge in the late Tertiary evolution of the margin: Journal of Geophysical Research: Solid Earth (1978–2012), v. 106, no. B4, p. 6325-6345.
Zajacz, Z., and Halter, W., 2009, Copper transport by high temperature, sulfur-rich magmatic vapor: Evidence from silicate melt and vapor inclusions in a basaltic andesite from the Villarrica volcano (Chile): Earth and Planetary Science Letters, v. 282, no. 1, p. 115-121.
Zellmer, G., Iizuka, Y., Miyoshi, M., Tamura, Y., and Tatsumi, Y., 2012, Lower crustal H2O controls on the formation of adakitic melts: Geology, v. 40, no. 6, p. 487-490.

Yáñez, G., Cembrano, J., Pardo, M., Ranero, C., and Selles, D., 2002, The Challenger–Juan Fernández–Maipo major tectonic transition of the Nazca–Andean subduction system at 33–34 S: geodynamic evidence and implications: Journal of South American Earth Sciences, v. 15, no. 1, p. 23-38.
Yáñez, G. A., Ranero, C. R., Huene, R., and Díaz, J., 2001, Magnetic anomaly interpretation across the southern central Andes (32–34 S): The role of the Juan Fernández Ridge in the late Tertiary evolution of the margin: Journal of Geophysical Research: Solid Earth (1978–2012), v. 106, no. B4, p. 6325-6345.

Zajacz, Z., and Halter, W., 2009, Copper transport by high temperature, sulfur-rich magmatic vapor: Evidence from silicate melt and vapor inclusions in a basaltic andesite from the Villarrica volcano (Chile): Earth and Planetary Science Letters, v. 282, no. 1, p. 115-121.
Zellmer, G., Iizuka, Y., Miyoshi, M., Tamura, Y., and Tatsumi, Y., 2012, Lower crustal H2O controls on the formation of adakitic melts: Geology, v. 40, no. 6, p. 487-490.

FIGURE CAPTIONS

Figure 1. Location of the Don Manuel Igneous Complex (DMIC) study area, major volcanoes, and major porphyry copper deposits in central Chile.

Figure 2. (A) Geological map of the region around 34°S, including the locations of El Teniente porphyry copper deposit and Maipo volcano relative to the Don Manuel Igneous Complex (DMIC). (B) Inset shows the location of the Paredones and Don Manuel Principal areas within the study area. Map modified after Servicio National de Geología y Minería (2002) and (Sruoga et al., 2005).

Figure 3. (A) Geological map of the Don Manuel area showing the surface geology, location of the Paredones and Don Manuel Principal sections of the study area, and the drill hole locations. Copper sulfides are confined to the Don Manuel Principal area. Map modified after (Candia et al., 2009). (B) Schematic geologic cross-section through the mineralized area at Don Manuel Principal. The cross-cutting relationships shown are dominantly based on logging by the lead author, supplemented by logs of surface samples and drill cores from BHP Billiton. Quartz monzonite dikes have intruded the Coya Machali Formation, followed by the emplacement of the equigranular phase of the biotite tonalite. A porphyritic phase of the biotite tonalite was emplaced after the equigranular phase of the biotite tonalite. A series of intermediate porphyry dikes cut the previous intrusions and are in turn cut by later basaltic andesite dikes.

Figure 4. Don Manuel Igneous Complex (DMIC) units sampled from Don Manuel Principal core. (A) Hornfelsed lacustrine sedimentary facies of the Coya Machali Formation showing a layer replaced by chalcopyrite and calc-silicate minerals (core DM7, depth: 77.25 m); (B) Intermediate porphyry with a chalcopyrite-quartz vein (core DM8, depth: 438.0 m); (C) Quartz monzonite (core DM6, depth: 425.8 m); (D) Equigranular biotite tonalite with mafic enclaves (core DM2, depth: 107.9 m); (E) Porphyryitic biotite tonalite (core DM4, depth: 472.4 m); (F) Intermediate porphyry (core DM5, depth: 441.2 m); and (G) Basaltic andesite (core DM4, depth: 477.2 m). Abbreviation: Ccp = chalcopyrite.

Figure 5. Characteristic macroscopic textures of the intrusive units of the Don Manuel Igneous Complex (DMIC) in the Don Manuel Principal drill core. The intermediate porphyry dikes may show a much broader range of textures than shown here. (A) Quartz monzonite with biotite (core DM6, depth: 120.6 m); (B) Porphyritic biotite tonalite containing both biotite and amphibole (core DM4, depth: 472.4 m); (C) Equigranular biotite tonalite with only biotite in this particular sample (core DM2, depth: 14.15 m); (D) Intermediate porphyry dike containing only biotite as ferromagnesian phenocryst (IPD1) (core DM5, depth: 168.5 m); (E) Intermediate porphyry dike containing both biotite and amphibole as ferromagnesian phenocrysts (IPD2) (core DM5, depth: 443.0 m); (F) Intermediate porphyry dike containing amphibole as the only ferromangnesian phenocryst (IPD3) (core DM6, depth: 465.3 m); (G) Basaltic andesite dike with amphibole phenocrysts (core DM6, depth: 534.8 m). Abbreviations: Bt = biotite, Ksp = potassium feldspar, Am = amphibole, Pl = plagioclase, Py = pyrite, Qtz = quartz.

Figure 6. Photomicrographs of the Don Manuel Igneous Complex (DMIC) units in the drill core from Don Manuel Principal showing (A) Quartz monzonite with plagioclase phenocrysts; cross-polarized light (core DM6, depth: 120.6 m); (B) Biotite tonalite with plagioclase, quartz and

biotite; cross-polarized light (core DM4, depth: 285.3 m); (C) Intermediate porphyry dike with plagioclase and amphibole phenocrysts; cross-polarized light (core DM6, depth: 527.8 m); (D) Miarolitic cavity filled with quartz, pyrite and epidote; cross-polarized light (core DM3, depth: 563.0 m); (E) Basaltic andesite dike, with plagioclase and amphibole phenocrysts; cross-polarized light (core DM5, depth: 503.0 m); (F) Contact between intermediate porphyry dike and basaltic andesite with plagioclase phenocryst; cross-polarized light (core DM6, depth: 546.0 m). Photomicrographs of DMIC units from the Parendones area showing (G) Rhyolite with plagioclase phenocrysts in a finer groundmass of quartz, plagioclase and potassium feldspar; cross-polarized light (sample location: 34°13'55.2"S, 70°4'48"W); (H) Basaltic andesite dike with clinopyroxene phenocryst; cross-polarized light (sample location: 34°13'44.4"S, 70°5'2.4"W); Abbreviations: Bt = biotite, Ep = epidote, Am = amphibole, Cpx = clinopyroxene, Pl = plagioclase, Py = pyrite, Qtz = quartz.

Figure 7. Representative textural relationships within the intermediate porphyry dikes of the Don Manuel Igneous Complex (DMIC): (A) Enclaves within an intermediate porphyry dike (core DM3, depth: 298.0 m); (B) Intermediate porphyry dike showing flow zones, diffuse contacts between magma pulses, and microenclaves (core DM3, depth: 168.1 m). Flow zones suggest magma mixing produced this hybridized texture.

Figure 8. Irregular contact between the rhyolite (bottom) and a basaltic andesite dike (top) in outcrop in the Paredones region of the study area.

Figure 9. Total alkalis vs silica (TAS) diagram after Le Maitre et al. (2002) of the Don Manuel Igneous Complex (DMIC) whole rock samples. DMIC samples range from basaltic andesites through to rhyolites (anhydrous normalized).

1686 Figure 10. Selected major element vs. SiO_2 Harker diagrams for the Don Manuel Igneous Complex
1687 (DMIC). Total Fe is plotted as FeO*. Symbols are the same as in Figure 9.

1688 Figure 11. Whole-rock REE concentrations normalized to average chondrite (Sun and
1689 McDonough, 1989) for the rocks of the Don Manuel Igneous Complex (DMIC).

1690 Figure 12. Plots of (A) Sr/Y vs. Y and (B) La/Yb vs. Yb for the rocks of the Don Manuel Igneous
1691 Complex (DMIC). Fields for adakites and normal arc trends are after Defant and Drummond
1692 (1993) and (Castillo, 2012). Symbols are the same as in Figure 9.

1693 Figure 13. Typical zoning profiles from core to rim of anorthite content (mol. %) in plagioclase
1694 phenocrysts from the rhyolite and basaltic andesite dikes from the Paredones area. White arrows
1695 mark the line of each traverse. Anorthite zoning is mostly absent in the rhyolite and is characterized
1696 by a slow decay towards the rim in the basaltic andesite.

1697 Figure 14. Typical zoning profiles from core to rim of anorthite content (mol. %) in plagioclase
1698 phenocrysts from the intermediate porphyry dikes from Don Manuel Principal drill core. All
1699 phenocryst types can be found in the same sample. Arrows mark the line of each traverse.

1700 Figure 15. CA-ID-TIMS $^{206}Pb/^{238}U$ fraction dates (corrected for initial ^{238}U–^{230}Th disequilibrium
1701 with $Th/U_{magma} \sim 3.5$, see DR3) and weighted mean dates for each unit of the Don Manuel Igneous
1702 Complex (DMIC). Weighted mean dates are interpreted as emplacement ages. All uncertainties
1703 are shown at the 2σ confidence level.

1704 Figure 16. Whole rock argon data for the Don Manuel Igneous Complex (DMIC) basaltic andesite
1705 dikes (see Table 4). $^{40}Ar/^{39}Ar$ step-heating plateau diagrams including $\%^{40}Ar^*$, K/Ca and age vs.
1706 $\%^{39}Ar$ released per step are shown on the left. The inverse isochron analysis on the right shows an

1707 age and composition of the trapped component for a number of points (n). The ages presented in
1708 the plateau diagram (left panel) are calculated using air as a trapped component.

1709 Figure 17. Summary of the Don Manuel Igneous Complex (DMIC) emplacement events including
1710 CA-ID-TIMS U-Pb zircon dates (circles), whole-rock $^{40}Ar/^{39}Ar$ dates (squares), and observed
1711 mafic enclaves within dated units (triangles). Gray filled circles indicate strongly mineralized
1712 units. Data are given in Figure 15, Figure 16 and Table 3 and Table 4. IPD, intermediate porphyry
1713 dike.

1714 [1]GSA Data Repository items 2016xxx, analytical methods and additional analytical results are
1715 available online at www.geosociety.org/pubs/ft20XX.htm, or on request from
1716 editing@geosociety.org or Documents Secretary, GSA, P.O. Box 9140, Boulder, CO 80301,
1717 USA.

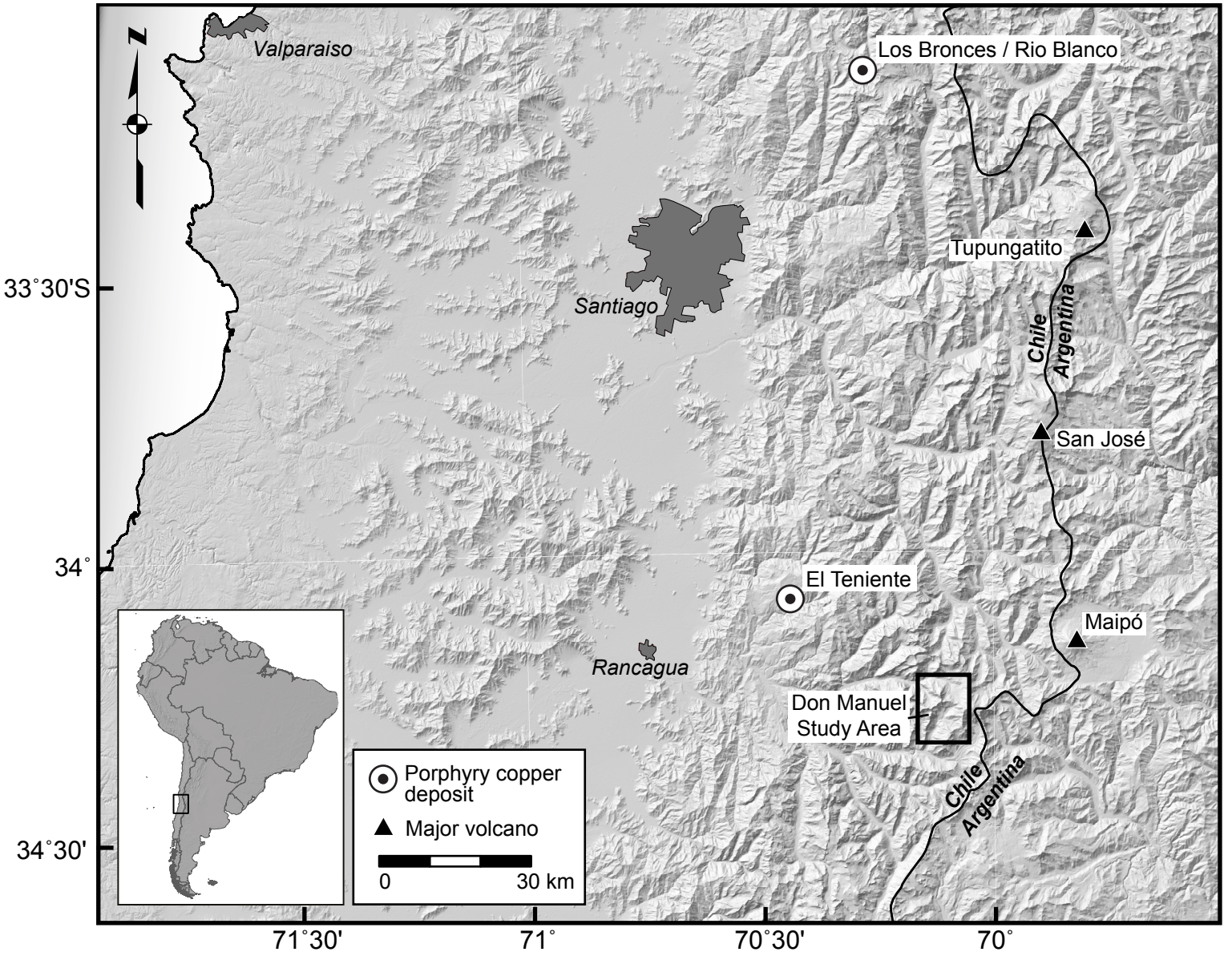

Gilmer, Figure 1, B31524

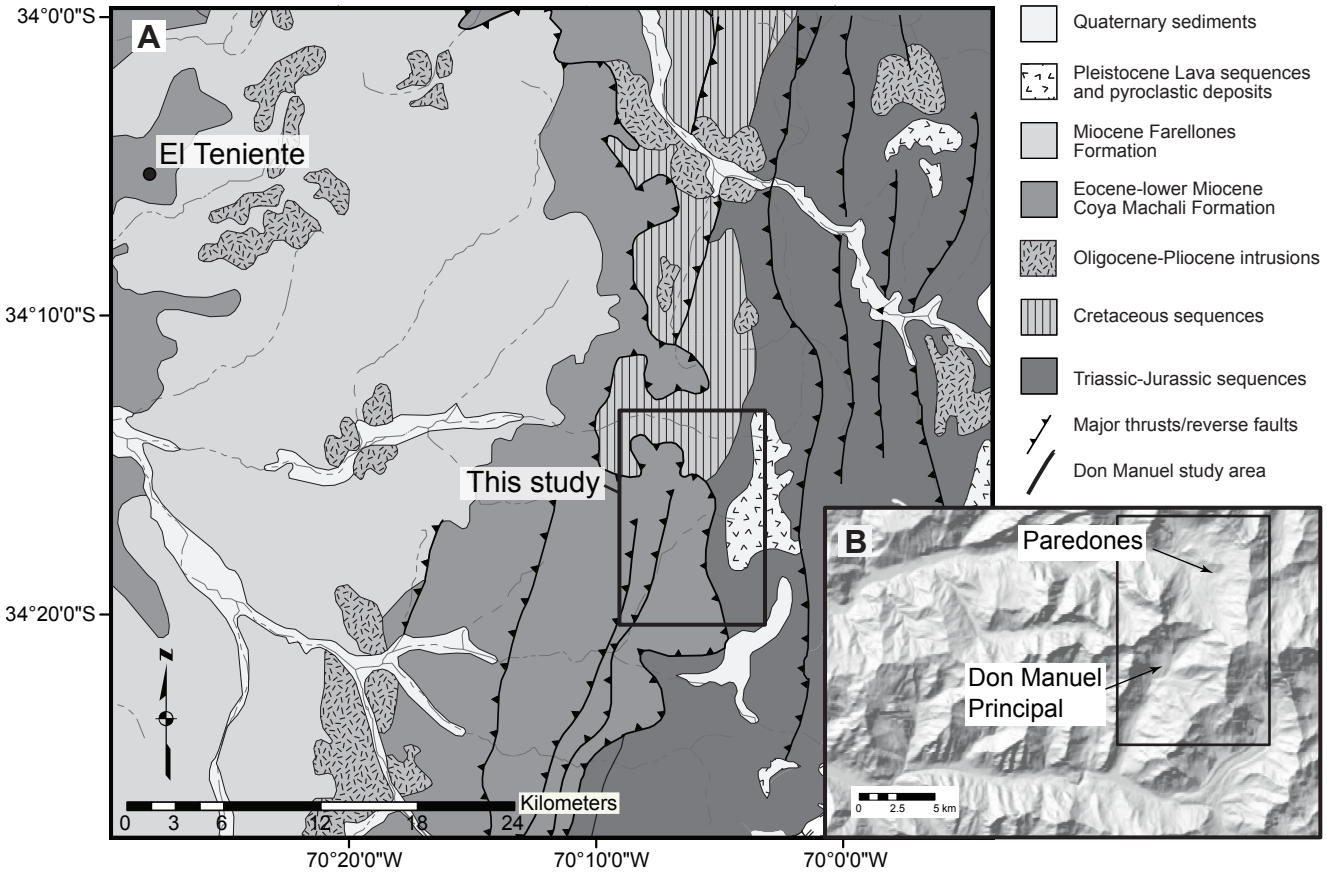
34°0'0"S
34°10'0"S
34°20'0"S
A
El Teniente
This study
B
Paredones
Don Manuel
Principal
0 2.5 5 km
N
0 3 6 12 18 24
Kilometers
70°20'0"W
70°10'0"W
70°0'0"W
Quaternary sediments
Pleistocene Lava sequences and pyroclastic deposits
Miocene Farellones Formation
Eocene-lower Miocene Coya Machali Formation
Oligocene-Pliocene intrusions
Cretaceous sequences
Triassic-Jurassic sequences
Major thrusts/reverse faults
Don Manuel study area

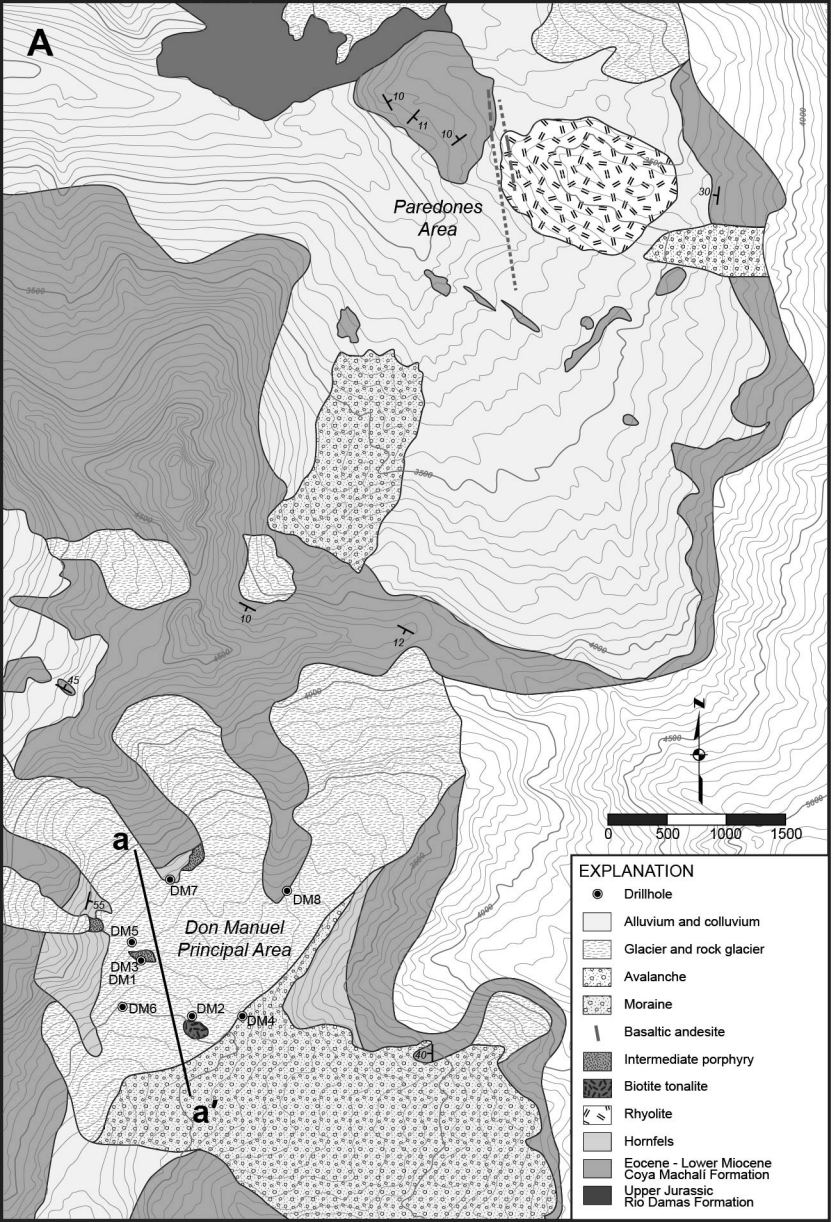
A
Paredones Area
Don Manuel Principal Area
a
a'
DM7
DM8
DM5
DM3
DM1
DM6
DM2
DM4
0 500 1000 1500
EXPLANATION
Drillhole
Alluvium and colluvium
Glacier and rock glacier
Avalanche
Moraine
Basaltic andesite
Intermediate porphyry
Biotite tonalite
Rhyolite
Hornfels
Eocene - Lower Miocene Coya Machali Formation
Upper Jurassic Rio Damas Formation

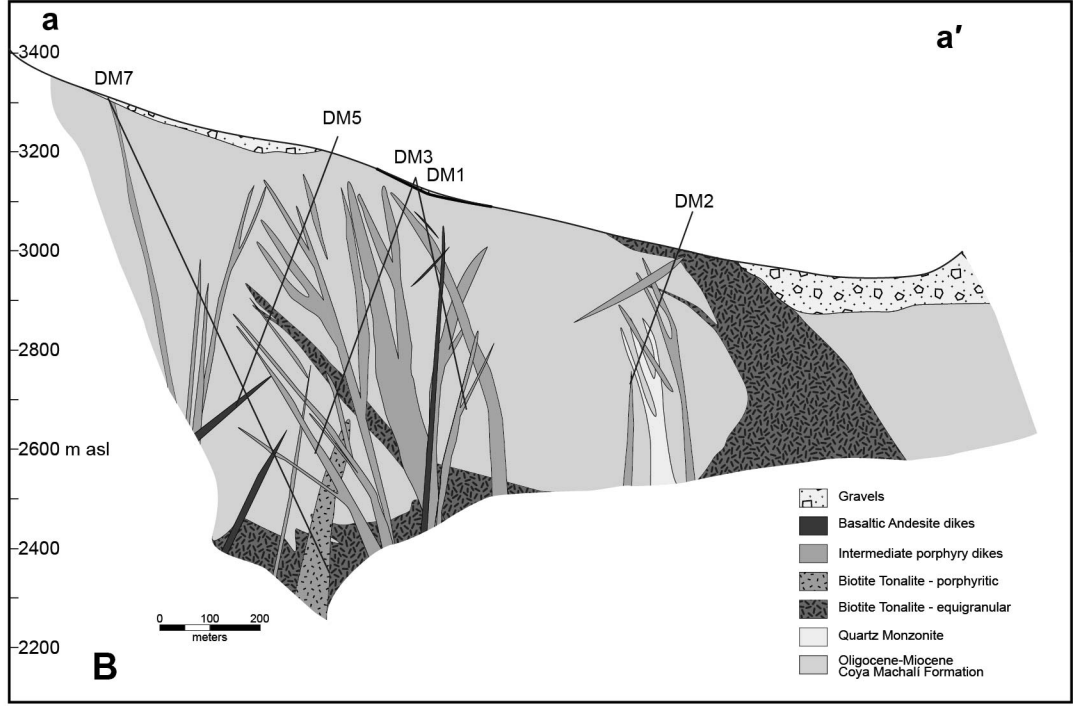
a
a'
3400
3200
3000
2800
2600 m asl
2400
2200
DM7
DM5
DM3
DM1
DM2
0 100 200
meters
B
Gravels
Basaltic Andesite dikes
Intermediate porphyry dikes
Biotite Tonalite - porphyritic
Biotite Tonalite - equigranular
Quartz Monzonite
Oligocene-Miocene Coya Machali Formation

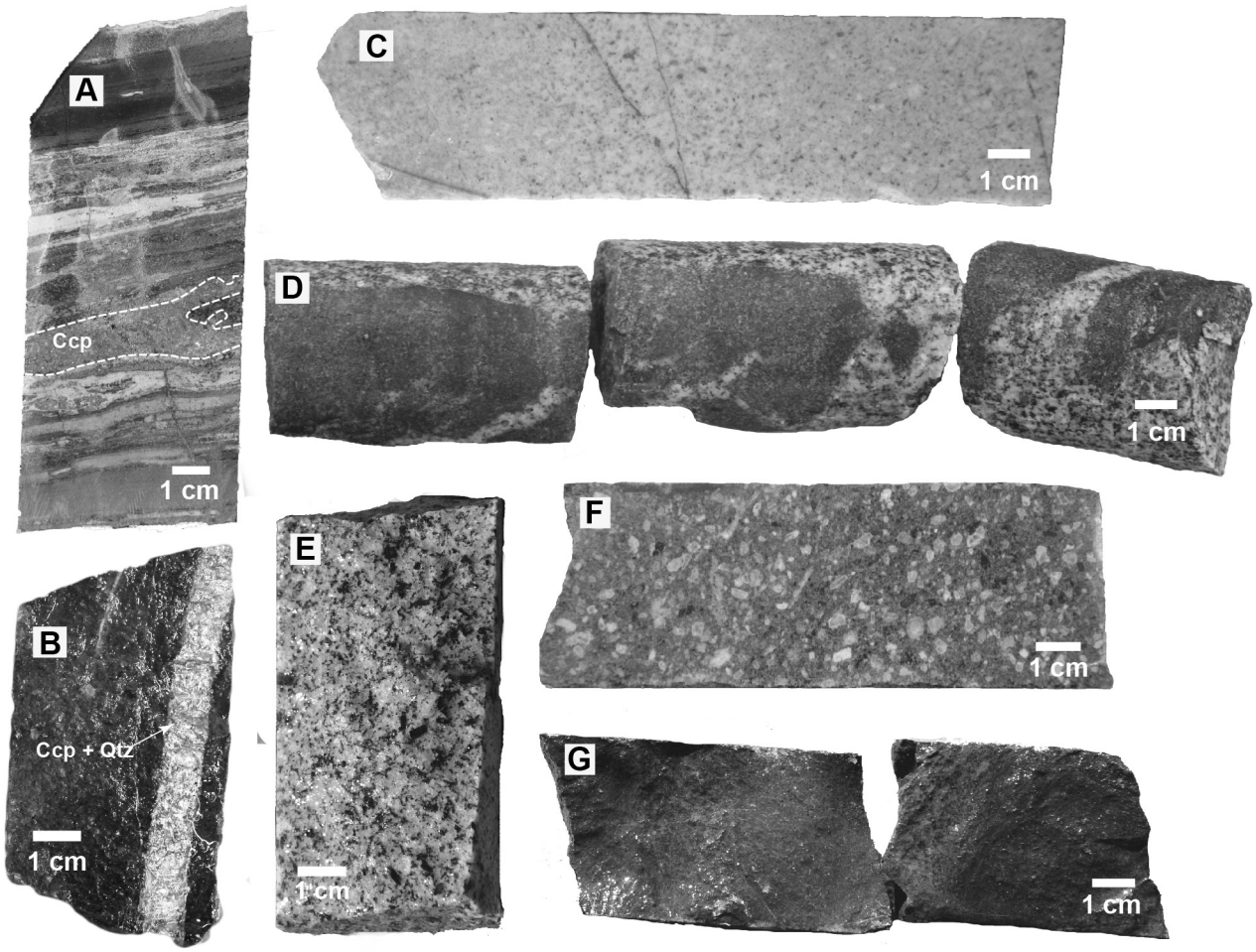

Gilmer, Figure 4, B31524

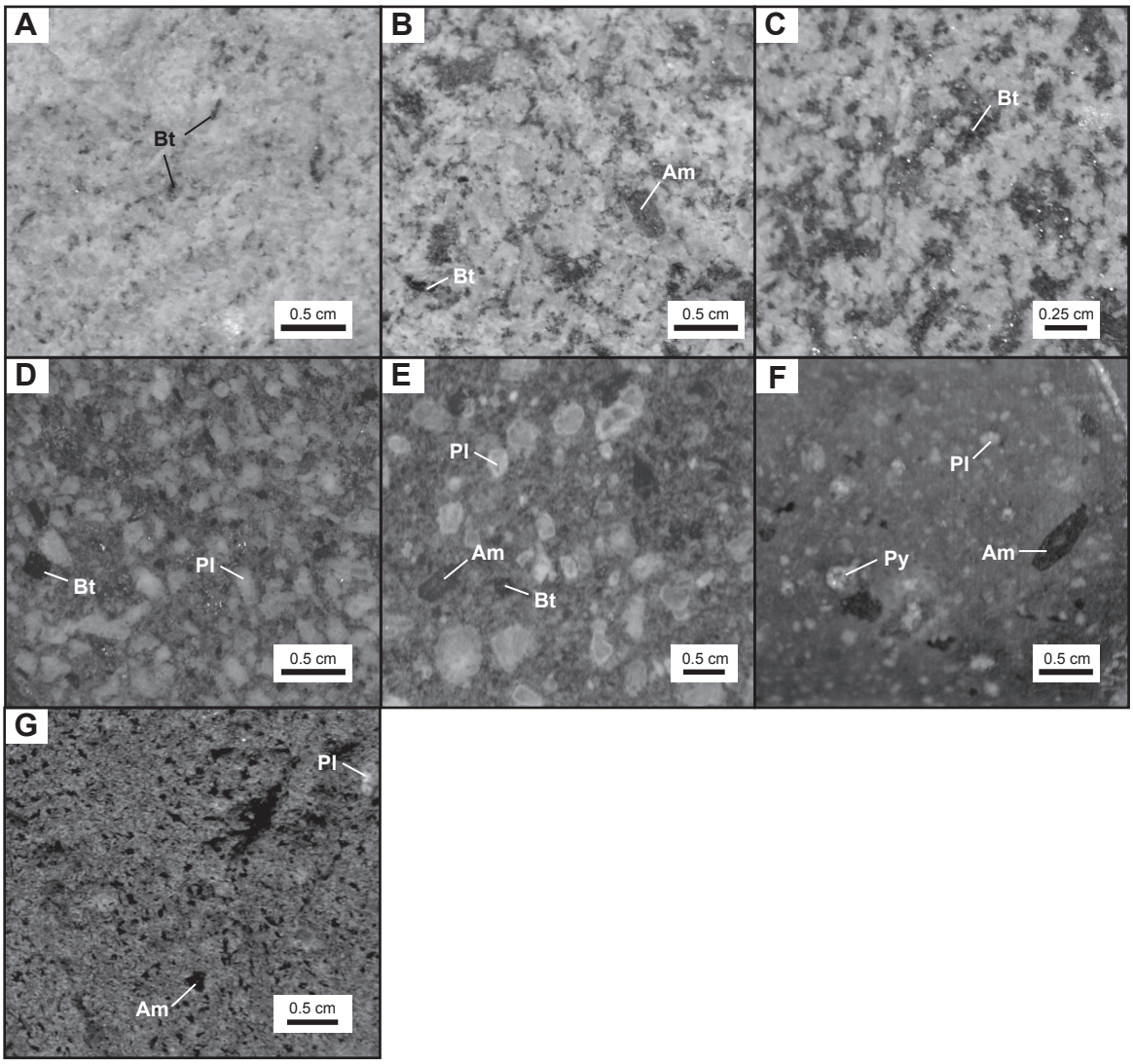

Gilmer, Figure 5, B31524

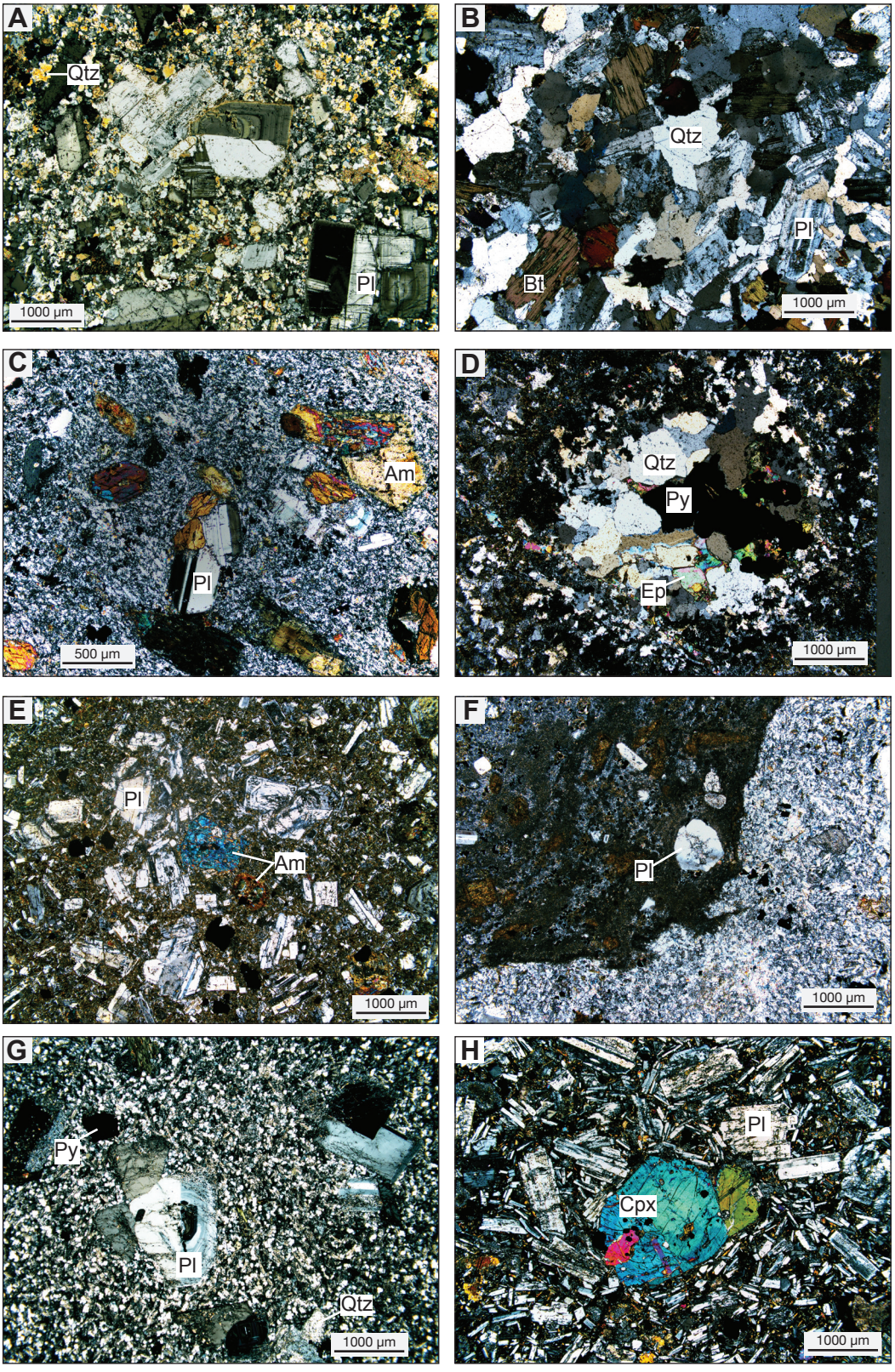

Gilmer, Figure 6, B31524

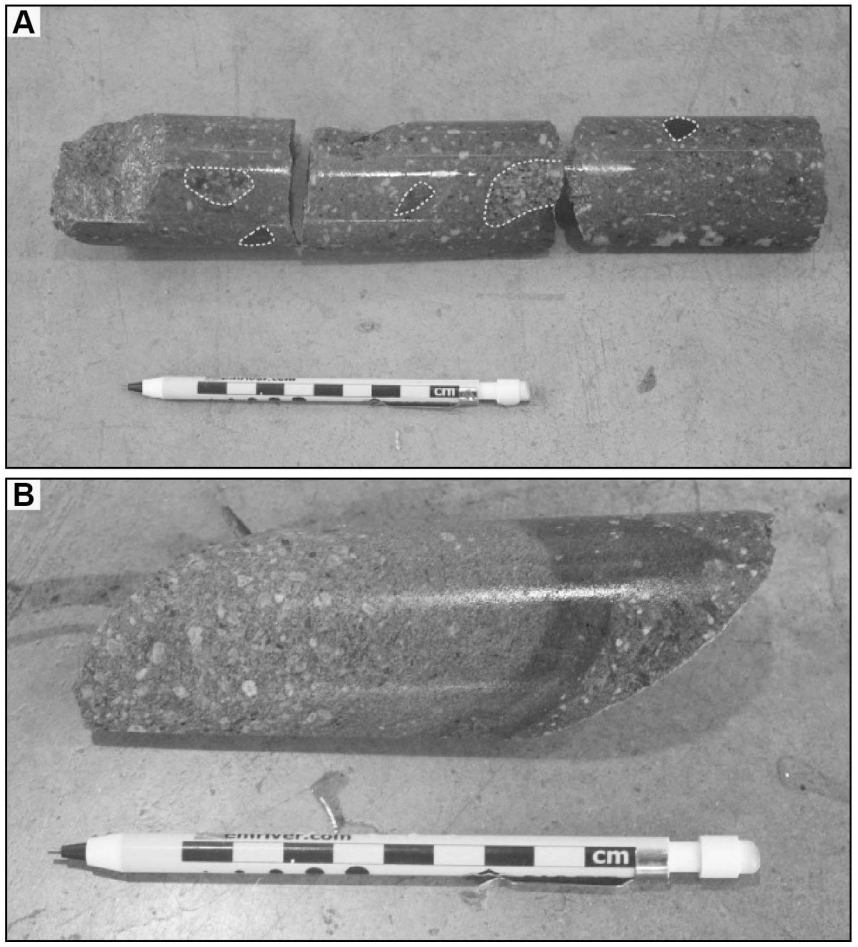

Gilmer, Figure 7, B31524

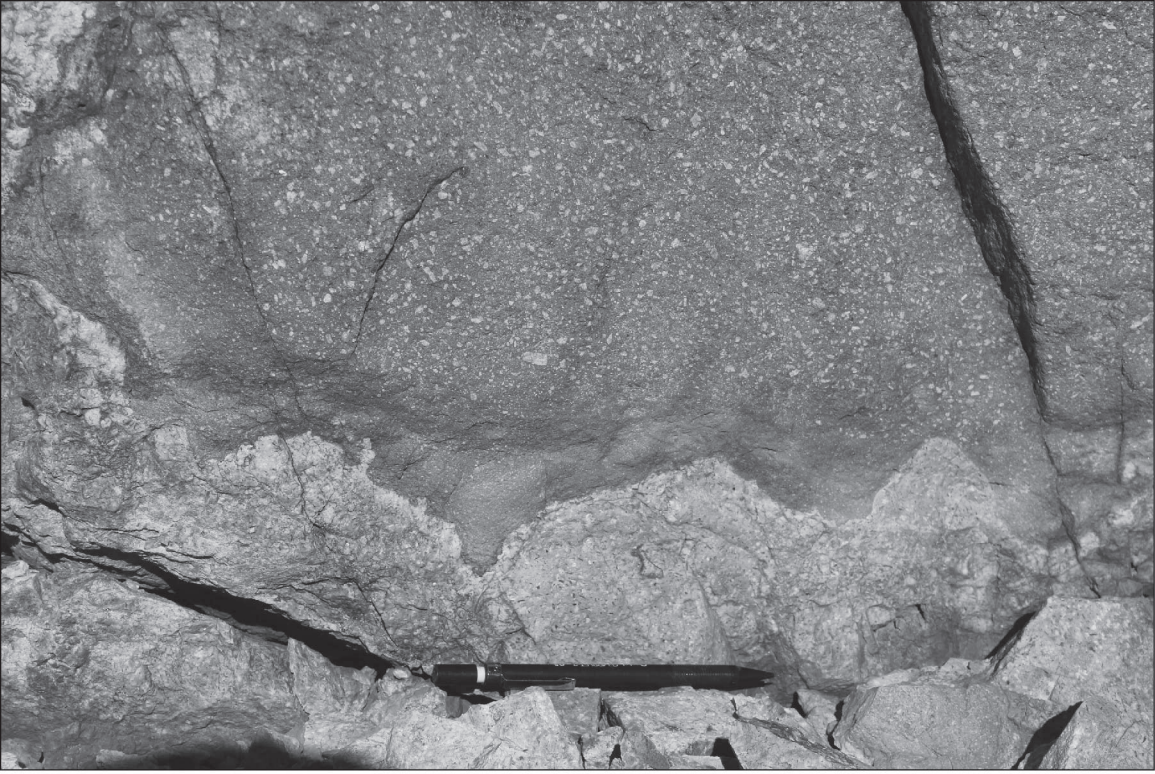

Gilmer, Figure 8, B31524

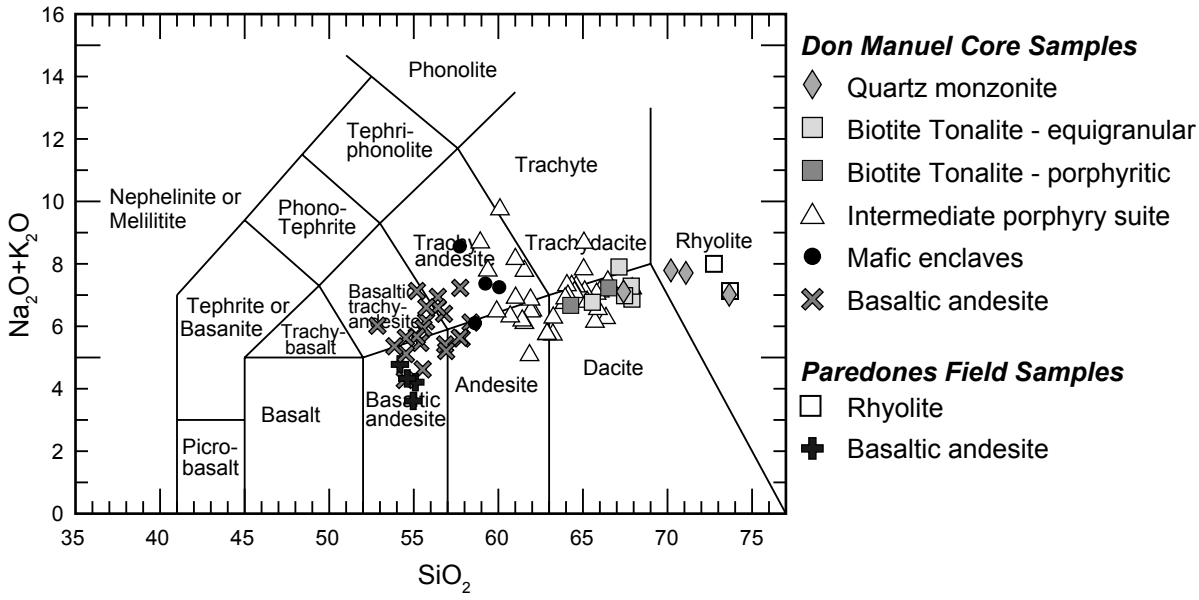

Gilmer, Figure 9, B31524

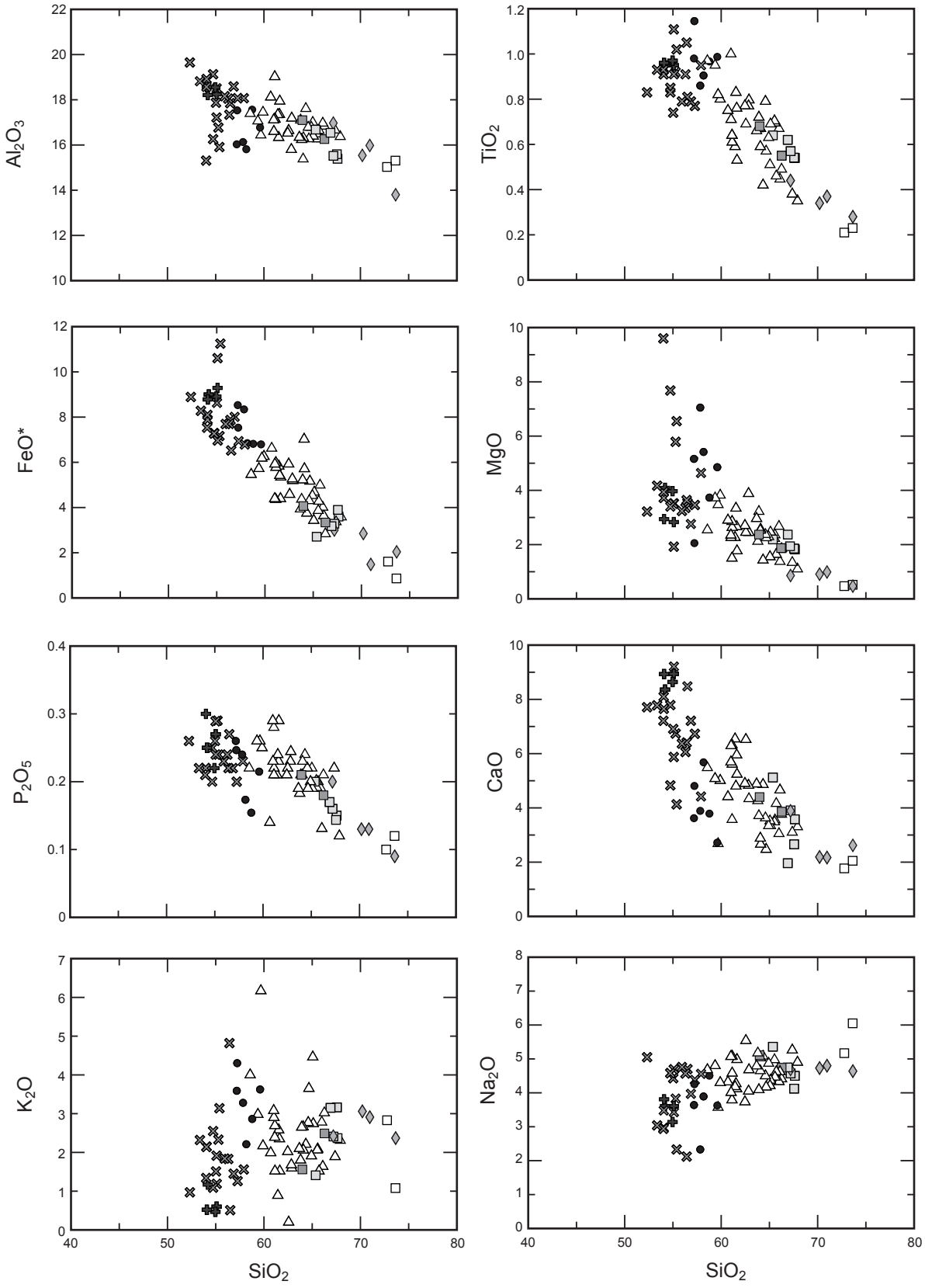

Gilmer, Figure 10, B31524

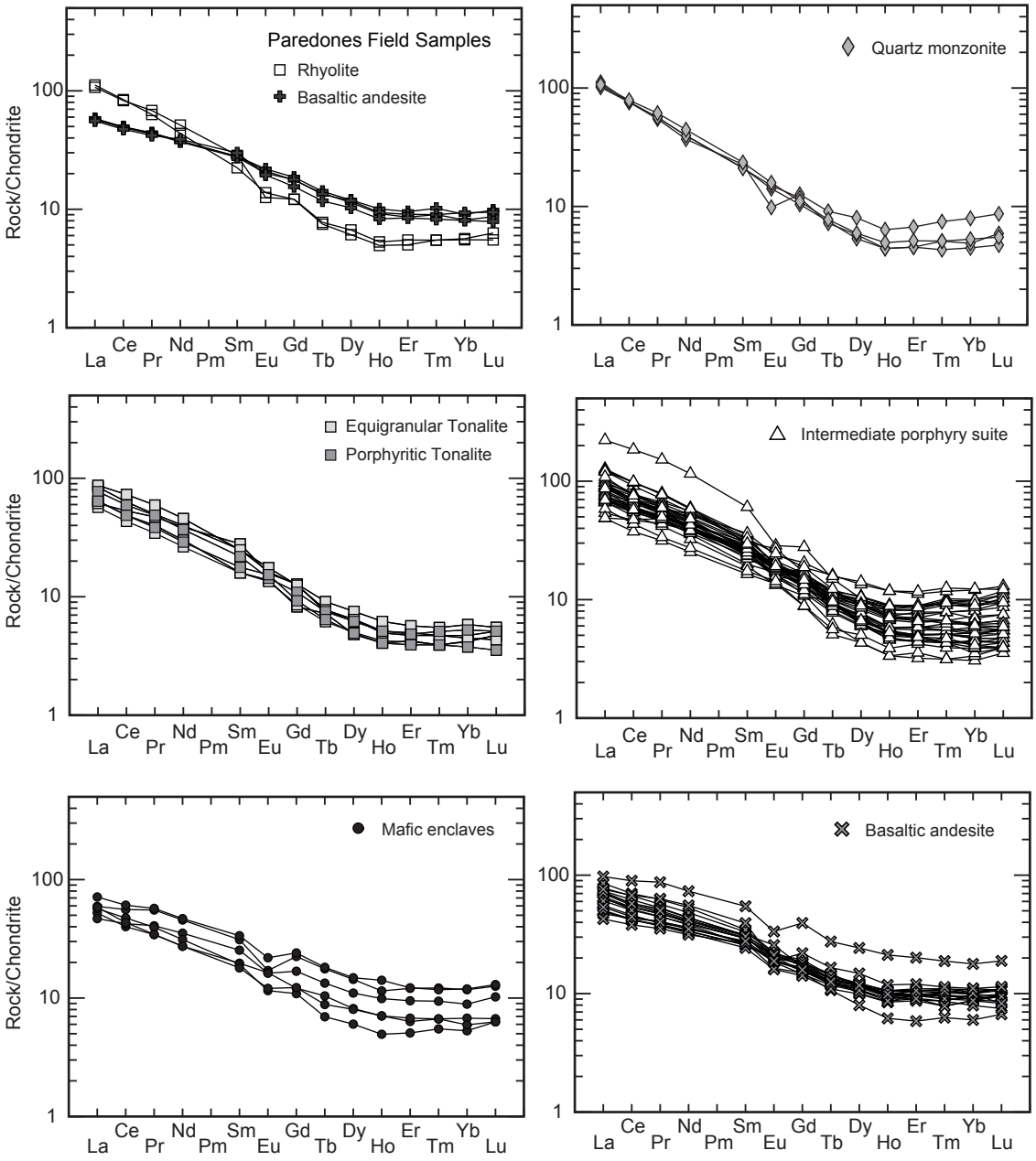

Gilmer, Figure 11, B31524

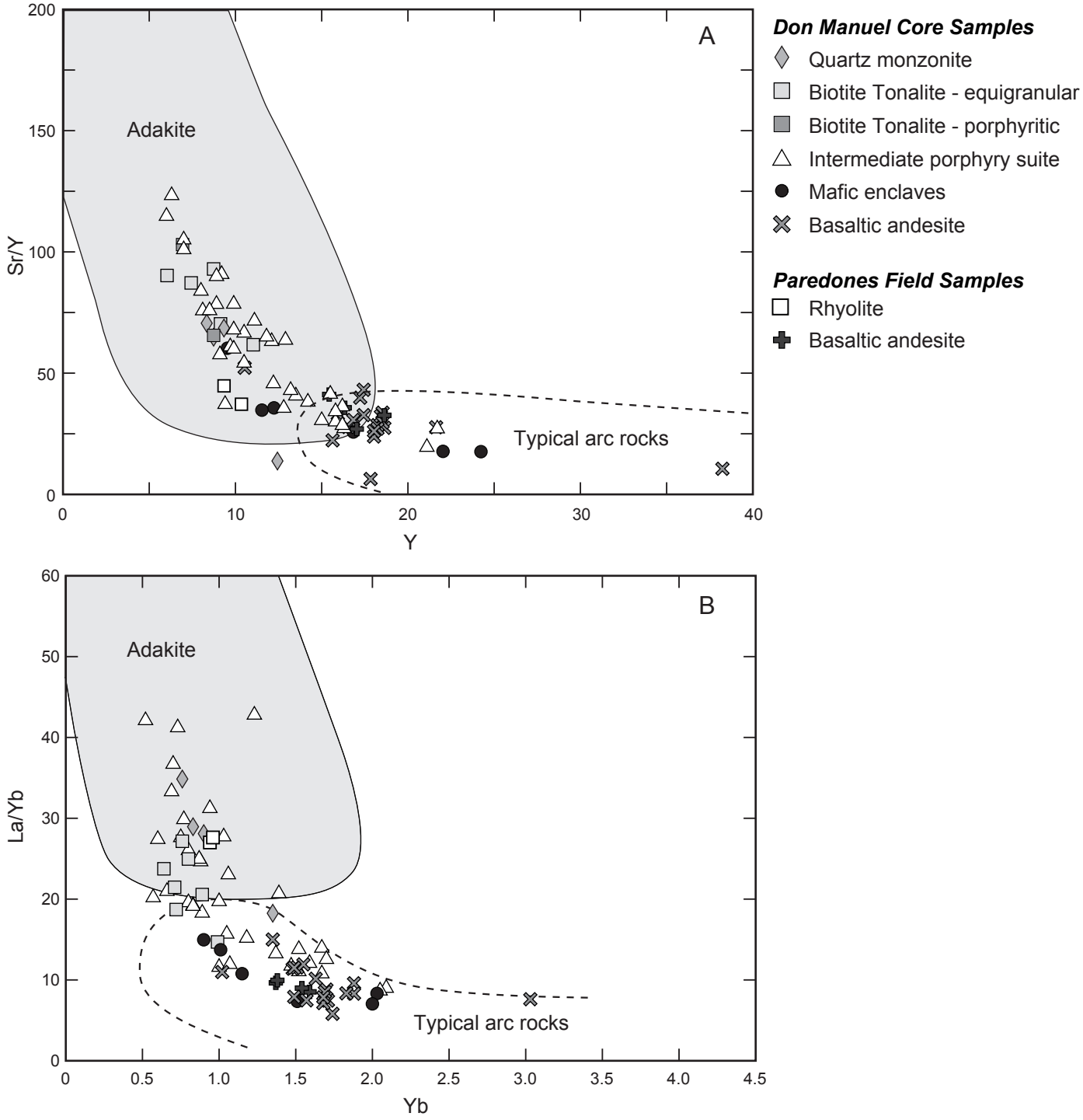

Gilmer, Figure 12, B31524

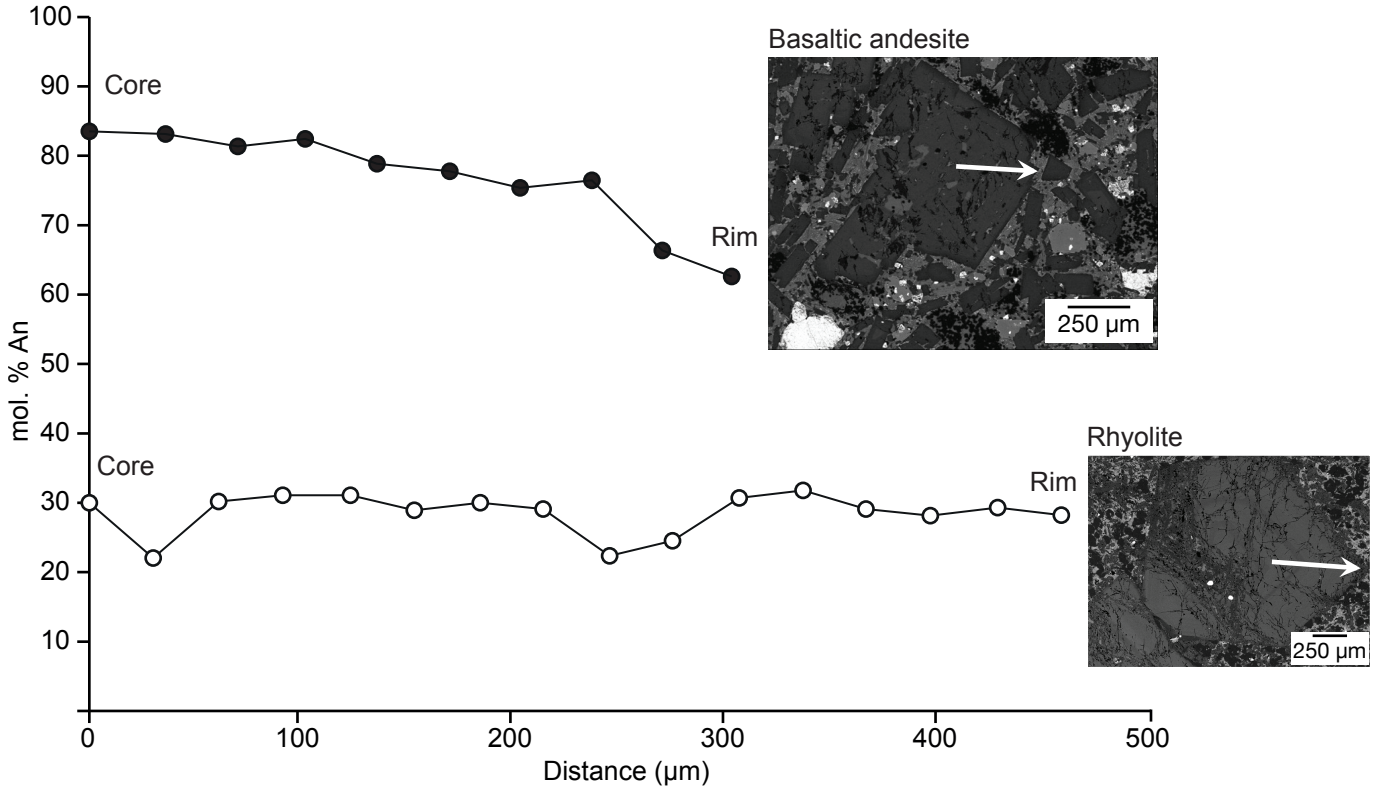

Gilmer, Figure 13, B31524

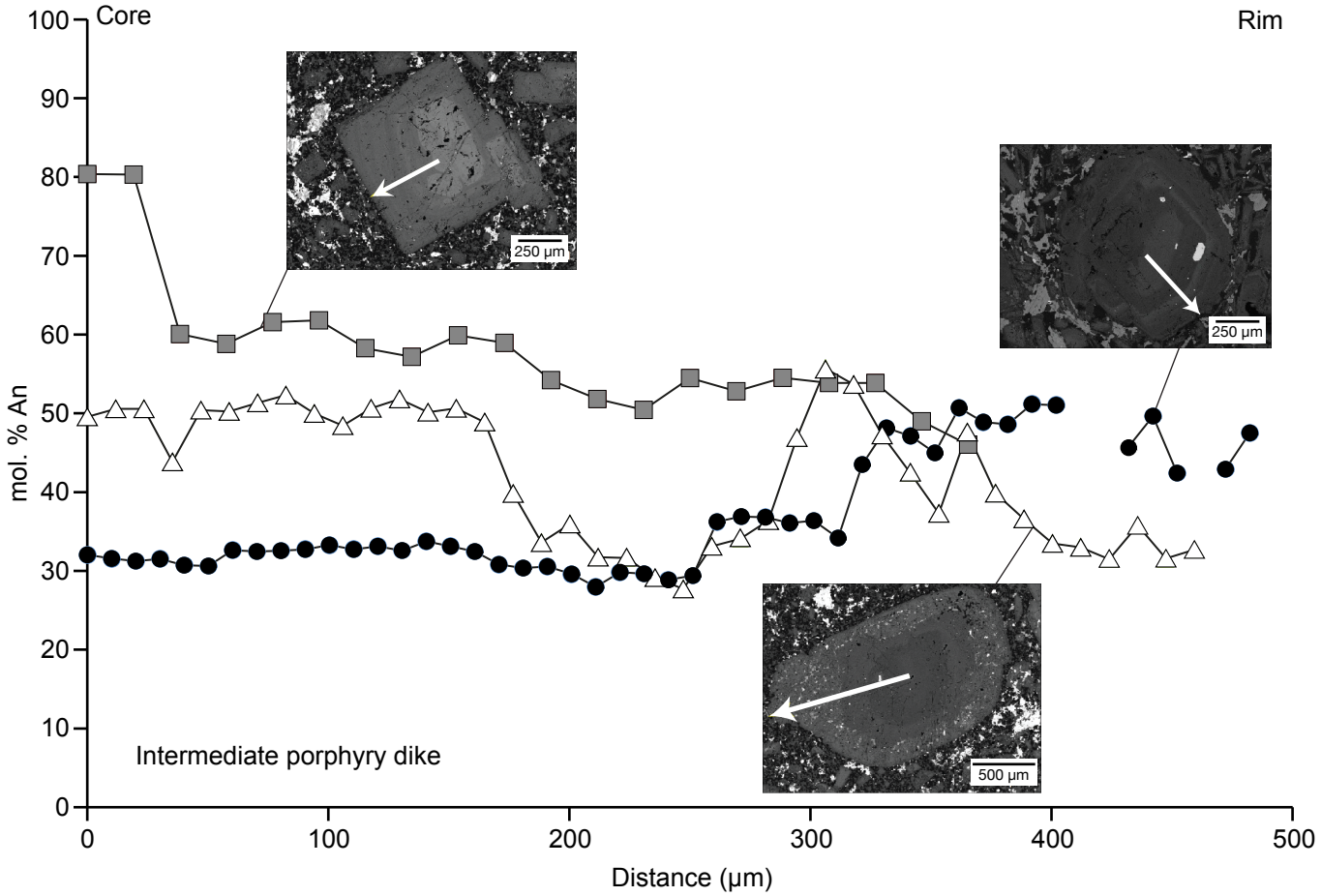

Gilmer, Figure 14, B31524

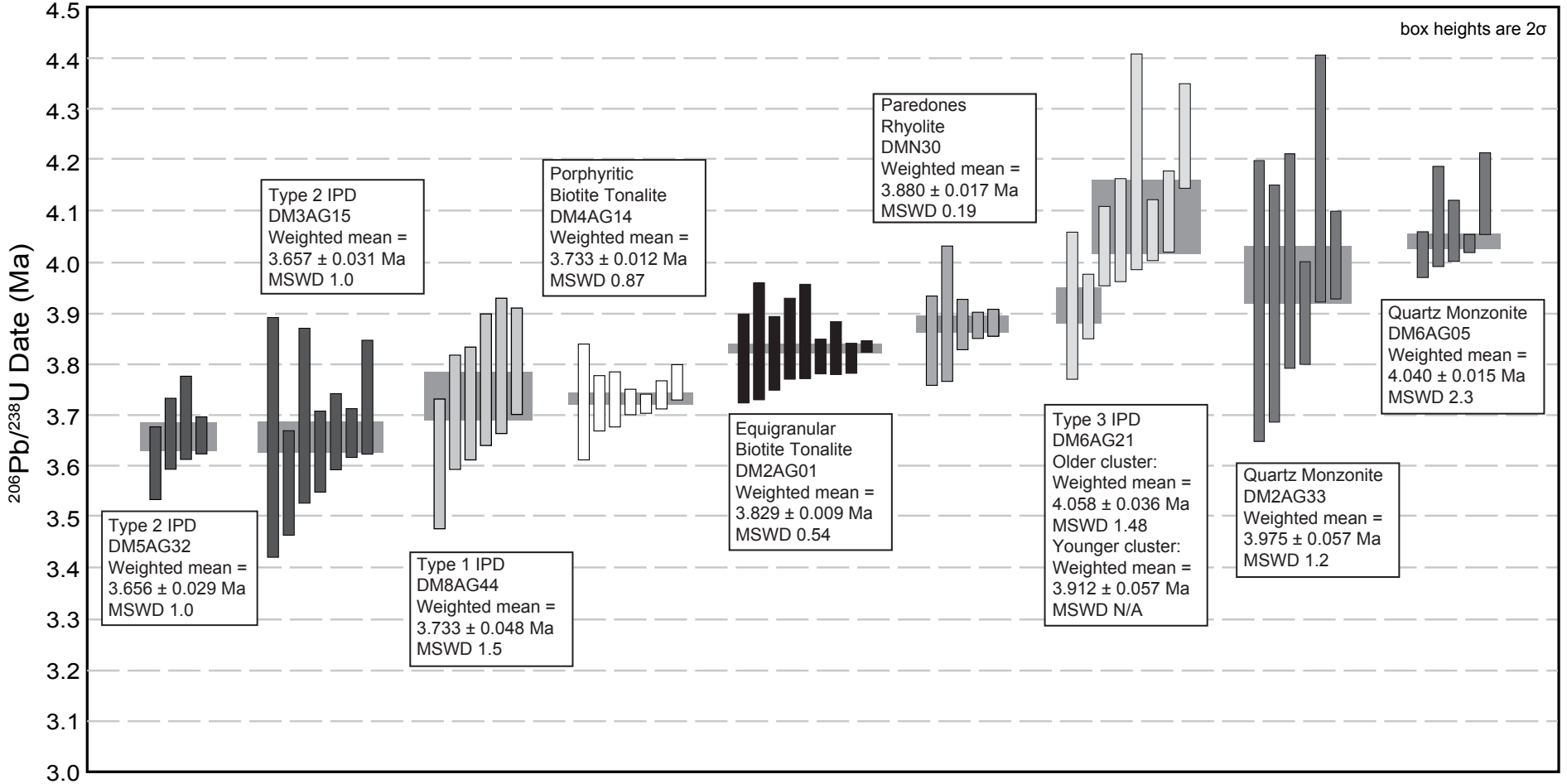

Gilmer, Figure 15, B31524

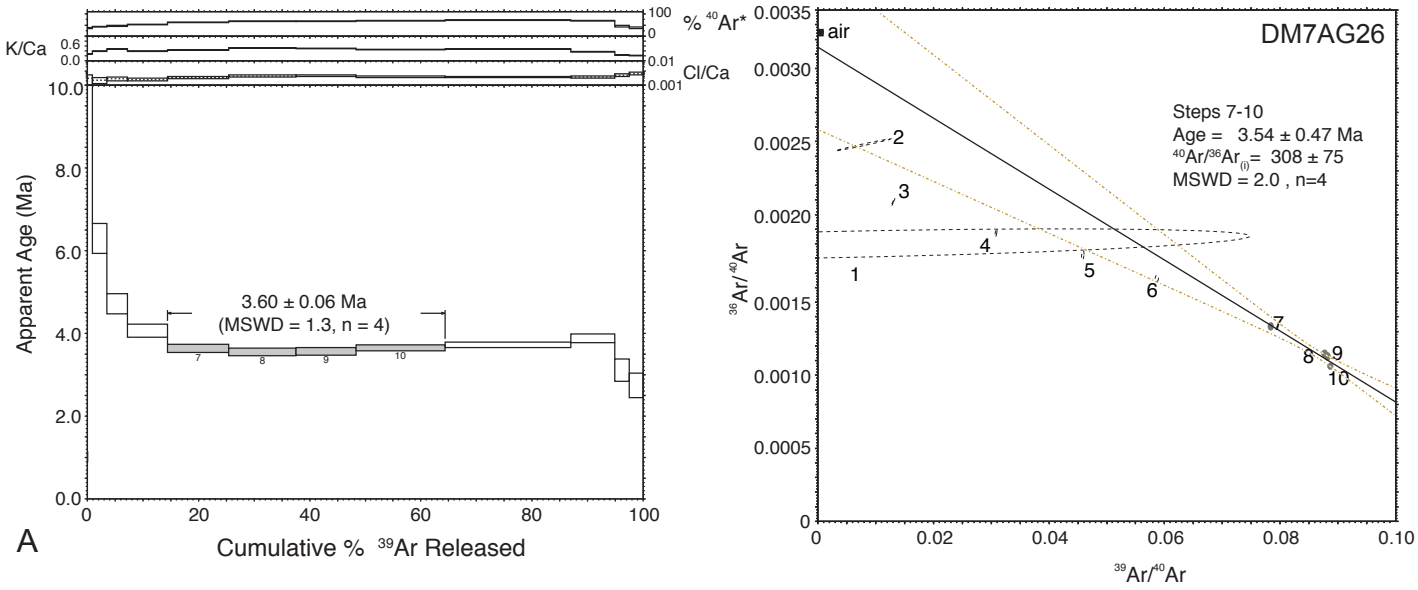

A

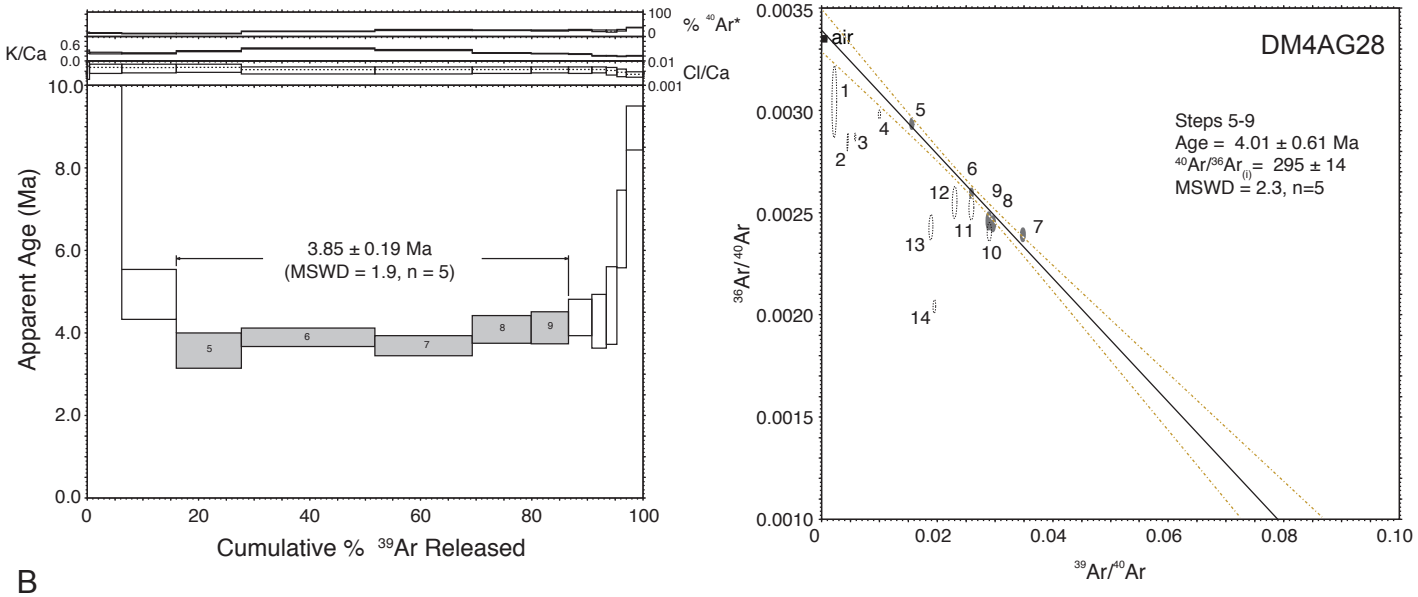

B

Gilmer, Figure 16, B31524

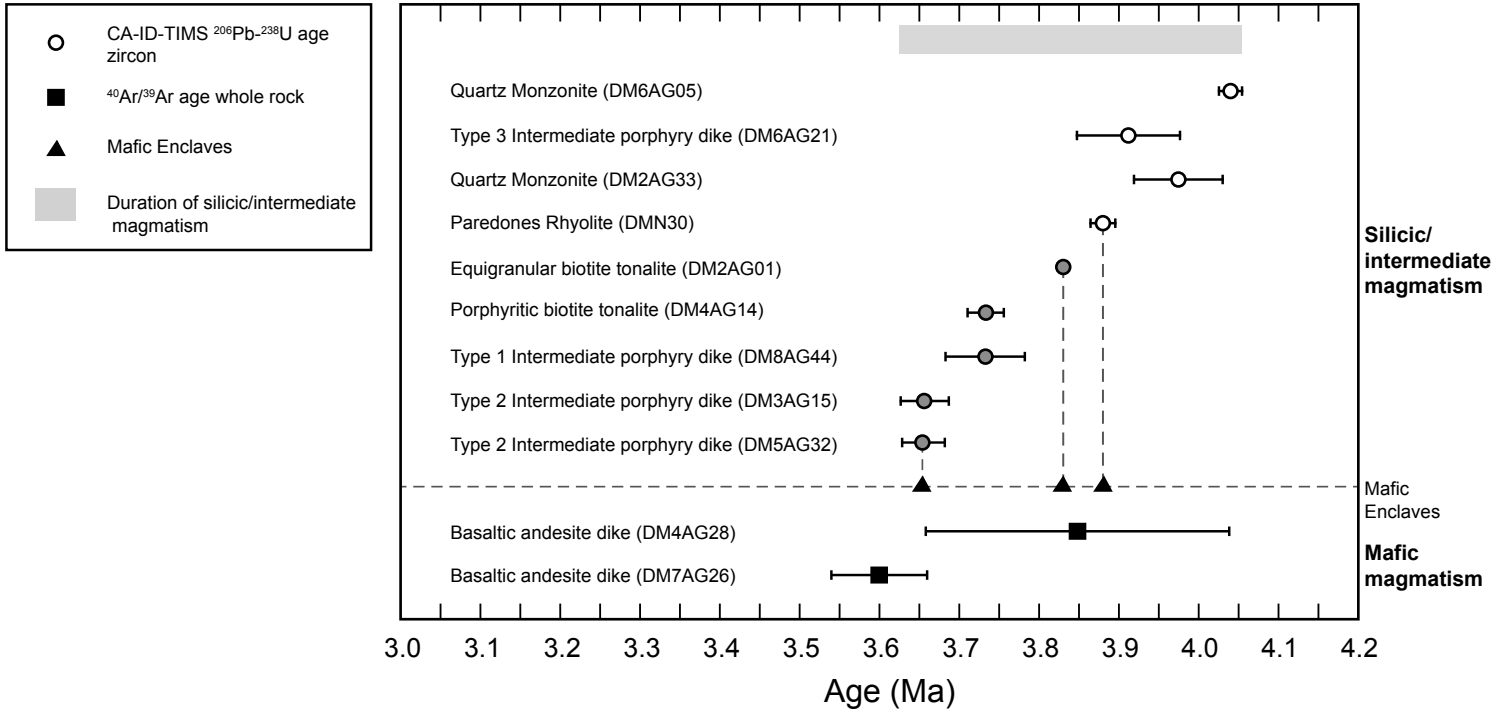

Gilmer, Figure 17, B31524

TABLE 1. REPRESENTATIVE BULK ROCK CHEMICAL ANALYSES OF THE DON MANUEL IGNEOUS COMPLEX

	Don Manuel Principal units													Paredones units			
Sample	DM2AG33	DM6AG05	DM2AG01	DM4AG14	DM5AG13	DM6AG11	DM6AG21	DM8AG53	DM2AG47	DM1AG10	DM5AG07	DM6AG17	DM8AG40	DMN30	DMN36	DMN16	DMN17
Rock Type	QM	QM	BT	BT	IPD	IPD	IPD	IPD	ME	ME	BA	BA	BA	PR	PR	PBA	PBA
SiO_2	68.79	69.79	67.33	62.95	63.18	59.77	61.71	60.38	54.49	55.89	55.23	54.02	51.38	71.7	71.57	52.52	51.31
TiO_2	0.34	0.36	0.54	0.67	0.56	0.8	0.68	0.58	1.09	0.83	0.92	0.82	0.82	0.21	0.22	0.92	0.9
Al_2O_3	15.22	15.71	15.54	16.82	15.9	15.86	16.41	17.04	16.69	15.59	17.75	18.89	19.3	14.81	14.88	17.73	17.24
Fe_2O_3*	0.99	N.D.	1.06	N.D.	N.D.	1.38	N.D.	N.D.	N.D.	N.D.	1.86	N.D.	N.D.	0.37	N.D.	N.D.	2.48
FeO	1.90	1.46	2.93	4.00	5.05	4.02	4.51	5.73	7.17	8.06	5.97	7.18	8.73	1.25	0.84	8.52	6.29
MnO	0.05	0.03	0.03	0.06	0.02	0.06	0.1	0.07	0.06	0.05	0.14	0.11	0.1	0.07	0.06	0.16	0.17
MgO	0.89	0.98	1.85	2.34	2.2	3.24	2.41	2.22	1.96	6.81	3.37	3.36	3.16	0.46	0.5	3.8	3.88
CaO	2.15	2.13	2.65	4.33	2.41	4.66	6.43	6.43	4.58	3.76	6.03	7.69	7.57	1.74	1.99	8.26	7.91
Na_2O	4.64	4.72	4.11	5.03	4.07	4.15	5.46	4.11	4.05	2.25	4.61	4.52	4.96	5.09	5.89	3.01	3.41
K_2O	3.00	2.87	3.15	1.53	3.56	2.51	0.19	0.87	4.1	3.17	1.78	1.08	0.96	2.79	1.05	0.45	1.11
P_2O_5	0.13	0.13	0.14	0.21	0.18	0.24	0.21	0.21	0.23	0.24	0.25	0.25	0.26	0.1	0.12	0.21	0.24
LOI†	1.32	0.95	1.16	0.57	2.43	2.31	2.06	0.56	3.86	1.9	1.61	1.48	0.52	0.99	2.43	3.1	4.03
Total	99.41	99.13	100.49	98.51	99.58	98.99	100.2	98.2	98.29	98.55	99.51	99.4	97.75	99.57	99.54	98.67	98.98
S§	<0.02	0.54	0.58	<0.02	2.88	0.83	1.61	0.02	2.98	1.79	<0.02	1.24	<0.02	<0.02	<0.02	<0.02	<0.02
Sc	2.40	3.10	6.80	8.30	7.1	9.8	8.1	10.5	19.5	16.6	17.1	15.7	13.8	2.6	2.2	18.1	18.4
V	38.80	52.70	80.70	111.20	98.7	126	117.5	120.1	188.8	160.2	198.8	185.5	177.5	18.8	25.3	204.2	201.1
Cr	10.60	6.60	35.40	35.80	41.8	85.8	31.6	29.8	83.5	303.2	6.3	6.7	6.4	8.6	11.5	13.4	13.5
Co	5.70	3.50	10.60	10.00	21.7	11.8	8.2	9.7	34.2	11.9	12.5	10.4	18.1	2.8	1.2	23.1	23
Ni	16.60	4.50	15.20	15.80	13.8	22.4	55.1	25.4	46.9	113.3	13.6	7.7	17.2	16.4	2.9	69.9	15.1
Zn	48.20	10.10	24.80	39.00	12.8	25.8	37.5	67.9	44.2	35.4	45.7	37.2	62.8	24.8	6.9	85.3	73.9
Ga	20.10	16.50	19.50	17.60	18.9	19.9	17.7	17.2	19.7	19.8	15.9	19.2	25.8	19.7	18.8	19.4	17.8
Rb	70.20	56.90	144.50	46.70	120.1	93.8	5	45.3	117.5	210.2	77.2	46.6	48.9	67.7	30.9	7.6	19.8
Sr	565.00	586.90	542.30	711.60	688.4	794.3	766.8	586.3	429.3	573.8	551.4	625.5	600.4	436.9	394.7	608.8	460.2
Y	8.70	8.30	6.00	6.90	6	11.1	11.8	16.2	24.2	9.5	18.5	18.5	21.6	9.3	10.6	18.6	17
Zr	178.70	124.80	183.00	101.80	127.1	133.6	124.6	101.4	172.9	115.4	79.5	81.6	81.9	126.4	125.9	92.3	83.4
Nb	4.32	5.10	3.92	3.25	4.27	5.26	4.37	3.06	4.47	4.33	2.7	2.68	3.34	5.65	5.32	2.91	2.53
Sn	6.78	0.15	1.44	0.95	1.19	1.34	1.1	1.06	1.48	5.13	1.12	1.35	2.02	4.14	0.7	4.54	3.45

Cs	2.98	1.18	5.17	2.44	3.11	4.37	0.33	3.29	3.43	12.94	6.83	1.63	5.01	1.16	2.93	0.51	0.7
Ba	750.80	908.80	678.20	502.00	965.1	574.9	203.3	161.2	611.4	297.6	281.5	273.5	155.8	756.6	253.1	258.1	248.7
La	24.03	26.49	15.24	15.20	21.89	21.68	12.77	17.99	16.91	13.47	15.61	14.37	18.02	26.52	25.39	13.84	13.55
Ce	46.53	46.62	29.75	29.78	43.07	45.84	28.65	35.67	37.24	29.05	32.7	30.97	41.29	51.59	50.63	30.22	29.87
Pr	5.38	5.35	3.80	3.65	5.33	6.1	4.16	4.7	5.43	3.76	4.48	4.23	6.01	6	6.48	4.18	4.12
Nd	18.52	18.57	14.03	13.50	20.44	24.29	17.78	18.7	21.86	14.57	18.94	18.02	25.94	20.42	24	17.64	17.34
Sm	3.22	3.24	2.44	2.71	3.86	4.96	4.05	4.1	5.14	2.95	4.82	4.49	6.02	3.43	4.36	4.28	4.2
Eu	0.87	0.82	0.80	0.89	0.94	1.17	1.11	1.1	1.27	0.67	1.49	1.23	1.09	0.8	0.73	1.27	1.17
Gd	2.43	2.14	1.69	1.90	2.28	3.03	2.88	3.15	4.94	2.24	3.45	3.51	4.51	2.49	2.5	3.83	3.65
Tb	0.27	0.28	0.27	0.24	0.23	0.37	0.37	0.44	0.68	0.26	0.5	0.51	0.62	0.28	0.29	0.53	0.5
Dy	1.47	1.36	1.22	1.25	1.1	1.97	2.08	2.71	3.77	1.53	2.99	3.08	3.76	1.55	1.7	3.04	3
Ho	0.25	0.25	0.23	0.23	0.19	0.33	0.38	0.51	0.8	0.28	0.59	0.6	0.67	0.28	0.3	0.57	0.53
Er	0.75	0.75	0.70	0.65	0.53	0.97	1.06	1.47	2.02	0.84	1.73	1.77	1.99	0.83	0.91	1.58	1.5
Tm	0.13	0.11	0.10	0.10	0.08	0.15	0.17	0.24	0.3	0.14	0.26	0.27	0.29	0.14	0.14	0.26	0.23
Yb	0.83	0.76	0.71	0.64	0.52	0.88	1.07	1.67	2.03	0.9	1.88	1.69	1.88	0.96	0.94	1.54	1.59
Lu	0.15	0.12	0.12	0.09	0.09	0.13	0.17	0.24	0.33	0.16	0.27	0.28	0.29	0.16	0.14	0.25	0.24
Hf	4.28	3.27	4.21	2.61	3.3	3.47	3.14	2.66	4.43	3.05	2.18	2.22	2.24	3.46	3.27	2.59	2.34
Ta	0.37	0.37	0.35	0.26	0.3	0.35	0.28	0.19	0.33	0.28	0.16	0.16	0.17	0.44	0.41	0.17	0.18
Pb	19.72	9.03	6.68	5.16	4.91	5.73	5.65	4.05	6.25	2.92	2.69	2.15	3.96	16.97	5.22	5.13	5.31
Th	11.42	5.34	6.66	4.35	5.29	5.06	3.94	2.64	4.21	5.6	1.81	1.86	2.02	8.16	5.65	3.44	2.67
U	2.31	1.60	1.86	1.07	1.52	1.58	1.22	0.72	1.72	2.88	0.61	0.49	1.27	2.18	1.68	0.62	0.61

Note: QM—quartz monzonite; BT-biotite tonalite; IPD-intermediate porphyry dike; ME-mafic enclave; BA-basaltic andesite; PR-Paredones rhyodacite; PBA-Paredones basaltic andesite. Units in wt%.

*Fe^{2+}/Fe^{3+} by iron titration analysis at Acme Analytical Laboratories Ltd., Canada. †LOI—loss on ignition. §Sulfur analyzed separately at Acme Analytical Laboratories Ltd., Canada.

TABLE 2. REPRESENTATIVE COMPOSITIONS OF PLAGIOCLASE PHENOCRYSTS AND MICROPHENOCRYSTS

Sample	DM1AG31	DM1AG31	DM8AG53	DM8AG53	DM6AG11	DM6AG11	DM3AG38	DM3AG38	DMN30	DMN30	DMN16	DMN16	DM6AG05	DM6AG05	DM2AG23	DM2AG23	DM5AG34
Host	IPD	IPD	IPD	IPD	IPD	IPD	ME	ME	PR	PR	PBA	PBA	QM	QM	BT	BT	BA
	pheno.	micro-pheno.	pheno.	micro-pheno.	pheno.	micro-pheno.	micro-pheno.	micro-pheno.	pheno.	micro-pheno.	pheno.	micro-pheno.	pheno.	micro-pheno.	pheno.	micro-pheno.	pheno.
SiO_2	52.53	53.37	49.90	54.89	54.70	54.57	48.54	56.53	60.95	62.96	46.30	46.50	60.74	65.96	60.38	59.42	49.12
TiO_2	0.02	0.02	0.02	0.03	0.03	0.02	bdl	bdl	bdl	bdl	0.02	0.02	bdl	bdl	bdl	0.01	0.03
Al_2O_3	29.74	28.86	31.92	27.93	27.64	27.85	32.57	27.61	24.97	23.38	33.26	32.68	24.83	21.72	25.23	25.06	32.21
FeO	0.23	0.49	0.52	0.38	0.44	0.49	0.54	0.20	0.15	0.14	0.55	0.57	0.11	bdl	0.19	0.19	0.54
MnO	0.01	bdl	bdl	bdl	bdl	bdl	bdl	bdl	bdl	0.05	0.02	0.01	bdl	bdl	bdl	bdl	bdl
MgO	0.01	0.05	0.04	0.05	0.04	0.06	bdl	bdl	bdl	bdl	0.05	0.06	bdl	bdl	bdl	0.02	0.04
CaO	12.25	11.38	14.75	10.47	9.88	10.58	16.17	9.66	6.35	4.55	16.80	16.81	6.34	2.29	6.82	6.68	15.50
Na_2O	4.39	4.86	3.02	5.35	5.54	5.35	2.64	5.96	7.67	8.56	1.92	2.00	7.87	9.79	7.56	7.30	2.77
K_2O	0.14	0.27	0.08	0.13	0.17	0.18	0.05	0.19	0.30	0.64	0.06	0.03	0.25	0.18	0.20	0.24	0.07
BaO	0.02	0.00	bdl	bdl	0.02	bdl	bdl	bdl	0.02	0.11	bdl	bdl	bdl	bdl	0.03	0.05	bdl
SrO	0.23	0.21	0.15	0.14	0.37	0.37	0.11	0.14	0.23	0.20	0.11	0.11	0.26	0.09	0.12	0.18	0.15
Total	99.55	99.52	100.42	99.37	98.83	99.48	100.63	100.31	100.66	100.59	99.09	98.80	100.41	100.05	100.55	99.16	100.42
An%	60.21	55.51	72.63	51.58	49.12	51.69	76.99	46.71	30.86	21.88	82.58	82.13	30.38	11.33	32.89	33.09	75.26

Note: IPD-intermediate porphyry dike; ME-mafic enclave; QM-quartz monzonite; BT-biotite tonalite; BA-basaltic andesite; PR-Paredones rhyodacite; PBA-Paredones basaltic andesite. Units in wt%.

bdl = below detection limit

TABLE 3. U-Pb GEOCHRONOLOGY

	Dates (Ma)										Composition				Isotopic ratios							
Fraction	$^{206}Pb/^{238}U$ <Th>†	±2σ abs	$^{206}Pb/^{238}U$§	±2σ abs	$^{207}Pb/^{235}U$ §	±2σ abs	$^{207}Pb/^{206}Pb$ §	±2σ abs	Corr. coef.	% disc #	Th/U ††	Pb* (pg) §§	Pbc (pg) ##	Pb*/Pbc †††	$^{106}Pb/^{204}Pb$ §§§	$^{08}Pb/^{206}Pb$ ###	$^{206}Pb/^{238}U$ ###	±2σ %	$^{07}Pb/^{235}U$ ###	±2σ %	$^{07}Pb/^{206}Pb$ ###	±2σ %
DM2AG33																						
z1	**3.901**	**0.101**	3.801	0.102	3.785	1.186	-6.390	743.677	0.257	159.488	0.30	0.13	0.38	0.34	39.6	0.098	0.0005898	2.676	0.0037348	31.393	0.0459	30.815
z3	**3.925**	**0.275**	3.841	0.276	3.739	3.154	-61.791	2032.388	0.208	106.217	0.81	0.05	0.32	0.14	25.9	0.267	0.0005961	7.196	0.0036890	84.524	0.0449	83.326
z4	**8.701**	**0.045**	8.604	0.045	8.904	0.492	90.671	129.880	0.181	90.510	0.38	0.96	0.57	1.70	123.7	0.124	0.0013356	0.527	0.0088074	5.552	0.0478	5.481
z6	**3.920**	**0.232**	3.829	0.234	3.607	2.591	-142.155	1760.775	0.184	102.693	0.57	0.09	0.57	0.153	27.2	0.188	0.0005941	6.108	0.0035587	71.947	0.0435	71.076
z8	**4.164**	**0.242**	4.079	0.244	6.752	2.714	1106.828	782.084	0.270	99.631	0.78	0.05	0.28	0.18	27.9	0.256	0.0006330	5.977	0.0066720	40.322	0.0765	39.134
z9	**4.014**	**0.086**	3.925	0.087	3.314	1.007	-421.366	784.189	0.260	100.931	0.63	0.10	0.22	0.45	44.1	0.208	0.0006090	2.221	0.0032691	30.437	0.0389	29.936
z10	**4.004**	**0.210**	3.907	0.214	4.127	2.852	134.410	1568.242	0.491	97.093	0.40	0.04	0.19	0.21	30.8	0.133	0.0006063	5.472	0.0040726	69.240	0.0487	66.721
DM6AG05																						
z1	**4.036**	**0.017**	3.960	0.018	4.142	0.203	111.051	113.222	0.275	96.434	1.08	1.34	0.52	2.59	152.5	0.351	0.0006145	0.443	0.0040873	4.899	0.0483	4.796
z3	**4.060**	**0.059**	3.979	0.059	4.436	0.655	259.975	334.716	0.199	98.469	0.90	0.28	0.40	0.70	55.8	0.293	0.0006175	1.482	0.0043781	14.794	0.0514	14.571
z5	**4.088**	**0.096**	4.009	0.097	4.744	1.158	395.842	538.717	0.232	98.987	0.95	0.31	0.70	0.44	41.3	0.312	0.0006220	2.414	0.0046827	24.470	0.0546	24.026
z6	**4.014**	**0.044**	3.936	0.044	3.659	0.529	-175.359	353.309	0.306	102.244	0.98	0.47	0.47	0.998	71.4	0.319	0.0006107	1.125	0.0036096	14.474	0.0429	14.169
z7	**4.136**	**0.078**	4.047	0.079	4.368	0.915	185.133	478.449	0.267	97.814	0.65	0.26	0.50	0.52	48.1	0.213	0.0006280	1.957	0.0043110	20.983	0.0498	20.547
DMN30																						
8_zb	**3.847**	**0.086**	3.757	0.087	3.964	1.006	131.552	588.803	0.211	97.144	0.60	0.29	0.69	0.42	42.8	0.197	0.0005829	2.305	0.0039111	25.421	0.0487	25.038
z1	**8.443**	**0.148**	8.360	0.148	8.760	1.656	120.087	440.197	0.221	93.038	0.86	1.12	1.93	0.58	49.9	0.278	0.0012977	1.774	0.0086647	18.990	0.0484	18.679
z2	**3.879**	**0.049**	3.796	0.049	4.335	0.557	315.066	287.498	0.234	98.795	0.82	0.22	0.27	0.80	62.2	0.269	0.0005890	1.304	0.0042784	12.882	0.0527	12.640
z3	**3.879**	**0.026**	3.790	0.026	4.021	0.296	144.761	170.616	0.195	97.382	0.65	0.66	0.47	1.40	98.8	0.212	0.0005880	0.698	0.0039676	7.377	0.0490	7.273
z5	**3.902**	**0.133**	3.827	0.135	7.809	1.954	1514.258	441.474	0.544	99.747	1.08	0.10	0.25	0.41	38.8	0.353	0.0005938	3.524	0.0077208	25.124	0.0943	23.394
z6	**7.869**	**0.043**	7.789	0.044	8.024	0.617	79.130	180.611	0.233	90.157	0.91	0.52	0.28	1.86	118.8	0.295	0.0012089	0.560	0.0079333	7.716	0.0476	7.605
z7	**3.884**	**0.027**	3.792	0.027	4.085	0.323	180.547	179.389	0.354	97.900	0.55	0.28	0.19	1.47	105.1	0.182	0.0005884	0.719	0.0040311	7.922	0.0497	7.697
DM4AG14																						
10_006	**3.727**	**0.115**	3.650	0.116	4.052	1.308	250.137	731.668	0.219	98.541	1.02	0.22	0.65	0.34	35.8	0.334	0.0005663	3.170	0.0039983	32.338	0.0512	31.795
10_011	**3.741**	**0.028**	3.695	0.028	3.827	0.322	87.807	195.730	0.287	95.792	2.01	1.23	0.65	1.88	98.4	0.653	0.0005734	0.755	0.0037764	8.440	0.0478	8.255
z2	**3.725**	**0.055**	3.634	0.055	3.982	0.625	219.736	357.748	0.216	98.346	0.60	1.38	2.18	0.63	55.0	0.196	0.0005639	1.526	0.0039293	15.718	0.0506	15.461
z3	**3.724**	**0.019**	3.683	0.019	3.836	0.206	101.205	124.984	0.221	96.361	2.19	2.81	1.04	2.69	129.4	0.709	0.0005715	0.513	0.0037853	5.375	0.0481	5.285
z4	**3.727**	**0.025**	3.673	0.025	3.969	0.285	187.961	164.798	0.226	98.046	1.74	0.80	0.43	1.89	103.0	0.567	0.0005699	0.689	0.0039168	7.204	0.0499	7.081
z5	**3.766**	**0.035**	3.732	0.035	4.144	0.383	251.211	210.209	0.186	98.515	2.38	1.24	0.83	1.49	77.6	0.771	0.0005790	0.934	0.0040900	9.264	0.0513	9.137
Z8	**3.732**	**0.055**	3.703	0.028	3.694	0.350	-2.466	222.780	0.374	250.160	2.57	1.42	0.66	2.15	101.2	0.830	0.0005747	0.768	0.0036446	9.498	0.0460	9.238
DM2AG01																						
z5	**3.849**	**0.080**	3.756	0.081	4.266	0.928	302.417	487.568	0.240	98.758	0.51	0.76	1.70	0.44	44.6	0.167	0.0005828	2.144	0.0042101	21.801	0.0524	21.388
z6	**3.833**	**0.011**	3.732	0.011	3.994	0.124	165.050	71.459	0.258	97.739	0.23	0.85	0.27	3.12	220.1	0.076	0.0005790	0.302	0.0039408	3.122	0.0494	3.057
z8	**3.831**	**0.052**	3.739	0.052	3.867	0.586	84.294	355.513	0.190	95.564	0.55	0.43	0.64	0.67	57.8	0.180	0.0005802	1.398	0.0038156	15.188	0.0477	14.985
z9	**3.810**	**0.029**	3.724	0.029	3.532	0.329	-125.806	226.155	0.249	102.960	0.73	0.36	0.28	1.31	92.6	0.240	0.0005779	0.774	0.0034843	9.320	0.0438	9.158
z10	**3.814**	**0.033**	3.732	0.033	3.619	0.372	-71.544	247.649	0.223	105.217	0.89	0.26	0.22	1.17	81.7	0.292	0.0005792	0.893	0.0035701	10.296	0.0447	10.134

z11	**3.810**	**0.087**	3.728	0.088	3.588	1.019	-89.611	686.796	0.232	104.160	0.85	0.15	0.33	0.44	42.2	0.279	0.0005784	2.357	0.0035395	28.460	0.0444	28.008
z12	**3.864**	**0.093**	3.774	0.093	3.941	1.034	107.166	612.532	0.193	96.479	0.61	0.21	0.55	0.39	40.6	0.201	0.0005856	2.476	0.0038885	26.293	0.0482	25.929
z13	**3.821**	**0.072**	3.735	0.073	4.093	0.833	220.134	464.189	0.214	98.303	0.77	0.11	0.22	0.52	46.9	0.252	0.0005796	1.944	0.0040395	20.388	0.0506	20.062
z14	**3.844**	**0.115**	3.760	0.116	4.572	1.267	456.353	608.194	0.171	99.176	0.80	0.22	0.69	0.32	36.0	0.261	0.0005835	3.075	0.0045132	27.769	0.0561	27.412
DM6AG21																						
8_z001	**3.911**	**0.063**	3.834	0.065	4.035	3.883	125.949	2259.073	0.281	96.956	1.02	0.12	1.00	0.12	24.2	0.333	0.00059493	1.700	0.0039821	96.426	0.0486	95.963
8_z010	**4.063**	**0.059**	3.986	0.061	4.138	3.623	93.657	2067.319	0.284	95.744	1.05	0.09	0.68	0.13	24.9	0.341	0.00061853	1.538	0.0040839	87.716	0.0479	87.291
z1	**4.195**	**0.209**	4.122	0.217	3.494	5.889	-411.126	4335.140	0.575	101.003	1.18	0.03	0.31	0.10	23.4	0.386	0.00063969	5.262	0.0034472	168.812	0.0391	165.840
z2	**3.913**	**0.143**	3.838	0.149	4.371	5.759	308.945	2964.159	0.489	98.758	1.09	0.04	0.40	0.09	22.7	0.356	0.00059556	3.889	0.0043143	132.036	0.0526	130.179
z3	**4.062**	**0.100**	3.990	0.104	5.333	3.747	663.403	1481.748	0.501	99.399	1.18	0.05	0.31	0.15	25.6	0.385	0.00061915	2.607	0.0052665	70.434	0.0617	69.164
z4	**4.245**	**0.101**	4.191	0.105	5.628	5.538	673.813	2092.798	0.332	99.378	1.75	0.09	0.83	0.11	22.9	0.569	0.00065032	2.509	0.0055585	98.660	0.0620	97.855
z5	**4.099**	**0.078**	4.033	0.082	7.316	3.152	1287.811	826.375	0.408	99.687	1.40	0.07	0.37	0.18	26.66	0.454	0.00062583	2.033	0.0072307	43.238	0.0838	42.450
z6	**4.031**	**0.077**	3.968	0.079	4.656	2.349	376.558	1119.163	0.432	98.946	1.48	0.08	0.35	0.23	29.02	0.483	0.00061578	1.993	0.0045961	50.573	0.0542	49.744
DM5AG32																						
z2	**3.663**	**0.070**	3.598	0.070	3.860	0.779	170.484	465.555	0.197	97.890	1.40	0.52	0.88	0.59	46.7	0.458	0.00055826	1.951	0.0038083	20.232	0.0495	19.939
z4	**3.842**	**0.095**	3.767	0.096	4.303	1.120	315.171	574.345	0.370	98.805	1.11	0.18	0.38	0.48	42.8	0.364	0.00058458	2.537	0.0042464	26.082	0.0527	25.252
z5	**3.660**	**0.037**	3.568	0.038	3.886	0.420	205.784	246.961	0.215	98.266	0.55	0.39	0.43	0.91	71.8	0.181	0.00055368	1.052	0.0038348	10.822	0.0503	10.646
z6	**3.604**	**0.072**	3.512	0.073	1.956	1.040	-1668.366	1800.471	0.577	100.211	0.54	0.17	0.27	0.61	54.9	0.179	0.00054499	2.091	0.0019278	53.223	0.0257	52.044
z8	**3.695**	**0.083**	3.611	0.084	3.888	1.033	178.901	595.787	0.487	97.981	0.82	0.19	0.36	0.53	47.4	0.268	0.00056038	2.336	0.0038367	26.612	0.0497	25.557
DM8AG44																						
z1	**3.720**	**0.110**	3.639	0.109	2.609	1.269	-870.952	1385.057	0.242	100.418	0.91	0.18	0.53	0.35	37.1	0.299	0.00056468	3.007	0.0025732	48.709	0.0331	48.070
z2	**3.766**	**0.128**	3.683	0.128	4.177	1.452	299.198	780.072	0.230	98.769	0.84	0.15	0.50	0.30	34.4	0.274	0.00057147	3.474	0.0041221	34.832	0.0523	34.199
z3	**3.602**	**0.126**	3.508	0.127	2.551	1.440	-830.850	1598.996	0.183	100.422	0.47	0.25	1.02	0.25	33.4	0.156	0.00054427	3.626	0.0025151	56.533	0.0335	55.982
z4	**7.588**	**0.323**	7.502	0.324	8.970	3.978	423.264	969.511	0.298	98.228	0.72	0.26	1.08	0.24	31.6	0.234	0.00116436	4.326	0.0088736	44.540	0.0553	43.446
z5	**3.703**	**0.111**	3.613	0.112	4.271	1.250	392.942	646.460	0.213	99.080	0.64	0.19	0.59	0.32	36.3	0.211	0.0005607	3.089	0.0042155	29.317	0.0546	28.816
z6	**3.802**	**0.104**	3.711	0.105	5.313	1.420	809.055	536.205	0.456	99.541	0.56	0.14	0.36	0.39	40.9	0.185	0.00057577	2.827	0.0052463	26.793	0.0661	25.628
z7	**3.793**	**0.132**	3.705	0.133	4.344	1.712	374.544	865.624	0.331	99.011	0.68	0.24	0.83	0.29	34.57	0.224	0.00057492	3.584	0.0042872	39.498	0.0541	38.461
DM3AG15																						
z1	**3.629**	**0.079**	3.558	0.079	3.690	0.879	90.481	555.046	0.250	96.068	1.23	0.23	0.45	0.52	44.0	0.402	0.00055207	2.226	0.0036402	23.879	0.0478	23.423
z2	**3.568**	**0.101**	3.491	0.102	2.827	1.226	-533.132	1144.155	0.288	100.655	1.06	0.34	0.89	0.38	38.1	0.346	0.00054175	2.925	0.002788	43.431	0.0373	42.681
z4	**4.794**	**0.163**	4.716	0.164	5.979	1.849	549.350	664.956	0.215	99.142	1.01	0.20	0.66	0.31	34.3	0.328	0.00073186	3.475	0.0059054	31.010	0.0585	30.452
z6	**3.667**	**0.074**	3.576	0.075	3.602	0.828	20.859	546.193	0.184	82.856	0.58	0.50	1.11	0.45	44.7	0.191	0.0005549	2.085	0.0035536	23.041	0.0465	22.749
z7	**3.665**	**0.047**	3.579	0.048	3.627	0.540	35.652	349.437	0.277	89.960	0.76	0.90	1.14	0.79	62.5	0.249	0.00055541	1.333	0.0035789	14.909	0.0468	14.595
z8	**3.657**	**0.234**	3.583	0.234	4.045	2.613	288.694	1456.476	0.200	98.759	1.13	0.17	1.04	0.17	26.6	0.371	0.00055593	6.536	0.0039916	64.721	0.0521	63.733
z9	**3.735**	**0.111**	3.653	0.112	4.783	1.265	618.101	560.060	0.243	99.409	0.90	0.20	0.58	0.35	36.79	0.294	0.0005669	3.055	0.0047215	26.520	0.0604	25.946
z10	**3.699**	**0.170**	3.634	0.170	4.330	1.926	410.583	979.703	0.214	99.115	1.43	0.16	0.62	0.25	30.07	0.467	0.0005639	4.680	0.0042731	44.568	0.0550	43.806

† Corrected for initial Th/U disequilibrium using radiogenic 208Pb and Th/U[magma] = 3.50000.

§ Isotopic dates calculated using the decay constants λ238 = 1.55125E-10 and λ235 = 9.8485E-10 (Jaffey et al. 1971).

% discordance = 100 - (100 * ($^{206}Pb/^{238}U$ date) / ($^{207}Pb/^{206}Pb$ date))

†† Th contents calculated from radiogenic 208Pb and the 207Pb/206Pb date of the sample, assuming concordance between U-Th and Pb systems.

§§ Total mass of radiogenic Pb.

Total mass of common Pb.

††† Ratio of radiogenic Pb (including 208Pb) to common Pb.

§§§ Measured ratio corrected for fractionation and spike contribution only.

Measured ratios corrected for fractionation, tracer and blank.

TABLE 4. $^{40}Ar/^{39}Ar$ GEOCHRONOLOGY FOR DON MANUEL PRINCIPAL BASALTIC ANDESITE DIKES

Sample	Material	J	±1σ	**Integrated age (Ma)**	±1σ	%radiogenic ^{40}Ar	int. $^{40}Ar^*/^{39}Ar_K$	**Plateau age (Ma)**	±1σ w/o J	±1σ w/ J	MSWD	Prob.	steps	n/n-total	%gas	mol ^{39}Ar	Ca/K	±1σ Ca/K	**Isochron age (Ma)**	±2σ	±2σ (%)	$^{40}Ar/^{36}Ar(i)$	±2σ	MSWD	p	n
DM4AG28	Groundmass	2.49E-04	1.45E-06	4.7	0.2	19.2	10.380	3.85	0.18	0.19	1.9	0.1	5-9	5/13	70.6	4.54E-16	2.82	0.30	4.01	0.61	10.0	295	14	2.3	0.08	5
DM7AG26	Groundmass	2.62E-04	9.50E-07	3.8	0.1	59.9	8.129	3.60	0.05	0.06	1.3	0.26	7-10	4/12	50	1.75E-15	2.17	0.10	3.54	0.47	9.4	308	75	2.0	0.14	4

Notes: Samples were irradiated in the Oregon State University reactor, Cd-shielded facility. Alder Creek sanidine (1.2056 ± 0.0019 (1σ) Ma, Renne et al. 2011) was used to establish neutron flux values (J). Decay constants are listed in Renne et al. (2011).

Nucleogenic production ratios:		Isotopic constants and decay rates:	
$(^{36}Ar/^{37}Ar)Ca$	2.64×10^{-4}	$\lambda(^{40}K_e)/yr$	$5.757 \pm 0.016 \times 10^{-11}$
$(^{39}Ar/^{37}Ar)Ca$	6.5×10^{-4}	$\lambda(^{40}K_\beta)/yr$	$4.955 \pm 0.013 \times 10^{-10}$
$(^{38}Ar/^{37}Ar)Ca$	0.196 ± 0.00816 × 10−4	$\lambda(^{37}Ar)/d$	$1.983 \pm 0.0045 \times 10^{-2}$
$(^{40}Ar/^{39}Ar)K$	8.5×10^{-3}	$\lambda(^{39}Ar)/d$	$7.068 \pm 0.0788 \times 10^{-6}$
$(^{38}Ar/^{39}Ar)K$	$1.22 \pm 0.0027 \times 10^{-2}$	$\lambda(^{36}Cl)/d$	$6.308 \pm 0 \times 10^{-9}$
$(^{36}Ar/^{38}Ar)Cl$	$2.629 \pm 0.011 \times 10^{2}$	$(^{40}Ar/^{36}Ar)_{Atm}$	298.56 ± 0.31
$^{37}Ar/^{39}Ar$ to Ca/K	1.96	$(^{40}Ar/^{38}Ar)_{Atm}$	1583.5 ± 2.5
$^{38}Ar/^{39}Ar$ to Cl/K	2.9	$^{40}K/K_{Total}$	0.01167 ± 0.00002

GSA Data Repository

Geology of the Don Manuel igneous complex, central Chile: relationship between igneous processes in volcanic and porphyry copper systems

Amy K. Gilmer[1*], R. Stephen J. Sparks[1], Alison C. Rust[1], Simon Tapster[2], Adam D. Webb[3],

and Dan N. Barfod[4]

[1]School of Earth Sciences, University of Bristol, Wills Memorial Building, Bristol BS8 1RJ, UK.
[2]NERC Isotope Geoscience Laboratory, British Geological Survey, Keyworth, Nottingham NG12 5GG, UK.
[3]BHP Billiton, Cerro El Plomo 6000, Santiago, RM, Chile.
[4] NERC Argon Isotope Facility, SUERC, East Kilbride G75 0QF, UK

Contents:

References for Data Repository

DR1. Whole rock geochemistry methods.

A mass of 0.1 g ± 0.002 of sample was measured, placed in a platinum crucible with 0.4 g ± 0.005 lithium metaborate flux (Alfa Aesar Spectroflux 100B) and 0.5 mL of lithium iodide 25% solution (Alfa Aesar) that was used as a non-wetting agent, and fused in a Claisse FLUXY automated fusion system. The melt was automatically poured into a Teflon beaker with 50 ml of 4% HNO_3 acid solution and stirred until completely dissolved. One mL of 100 ppm rhodium spike solution was added as an internal standard. All samples were diluted to 100 mL with 18.2 MΩ deionized water, resulting in a spiked rock solution in 2% HNO_3. Solutions were then analyzed for bulk composition using Inductively Coupled Plasma – Optical Emission Spectrometry (ICP-OES) using a JY Horiba ULTIMA2. Analyses of trace and rare earth elements were performed on some solutions that were first further diluted by 10 times with 2% HNO_3 spiked to correct for instrument drift at low and high masses (5 ppb In and Tl internal standards). These solutions were analyzed using a Thermo Elemental X Series (X7) ICP-MS system. Calibration was carried out using reagent blank and international certified reference materials (CRM) (DTS-1, W2, BIR1, MRG1, JA2, STM-1 and JG3) and JA2, JG1a and JB1a as secondary standards. The relative analytical errors (±2σ) for major elements were less than 1% (with the exception of Fe and Na, where the error was 2%) and about 5% for trace elements. The loss on ignition determination error is about 10%.

DR3. Zircon U-Pb geochronology

Sample preparation

Four samples were split using a hydraulic rock splitter to reduce the sample to manageable fragments for the jaw-crusher. The jaw-crusher is used to reduce the split sample to a size suitable for sieving. Sample concentrates were prepared from sieve fractions from 50 to 250 μm using a hand magnet, heavy liquid (LST, density at 2.85 g/mL), and a Frantz magnetic separator. Approximately 50 zircon grains from each sample were hand-picked from each concentrate. Grains were photographed in transmitted light (Figure DR3.1).

Zircon characterization

Grains were photographed in transmitted light (Figure DR3.1). Additional zircons from each sample were mounted in epoxy disks and polished to expose a cross-section through the grain. Zircons were then imaged in BSE and Cathodoluminescence (CL) at the British Geological Survey, and at the University of Bristol to (Figure DR3.2). CL imaging was done to texturally characterize each sample's zircon population. Zircons typically showed mixed populations of: 1) multifaceted crystals with large, rounded and resorbed antecrystic cores with late-stage discordant rims; and 2) elongate or prismatic zircons which showed simpler growth evolution within their CL images. For the zircon grains or fragments that were dated we favoured the selection of elongate prismatic morphologies - as these were likely to contain the simplest growth histories that predated emplacement, and therefore give the best approximation of the emplacement age of their host intrusion. As DMIC zircons are typically small in size and have low concentrations of radiogenic Pb, we generally favoured dating whole zircons or fragments rather than those that had been CL imaged due to the reduced mass resulting from polishing.

Methods

Sample preparation and analyses for Chemical Abrasion Isotope Dilution Thermal Ionisation Mass spectrometry were carried out at the NERC Isotope Geosciences Laboratory (NIGL), British Geological Survey, Keyworth, UK. Methodology and instrumentation follows those described by Tapster et al. (2016). The important points are outlined here: Zircons were thermally annealed and chemically abraded prior to dissolution (Mattinson, 2005); The mixed ^{205}Pb–^{233}U–^{235}U EARTHTIME solutions (ET535; (Condon et al., 2015; McLean et al., 2015); Common Pb was attributed to the NIGL laboratory blank isotopic composition and associated uncertainty based upon

repeat analysis of total procedural blanks during the analytical period, U blanks were assigned a value of 0.1 ± 0.01 pg (1σ); Processing of isotope measurements, data reduction, error propagation, and date calculation was conducted using the TRIPOLI software package (Bowring et al., 2011) and ET_Redux and related algorithms (McLean et al., 2011); $^{206}Pb/^{238}U$ zircon dates were corrected for initial Th/U disequilibrium between the crystallising zircon and its host magma, which leads to the preferential incorporation of ^{238}U and exclusion of ^{230}Th, a daughter isotope within the decay series of ^{238}U to ^{206}Pb. In turn, this leads to an eventual deficit in ^{206}Pb within the analysed zircons and younger apparent dates (Schärer, 1984). For the correction we assumed a $Th/U_{(melt)} = 3.5$ and concordance between the $^{206}Pb/^{238}U$ and $^{208}Pb/^{232}Th$ systems. Using the $\lambda^{230}Th$ of Cheng et al., (2000), and the $\lambda^{238}U$ of Jaffey et al., (1971) this correction results in an increase in $^{206}Pb/^{238}U$ dates on the order of ca. 100 kyr for individual fractions.

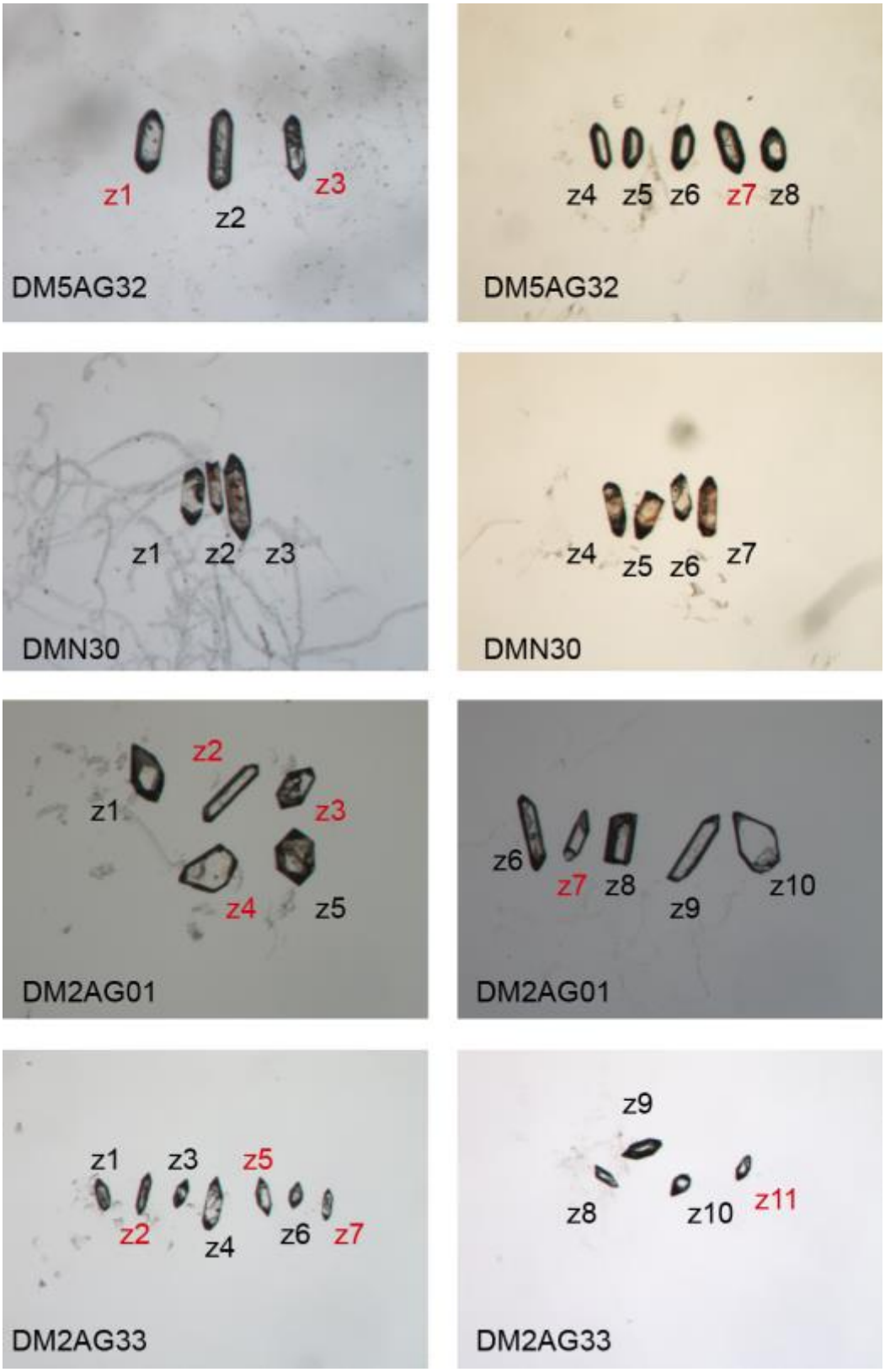

Figure DR3.1: Transmitted light images of annealed zircons. Red labels indicated zircons that were selected but were not analyzed. FOV=1.2 mm. Not all samples shown.

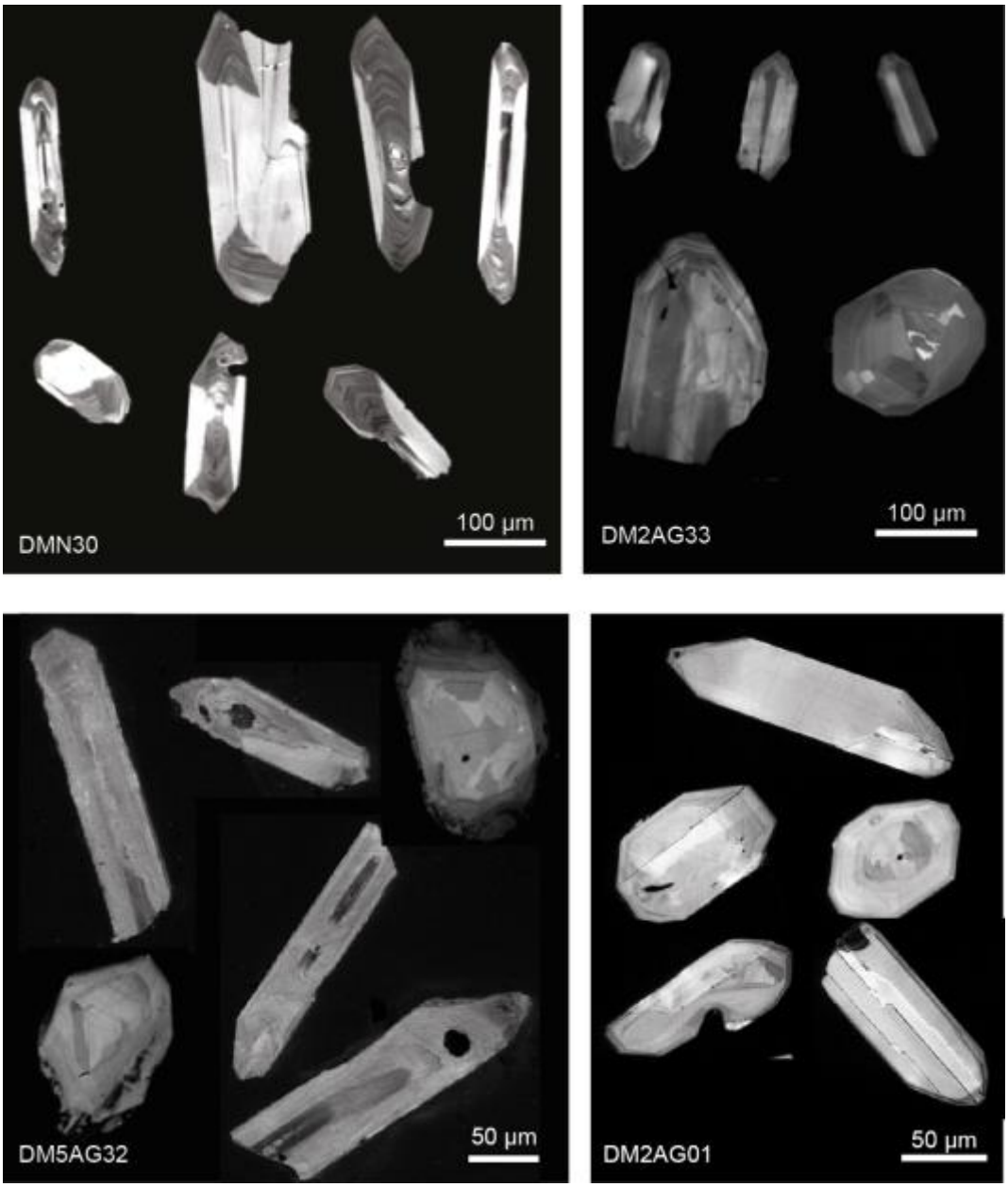

Figure DR3.2: CL images of representative zircons from dated samples. Not all samples shown.

DR4. $^{40}Ar/^{39}Ar$ geochronology

Sample preparation

Samples were trimmed to remove any weathering/staining using a diamond water saw. Six samples were split using a hydraulic rock splitter to reduce the sample to manageable fragments for the jaw-crusher. The jaw-crusher is used to reduce the split sample to a size suitable for sieving. Samples were sieved to obtain a 250-500 μm aliquot. They were then passed over with a strong hand magnet to remove any metal particles introduced during crushing. Dust was removed by washing the samples in deionized water in an ultrasonic bath for 10 minutes. Samples were leached in 3N HNO_3 for 20 minutes in an ultrasonic bath at 50°C. This was repeated until a clear solution was obtained. Samples were then rinsed with deionized water and then washed with deionized water in an ultrasonic bath for 10 minutes. Samples were then hand- picked under a binocular microscope and care was taken to remove all phenocrysts and altered grains. For each sample 1 g of groundmass separate was attained.

Methods

Samples and neutron flux monitors were placed in aluminium discs and stacked in quartz tubes. The relative positions of wells in the discs were precisely measured for later reconstruction of neutron flux gradients. The sample package was irradiated in the Oregon State University reactor, Cd-shielded facility. Alder Creek sanidine (1.2056±0.0019 (1σ) Ma, (Renne et al., 2011) was used to monitor ^{39}Ar production and establish neutron flux values (J) for the samples. Gas was extracted from samples via step-heating using a mid-infrared (10.6 μm) CO_2 laser with a non-gaussian, uniform energy profile and a 3.5 mm beam diameter. The samples were housed in a doubly-pumped ZnS-window laser cell and loaded into a copper planchette containing four 2.6 cm^2 square wells. Liberated argon was purified of active gases, e.g., CO_2, H_2O, H_2, N_2, CH_4, using three Zr-Al getters; one at 16°C and two at 400°C. Data were collected on a GVi instruments ARGUS V multi-collector mass spectrometer using a variable sensitivity faraday collector array in static collection (non-peak hopping) mode (Mark et al., 2009; Sparks et al., 2008). Time-intensity data are regressed to t_0 with second-order polynomial fits to the data. Mass discrimination was monitored on a daily basis by comparison to running-average values of an air standard. The average total system blank for laser extractions, measured between each sample run, was 2×10^{-15} mol ^{40}Ar, 1×10^{-17} mol ^{39}Ar, 2×10^{-17} mol ^{36}Ar. All data are blank, interference and mass discrimination corrected using the *MassSpec* software package (*MassSpec*, version 8.058, authored by Al Deino, Berkeley Geochronology Center, Version 8.058).

--- Atmospheric argon ratios and discrimination ---

($^{40}Ar/^{36}Ar$)atm	298.56 Â± 0.31
($^{40}Ar/^{38}Ar$)atm	1583.5 Â± 2.5

--- Minor irradiation parameters (see also Irradiation Data File) ---

($^{38}Ar/^{37}Ar$) Ca	0.0000196 Â± 8.160000e-7
($^{38}Ar/^{39}Ar$) K	0.0122 Â± 0.000027
P(36Cl/38Cl)	262.9 Â± 1.1

--- Decay constants ---

Lambda ^{40}K epsilon	5.757000e-11 ± 1.600000e-13
Lambda ^{40}K Beta	4.955000e-10 ± 1.340000e-12
Lambda ^{37}Ar	0.01983 ± 0.0000454
Lambda ^{39}Ar	7.068000e-6 ± 7.882200e-8
Lambda ^{36}Cl	6.308000e-9 ± 0

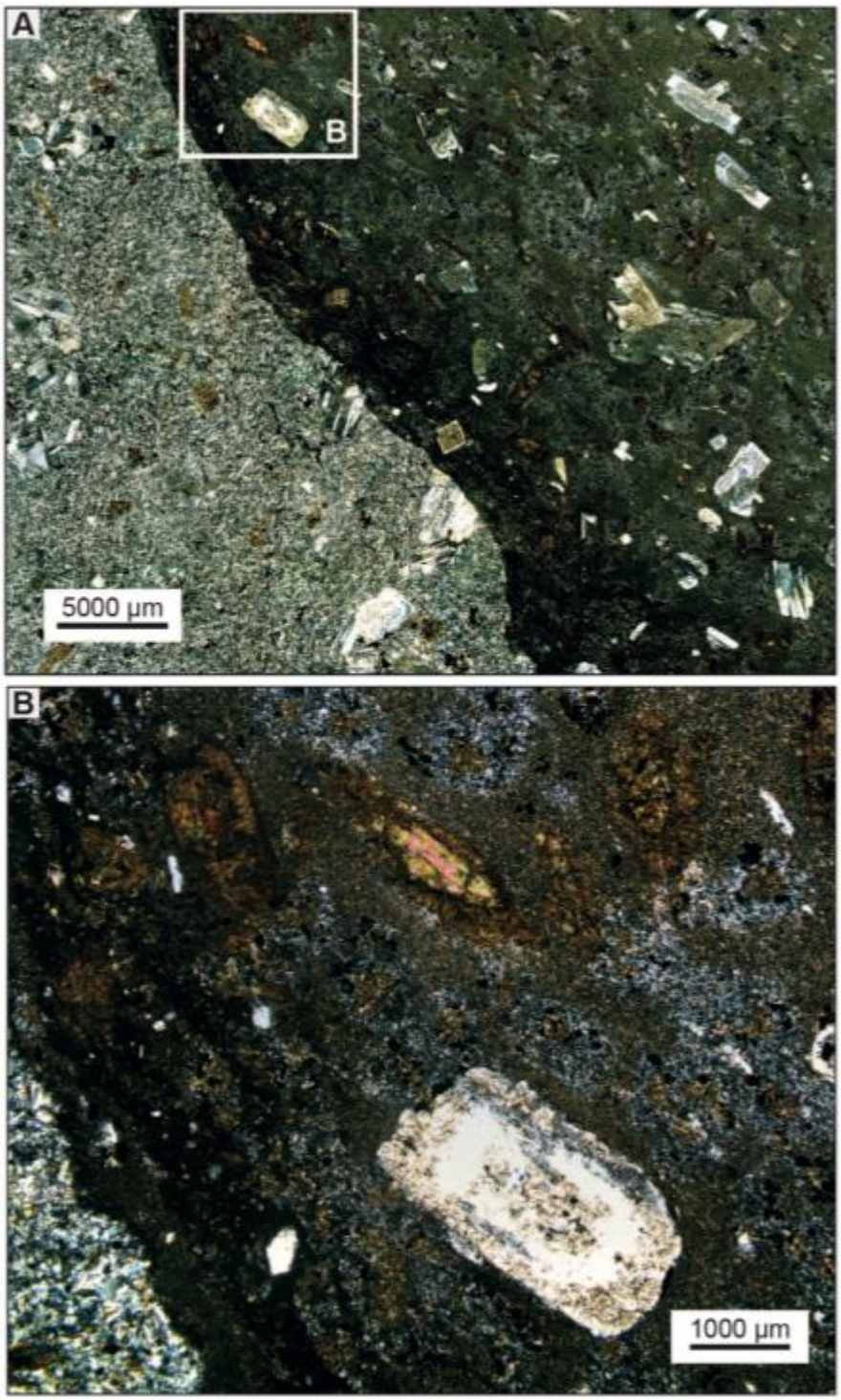

Figure DR5. (A) Mafic enclave in an intermediate porphyry dike showing plagioclase phenocryst likely entrained. (B) Inset showing significant secondary biotite alteration of mafic phases and groundmass.

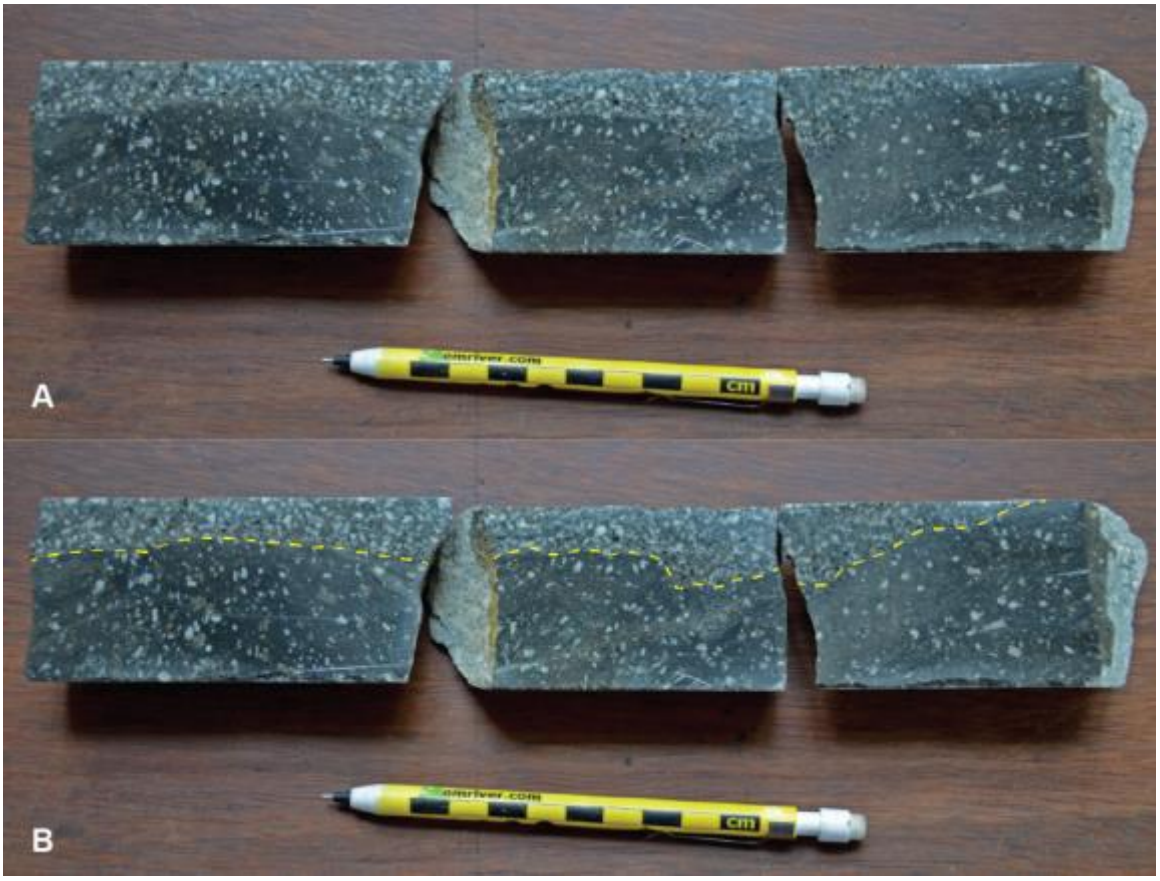

Figure DR6. (A) Internal ductile contact within a composite intermediate porphyry dike (IPD). Yellow dashed line follows the contact (B).

References

Bowring, J., McLean, N., and Bowring, S., 2011, Engineering cyber infrastructure for U-Pb geochronology: Tripoli and U-Pb_Redux: Geochemistry, Geophysics, Geosystems, v. 12, no. 6.

Cheng, H., Edwards, R., Hoff, J., Gallup, C., Richards, D., and Asmerom, Y., 2000, The half-lives of uranium-234 and thorium-230: Chemical Geology, v. 169, no. 1, p. 17-33.

Condon, D., Schoene, B., McLean, N., Bowring, S., and Parrish, R., 2015, Metrology and traceability of U–Pb isotope dilution geochronology (EARTHTIME Tracer Calibration Part I): Geochimica et Cosmochimica Acta, v. 164, p. 464-480.

Jaffey, A., Flynn, K., Glendenin, L., Bentley, W. t., and Essling, A., 1971, Precision measurement of half-lives and specific activities of U 235 and U 238: Physical Review C, v. 4, no. 5, p. 1889.

Mark, D., Barfod, D., Stuart, F., and Imlach, J., 2009, The ARGUS multicollector noble gas mass spectrometer: Performance for 40Ar/39Ar geochronology: Geochemistry, Geophysics, Geosystems, v. 10, no. 10.

Mattinson, J. M., 2005, Zircon U–Pb chemical abrasion ("CA-TIMS") method: combined annealing and multi-step partial dissolution analysis for improved precision and accuracy of zircon ages: Chemical Geology, v. 220, no. 1, p. 47-66.

McLean, N., Bowring, J., and Bowring, S., 2011, An algorithm for U-Pb isotope dilution data reduction and uncertainty propagation: Geochemistry, Geophysics, Geosystems, v. 12, no. 6.

McLean, N. M., Condon, D. J., Schoene, B., and Bowring, S. A., 2015, Evaluating uncertainties in the calibration of isotopic reference materials and multi-element isotopic tracers (EARTHTIME Tracer Calibration Part II): Geochimica et Cosmochimica Acta, v. 164, p. 481-501.

Renne, P. R., Balco, G., Ludwig, K. R., Mundil, R., and Min, K., 2011, Response to the comment by WH Schwarz et al. on "Joint determination of 40 K decay constants and 40 Ar*/40 K for the Fish Canyon sanidine standard, and improved accuracy for 40 Ar/39 Ar geochronology" by PR Renne et al.(2010): Geochimica et Cosmochimica Acta, v. 75, no. 17, p. 5097-5100.

Schärer, U., 1984, The effect of initial230Th disequilibrium on young UPb ages: the Makalu case, Himalaya: Earth and Planetary Science Letters, v. 67, no. 2, p. 191-204.

Sparks, R. S. J., Folkes, C. B., Humphreys, M. C., Barfod, D. N., Clavero, J., Sunagua, M. C., McNutt, S. R., and Pritchard, M. E., 2008, Uturuncu volcano, Bolivia: Volcanic unrest due to mid-crustal magma intrusion: American Journal of Science, v. 308, no. 6, p. 727-769.

Tapster, S., Condon, D., Naden, J., Noble, S., Petterson, M., Roberts, N., Saunders, A., and Smith, D., 2016, Rapid thermal rejuvenation of high-crystallinity magma linked to porphyry copper deposit formation; evidence from the Koloula Porphyry Prospect, Solomon Islands: Earth and Planetary Science Letters.